# First Characterization of a Class F Sortase and Establishment of a Microreactor-Based Assay for its Directed Evolution

**Inauguraldissertation**

zur

Erlangung der Würde eines Doktors der Philosophie

vorgelegt der

Philosophisch-Naturwissenschaftlichen Fakultät

der Universität Basel

von

**Salvatore Di Girolamo**

aus Italien

2020

Genehmigt von der Philosophisch-Naturwissenschaftlichen Fakultät der Universität Basel auf Antrag von

Prof. Dr. Florian Seebeck

Prof. Dr. Georg Lipps

Prof. Dr. Michael Nash

Basel, 21 Mai 2019

Prof. Dr. Martin Spiess

# Table of contents

# Abstract

Sortases are a family of enzymes responsible for the covalent anchoring of proteins to the cell wall of Gram-positive bacteria via a transpeptidation reaction. These cysteine transpeptidases specifically recognize and cleave a five amino acid long sorting motif on the target proteins and then catalyzed the formation of a new peptide bond between the C-terminus of the cleaved sorting motif and the free amino group of a cell wall component. The transpeptidation activity of the well-characterized class A sortase from *Staphylococcus aureus* (SaSrtA) and evolved variants thereof continues to see increasing use in a wide range of biotechnological applications (Sortagging). Due to low activity, sortases from classes other than class A are not currently used for this purpose and, with the exception of SaSrtA, laboratory evolution of other sortases has not been performed.

In the first part of this work, we report on the exploration of the natural diversity of sortases and describe the in-depth characterization of a sortase enzyme that belongs to the not-yet-investigated class F, sortase F from *Propionibacterium acnes* (PaSrtF). We showed that PaSrtF exhibits similar behaviour to the wild type SaSrtA in terms of catalytic activity and sequence specificity and demonstrated its usefulness for protein engineering applications.

In the second part of the work, the development of a novel assay for the screening of sortase variants with improved properties is described. Hydrogel bead-based microreactors, suitable for high-throughput screening using a large particle flow cytometer, were prepared and evaluated for their capability to act as individual evolutionary units that link sortases activity with a fluorescent readout.

The microreactor-based assay, developed and optimized with the wild type SaSrtA, was successfully validated with the newly characterized PaSrtF and can, therefore, be used for its directed evolution.

# List of abbreviations

| | |
|---|---|
| Å | Ångström $10^{-10}$ m |
| A | adenine |
| A, Ala | alanine |
| ADCs | antibody-drug conjugates |
| BaSrtB | sortase B from *Bacillus anthracis* |
| BaSrtD | sortase D from *Bacillus anthracis* |
| C | cytosine |
| C, Cys | cysteine |
| CaSrtD | sortase D from *Clostridium acetobutylicum* |
| CBM | carbohydrate-binding motif |
| COPAS | complex object parametric analysis and sorting |
| CpSrtD | sortase D from *Clostridium perfringens* |
| CV | column volume |
| CWSS | cell wall sorting signal |
| D, Asp | aspartic acid |
| Dabcyl | 4-{[4-(dimethylamino) phenyl]azo}benzoic acid |
| dATP | deoxyadenosine triphosphate |
| dCTP | deoxycytidine triphosphate |
| dGTP | deoxyguanosine triphosphate |
| dTTP | deoxythymidine triphosphate |
| dNTP | deoxynucleoside triphosphate |
| DMF | *N*,*N*-dimethylformamide |
| DMSO | dimethyl sulfoxide |
| DNPNTGDE | aspartic acid-asparagine-proline-asparagine-threonine-glycine-aspartic acid-glutamic acid |
| E, Glu | glutamic acid |
| EDANS | 5-[(2-aminoethyl)amino] naphthalene-1-sulfonic acid |
| ep-PCR | error-prone polymerase chain reaction |
| DNA | deoxyribonucleic acid |
| eSaSrtA | evolved sortase A from *Staphylococcus aureus* |
| eSrtA/D | chimeric sortase (evolved sortase A from *S. aureus*/sortase D from *B. anthracis*) |
| FITC | fluorescein isothiocyanate |
| G | guanidine |
| G, Gly | glycine |
| GCABs | gel-core alginate microbeads |
| GC-CAMs | gel-core chitosan-coated alginate microcapsules |
| GFP | green fluorescence protein |
| Gn-SrtA | N-terminally glycine-modified sortase A from *Staphylococcus aureus* |
| Gn-SrtB | N-terminally glycine-modified sortase B from *Bacillus anthracis* |
| Gn-SrtF | N-terminally glycine-modified sortase A from P*ropionibacterium acnes* |
| HC-CAMs | hollow-core chitosan-coated alginate microcapsules |
| His10 | polyhistidine tag |
| HPLC | high performance liquid chromatography |
| IPTG | isopropyl β-D-1-thiogalactopyranoside |
| K, Lys | lysine |
| kDa | kilo Dalton |
| L, Leu | leucine |
| LB | lysogeny broth |
| LC-MS | liquid chromatography-mass spectrometry |
| LPXTG | leucine-proline-any amino acid-treonine-glycine |
| LPETGE | leucine-proline-glutamic acid-treonine-glycine- glutamic acid |

| | |
|---|---|
| M, Met | methionine |
| MES | 2-(N-morpholino)ethanesulfonic acid |
| mRNA | messenger ribonucleic acid |
| MkSrtE | sortase E from *Methanopyrus kandleri* |
| MTT | 3-(4,5-dimethylthiazol-2-yl)-2,5-diphenyl tetrazolium bromide |
| N, Asn | asparagine |
| NMR | nuclear magnetic resonance |
| OD600 | optical density at 600 nm |
| P, Pro | proline |
| PAH | poly-allylamine hydrochloride |
| PaSrtF | sortase F from *Propionibacterium acnes* |
| PCR | polymerase chain reaction |
| PI | propidium iodide |
| PSS | poly-styrene sulfonate |
| Q, Gln | glutamine |
| *R*, Arg | arginine |
| $R_s$ | Stokes radius |
| S, Ser | serine |
| SaSrtA | sortase A from *Staphylococcus.aureus* |
| ScSrtE | sortase E from *Streptomyces coelicolor* |
| SDS-PAGE | sodium dodecyl sulphate-polyacrylamide gel electrophoresis |
| SrtA | sortase A |
| SrtB | sortase B |
| SrtF | sortase F |
| T | thymine |
| T, Thr | threonine |
| TB | terrific broth |
| TOF | time of flight |
| V, Val | valine |
| VvGT5 | *Vitis vinifera* glycosyltransferase 5 |
| WCE | whole cell extract |

# 1 Introduction

## 1.1 Biology and function of sortases

The cell wall of Gram-positive bacteria displays a wide subset of proteins that enable each microbe to communicate and interact with the surrounding environment. Among the strategies evolved by bacteria to immobilize proteins on the cell surface, the covalent anchoring of proteins to the cell wall is executed by sortase enzymes (Navarre and Schneewind, 1994).

Sortases are a family of membrane-anchored cysteine transpeptidases that either "sort" proteins by attaching them to the cell wall or participate in the construction of pili, proteinaceous filaments that extend from the cell surface.

The first and still the best characterized sortase family member sortase A from *Staphylococcus aureus* (SaSrtA) was identified in 1999 by Mazmanian and colleagues following the functional complementation of *S. aureus* mutants defective in the anchoring of surface proteins (Mazmanian et al., 1999).

The sortase A-mediated transpeptidation starts when the precursor of the target protein containing an N-terminal signal peptide and a C-terminal cell wall sorting signal (CWSS) is exported from the cytoplasm through the secretory (Sec) pathway. The CWSS consists of a conserved five amino acid long sorting motif LPXTG (where the third amino acid X can be variable) followed by a hydrophobic stretch and a C-terminal positively charged tail. The hydrophobic stretch and the positively charged tail presumably function by retaining the translocated polypeptide in the bilayer membrane and positioning the LPXTG motif for processing by the sortase enzyme (Ryan G Kruger et al., 2004; Navarre and Schneewind, 1994; Schneewind et al., 1992). Once sortase A binds the LPXTG sorting motif the thiol group of the cysteine in the active site nucleophilically attacks the carbonyl carbon of the threonine residue (T) cleaving the peptide bond between the threonine and the glycine (G) and creating an intermediate in which the sortase and the target protein are linked together through a thioester linkage. The intermediate is then resolved when the free amino group of the first glycine residue of the pentaglycine stretch of the cell wall precursor lipid II nucleophilically attacks the thioester linkage forming a new peptide bond between the target protein and the lipid II molecule (Ton-That et al., 1999) (**Figure 1.1**).

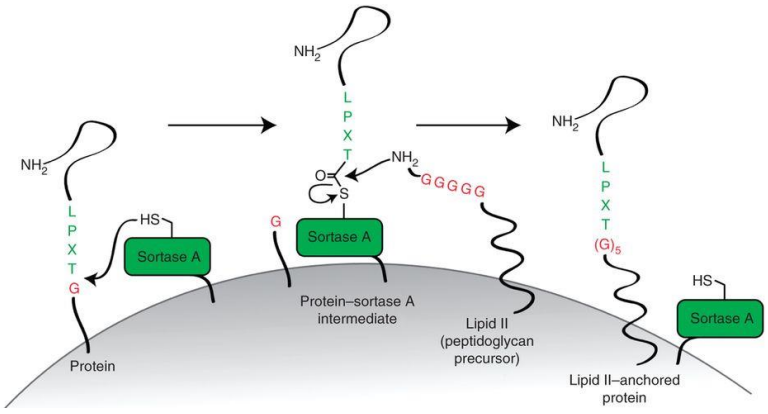


**Figure 1.1.** Mechanism of *S. aureus* sortase A-mediated surface protein anchoring to the cell wall. (Reproduced with permission from Guimaraes et al. 2013).

## 1.2 Classification of sortases

At present 9205 gene sequences encoding sortase enzymes have been identified within 3118 species most of them being Gram-positive bacteria. Only a handful of sortases have been found in Gram-negative bacteria or archaeal species (Comfort and Clubb, 2004; Finn et al., 2016; Pallen et al., 2001).

Based on their amino acid sequence and their function, Clubb and co-workers. (Spirig et al., 2011) divided sortases into six classes called class A to F. Although the nomenclature has considerably changed in the past (Comfort and Clubb, 2004; Dramsi et al., 2005) this system is now reflected in the conserved domain database of the NCBI, which, however, splits the sortase D class into two separate classes (D1 and D2). Most Gram-positive bacteria express more than one class of sortases that, in the course of the evolution, may have evolved different specificity for the pentapeptide sorting motif. Consequently, by recognizing their class-specific sorting motif, sortases belonging to different classes are predicted to operate non-redundantly to display or assemble distinct proteins on the cell surface (Comfort and Clubb, 2004). The phylogeny of the sortases along with their predicted recognition sequences is depicted in **figure 1.2**.

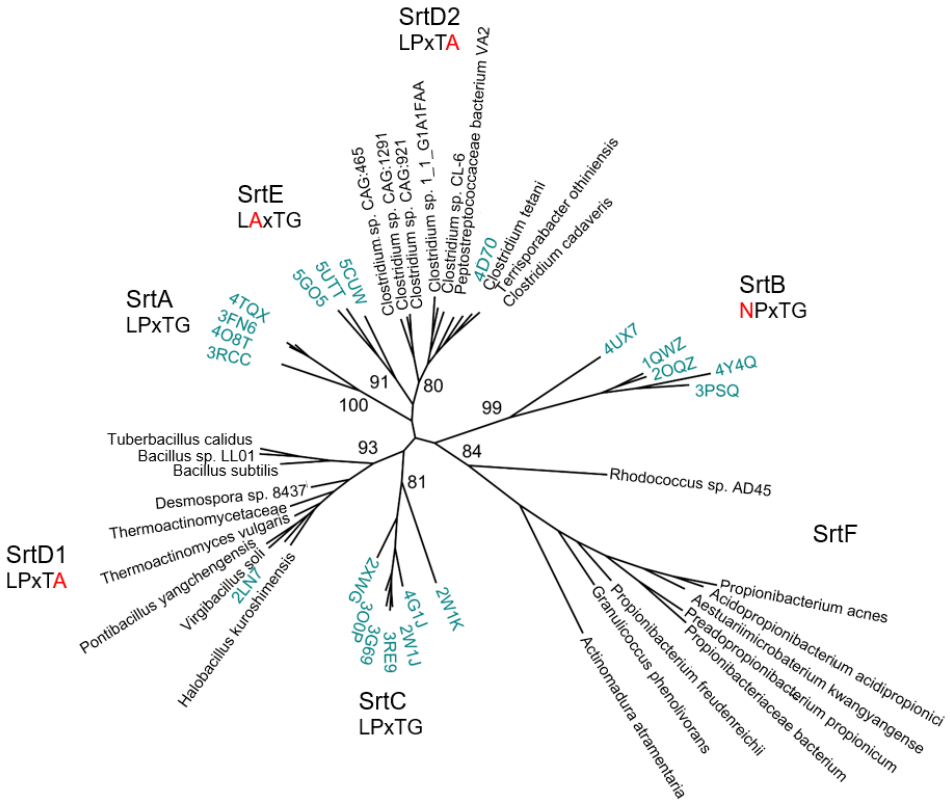


**Figure 1.2.** Neighbour-joining phylogenetic tree showing the evolutionary relationship among sortases. The tree was constructed from a multiple sequence alignment of representative structures of sortases from classes A, B, C, D1, D2 and E and additional sortase sequences of the classes D1, D2 and F. Leaves of the tree were labeled with the PDB code (green) or the species. For each class the bootstrap support and the consensus recognition sequence are indicated. Highlighted in red are positions differing from the sortase A recognition sequence (Di Girolamo et al., 2019).

Class A sortases are considered housekeeping enzymes as in different bacteria they anchor to the cell wall a large number of functionally distinct proteins. As an example, sortase A from *L. monocytogenes* was found to process up to 43 proteins (Boekhorst et al., 2005; Marraffini et al., 2006). Consistent with this observation is the fact that genes encoding for sortases A are generally not clustered with any of its substrates (Pallen et al., 2001). Proteins anchored by class A enzymes contain the LPXTG motif and possess several functions including bacterial adhesion, nutrient acquisition, host cell invasion, and immune system evasion (Navarre and Schneewind, 1999).

Sortases belonging to class B are less abundant then class A homologues and genes encoding for members of this class were found located within operons that also encode their substrates. For instance, genes encoding for sortase B from *Staphylococcus aureus* (Sa-SrtB) and for sortase B from *Bacillus anthracis* (Ba-SrtB) reside within the *isd* (iron-responsive surface determinant) locus, which also contains genes encoding for proteins involved in the heme uptake. Unlike class A sortases, specificity of class B members is less well-defined and recognition sequences NPKTG and NPQTN were reported for Ba-SrtB and Sa-SrtB respectively (Maresso et al., 2006; Mazmanian et al., 2003).

Class C sortases have a more specialized function and are used by Gram-positive bacteria to link pilin subunits via lysine–isopeptide bonds to construct pili that promote microbial adhesion and biofilm formation (Mandlik et al., 2008; Ton-That and Schneewind, 2003). More recently class B members were also found that assemble pili (Kang et al., 2011; Shaik et al., 2015). As for class B sortases, the genes encoding class C sortases are often located in gene clusters with their substrates and are often present in several copies per genome (Hendrickx et al., 2011). Similarly to class A sortases, sortases belonging to class C are predicted to process proteins harboring sorting signal with the LPXTG motif (Comfort and Clubb, 2004).

Less is known on sortases of the classes D and E. At present only two class D sortases have been characterized in *Bacillus anthracis* and *Clostridium perfringens* for which atomic structures have also been reported. Sortase D1 form *B. anthracis (*Ba-SrtD1, also known as Ba-SrtC) is required for the formation of infectious spores and it has been shown to specifically cleave proteins bearing the LPNTA motif and to attach them to the amino group of diaminopimelic acid in the envelope of sporulating cells (Marraffini and Schneewind, 2006, 2007; Scott A. Robson et al., 2012).

Sortase D2 from *C. perfringens* (CpSrtD2) was shown to be catalytically distinct from Ba-SrtD1 as it cleaves substrates bearing the LPQTGS recognition sequence. Interestingly, its catalytic activity was found enhanced in presence of magnesium making CpSrtD2 one of the two known sortases (the other being SaSrtA) whose activity is modulated by metal ions (Suryadinata et al., 2015).

Class E sortases share limited primary sequence homology to other sortases and are thought to also have a general housekeeping role. In fact, genes encoding class A and E sortases are never found in the same organism and, similar to class A sortases, genes encoding class E enzymes are not positioned adjacent to those encoding potential protein substrates (Comfort and Clubb, 2004). So far, two class E sortases have

been studied in more detail and their structures have been recently determined. Sortase E from *Streptomyces coelicolor* has been shown to anchor chaplin proteins to the cell surface that promote the transition from vegetative growth to aerial hyphae formation and appeared to prefer LAXTG substrates over LPXTG substrates (A. Duong et al., 2012; M. D. Kattke et al., 2016). Similarly, sortase E from *S. avermitilis* preferentially transpeptidates substrates with an LAXTG motif using nucleophiles with an N-terminal glycine residue (Das et al., 2017). Class F sortases are mainly present in the orders Actinomycetales and Bacillales but at present, none of them has been biochemically or structurally characterized. An overview of the sortase enzyme family is given in **table 1.**

**Table 1:** Overview of the sortase enzyme family. Sortases are grouped according to their sequence homology. The conserved domain (CD) code as well as the protein data base (PBD) code of representative structures are reported. The most common sorting motifs (with positions differing from sortase A sorting motif highlighted in red) and the function of the sortases are also given.

| Class | Conserved domain (CD) | Representative structure (PDB) | Sorting motif | Main function |
|---|---|---|---|---|
| A | cd06165 | 3FN6 | LPxTG | General |
| B | cd05826 | 1QWZ | NPxTG | Heme uptake, Pilus polymerization |
| C | cd05827 | 2WIJ | LPxTG | Pilus polymerization |
| D1 | cd05828 | 2LN7 | LPxTA | Spore formation |
| D2 | cd06166 | 4D70 | LPxTA | Spore formation |
| E | cd05830 | 5GO5 | LAxTG | General, Pilus attachment |
| F | cd05829 | - | - | Unknown |

## 1.3 Sortases structure and mechanism of action

Shortly after its discovery, the three-dimensional structure of the conserved domain of sortase A from *S. aureus* ($SaSrtA_{\Delta N59}$) was determined with NMR spectroscopy (Ilangovan et al., 2001). The structure revealed a unique eight-stranded β-barrel core formed by the interaction of two anti-parallel β sheets that includes two helices and several loops with the putative active site at the end of a hydrophobic depression that could accommodate the LPXTG substrate peptide. In addition, comparison of NMR spectra in the presence and absence of calcium allowed the positioning of the calcium binding site in proximity of the active site (Ilangovan et al., 2001). The overall structure of $SaSrtA_{\Delta N59}$ is depicted in **figure 1.3.**

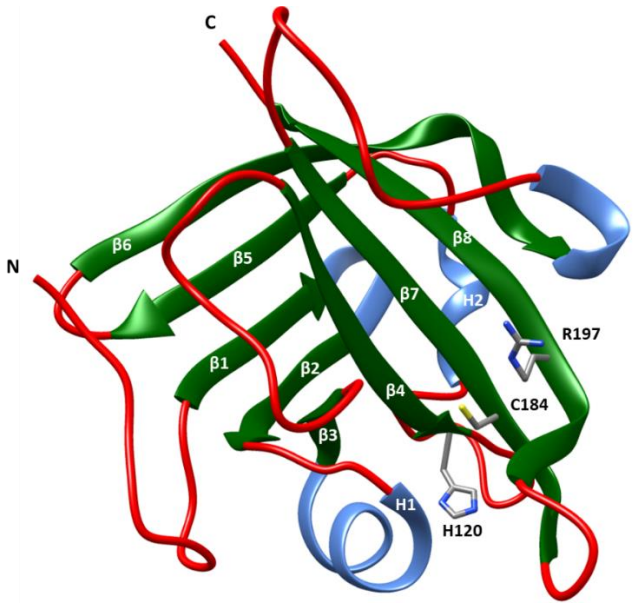


**Figure 1.3. Overall structure of SaSrtA**. $SrtA_{\Delta N59}$ adopts a three-dimensional β-barrel structure formed by the interaction of two anti-parallel β sheets (Ilangovan et al., 2001). The structure was generated from the atomic coordinates of 1T2P (Zong et al., 2004) using the program UCSF Chimera (Pettersen et al., 2004).

To better describe the substrate binding pocket, the X-ray structure of $SaSrtA_{\Delta N59}$ non-covalently complexed with its substrate was subsequently solved (Zong et al., 2004). Analysis of the complex structure revealed that the peptide bond between the threonine and the glycine residues of the ligand peptide was positioned between the conserved residues Cys184 and Arg197 but far from the His120 side chain that was thought to form along with Cys184 the catalytic thiolate-imidazolium ion pair found in the superfamily of cysteine proteases.

Although the conserved His120 and Arg197 were shown essential for efficient enzymatic activity (Marraffini et al., 2004; Ton-That et al., 2002), their role in catalysis remained controversial until detailed kinetic measurements supported a reverse protonation mechanism (Frankel et al., 2005). This mechanism

proposes that at any given time and at physiological pH only a small percentage (0.06%) of the total enzyme contains the Cys184 thiolate and His120 imidazolium forms and is competent for catalysis.

The reverse protonation mechanism was confirmed by analyzing the NMR structure of the $SaSrtA_{\Delta N59}$ covalently bound to a substrate analog to mimic the thioacyl catalytic intermediate (Suree et al., 2009). His120 would protonate the amide leaving group as the T-G peptide bond is broken and would deprotonate and activate the incoming terminal amine group of lipid II for nucleophilic attack on the thioacyl intermediate. By donating hydrogen bonds Arg197 would stabilizes both the positioning of the LPXTG substrate in the active site and the tetrahedral intermediates of catalysis (**figure 1.4**)

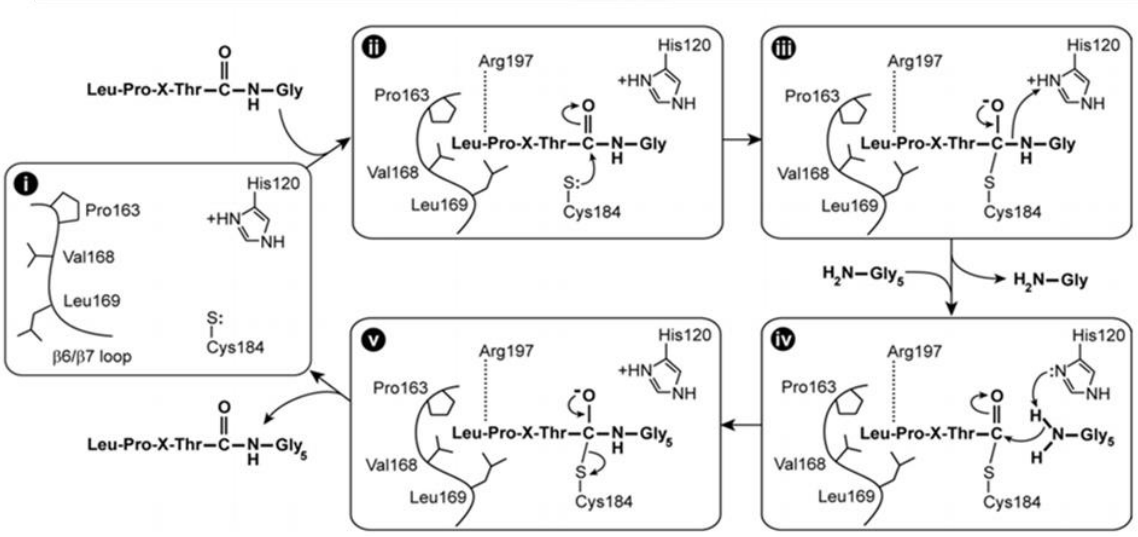


**Figure 1.4.** Proposed SrtA transpeptidation mechanism based on the structure of the $SrtA_{\Delta N59}$ in complex with a substrate analog. (***i)*** Active site of sortase A containing the flexible β6/β7 loop. (***ii)*** The β6/β7 loop closes upon binding of the sorting motif whose positioning is stabilized through the formation of hydrogen bonds with Arg197. The thiolate group of Cys184 attacks the carbonyl carbon of the threonine forming a tetrahedral intermediate. (***iii)*** His120 protonates the amide of the glycine residue as the peptide bond is broken. (***iv)*** The free amino group of the pentaglycine cross-bridge peptide of lipid II enters the active site and, upon activation by His120, nucleophilically attacks the intermediate. (***v)*** The formation of a second tetrahedral intermediate is followed by the rupture of the thioacyl linkage and the release of the transpeptidation product. (Reproduced with permission from Suree et al. 2009).

In addition, the NMR structure of $SaSrtA_{\Delta N59}$ bound to a substrate analog allowed to elucidate the molecular basis of substrate recognition. SaSrtA recognizes the LPXTG substrate through a large groove that leads into the active site. Residues in strands β4 and β7 form the floor of the groove, whereas the walls are formed by surface loops β6/β7, β7/β8, β3/β4, and β2/H1.

Comparison of NMR structures in presence and absence of the substrate analog revealed that the binding of the sorting motif induces two main structural changes. One concerns a 10 Å displacement of the β6/β7

loop towards the active site that (**i**) lead to the formation of a $3_{10}$ helix that appears to plays a key role in substrate recognition and (**ii**) allow the side chain of Glu171 (together with Glu105 and Glu108) to contact the calcium ion stabilizing the closed conformation (**figure 1.5 A**). The second structural change concerns a 13 Å displacement of the β7/β8 loop that creates a new groove that expose the side chain of His120 and that might represent the entry point for the lipid II substrate into the active site (Suree et al., 2009) (**figure 1.5 B**).

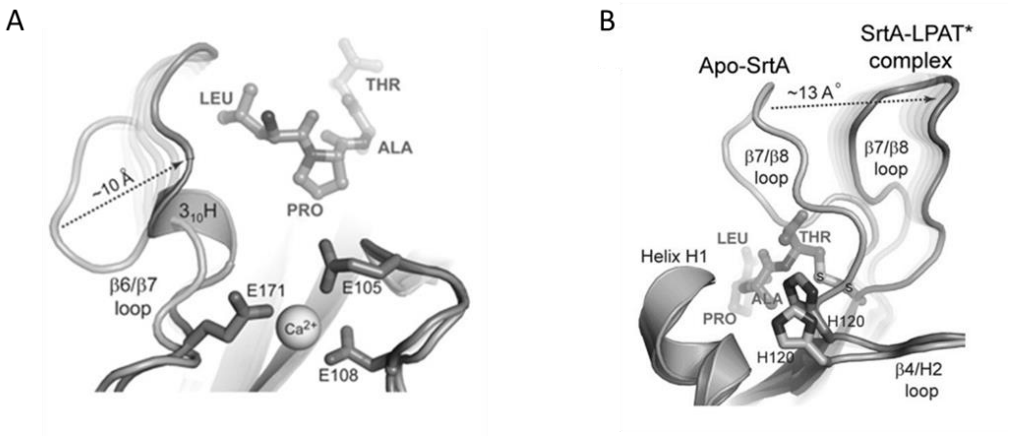


**Figure 1.5.** Binding of the sorting motif induces two main changes in the structure of SrtA. (**A**) Expanded view of the superposition of the average NMR structures of $SrtA_{\Delta N59}$ and of $SrtA_{\Delta N59}$ bound to a substrate analog showing that the displacement of β6/β7 loop towards the active site upon substrate binding causes the formation of a $3_{10}$ helix and allows the positioning of the calcium ion calcium into the calcium binding pocket. (**B**) Expanded view as in (A) showing that the substrate-dependent structural change in the β7/β8 loop unmasks a groove that might represent the entry point of the lipid II substrate. (Reproduced with permission from Suree et al. 2009).

At present, in addition to SaSrtA, structures have been reported for other class A sortases and for members of class B, C, D and E. Structural analysis have shown that sortases from different classes share a similar overall structure but with variable number of peripheral α-helices and other variations that likely effect the function and modulate the substrate specificity. For instance, an extended β6/β7 loop in sortase B from *S. aureus* is involved in recognizing the NPQTN sorting signal substrate (Jacobitz et al., 2014) while the two short additional N-terminal helices may play a role in anchoring substrates to buried portions of the cell wall (Marraffini and Schneewind, 2005). Still, in class C sortases, an elongated N-terminal region has been shown to work as a lid that occlude the active site and that might regulate the enzyme activity (Mandlik et al., 2008; Manzano et al., 2009, 2008).

Structural and computational studies of sortase A from *B. anthracis* and sortase B from *S. aureus* in complex with their sorting signals peptides have shown that class A and B sortases recognize their substrates and catalyze the transpeptidation reaction in a similar manner (Chan et al., 2015; Jacobitz et al., 2014). These results suggest that all the sortases may function using a similar mechanism of action.

## 1.4 Sortases as targets for anti-infective agents development

Many of the LPXTG bearing proteins attached to the cell wall of *S. aureus* by sortase A belong to the MSCRAMMs (microbial surface components recognizing adhesive matrix molecules). These proteins are virulence factors that play significant roles during staphylococcal infections including bacterial attachment to the extracellular matrix of host tissues, biofilm formation and immune response evasion (Foster et al., 2014). Over the last two decades, several studies have demonstrated the link between sortase A activity and *S. aureus* pathogenesis. In a pioneer study, Mazmanian and colleagues (Mazmanian et al., 2000) showed that gene knockout mutants of *srtA* resulted in defective surface expression of various LPXTG motif proteins and a defect in establishing renal abscesses and acute infection in mice. The reduced ability of an *S. aureus srtA* deletion mutant to infect the host was also demonstrated in several animal models (Weiss et al., 2004). SrtA activity was shown to promote *S. aureus* survival inside macrophages following phagocytosis, as *srtA* deletion mutants were found to be more susceptible to killing by macrophages (Kubica et al., 2008) and to promote biofilm formation as loss of SrtA in clinical isolates significantly reduced their ability to form biofilms (O'Neill et al., 2008). Similarly, the link between sortase activity and pathogenicity has been confirmed for others Gram-positive species such as *L. monocytogenes* (Bierne et al., 2002), *S. pneumonia* (Kharat and Tomasz, 2003), *Enterococcus faecalis* (Kemp et al., 2007) *and Streptococcus suis* (Vanier et al., 2008). All together, these studies have highlighted the potential of sortase inhibition for the treatment of Gram-positive related infectious diseases and, for this reason, the search of molecules that could inhibit sortase activity became an intensive area of research. The screening of natural or synthetic compound libraries as well as molecular modeling, pharmacophore hypotheses, 3D-QSAR models and virtual screening approaches allowed the identification and the characterization of a consistent number of reversible and irreversible SaSrtA inhibitors (Cascioferro et al., 2015). However, most of these compounds showed activity in the high micromolar range and because of this low potency, none of them has been developed as drug.

## 1.5 *In vitro* activity and specificity of sortases

Soon after its discovery, the proteolytic activity of SaSrtA towards peptides bearing the LPXTG motif and its transpeptidation reaction in presence of the nucleophile NH2-Gly3 were demonstrated by Ton-That and colleagues in two subsequent studies (Ton-That et al., 2000, 1999). In these studies, the authors also showed that SaSrtA cleaves the LPXTG motif between the threonine and the glycine and that in the absence of a nucleophile, the thioacyl intermediate is hydrolyzed, resulting in the cleavage of the LPETG motif without the formation of a new peptide bond. Later, beside determining the SaSrtA 3D structure, Ilangovan and colleagues found that the SaSrtA activity was increased by 8-fold in presence of calcium ions (Ilangovan et al., 2001). To determine the kinetic parameters of SaSrtA, FRET-based assays, that make use of sorting signal peptides containing donor and quencher fluorophores at each end, were initially employed (Ilangovan et al., 2001; Ton-That et al., 2000). However, limitations associated with the fluorescence inner filter effect quenching at high substrate concentration led to the development of HPLC-based methods enabling more accurate measurements (Frankel et al., 2005; Ryan G Kruger et al., 2004). Although published values for SaSrtA show a wide variation depending on the substrate sequence used, according to Frankel and colleagues transpeptidation occurs with a $k_{cat} = 0.28 \pm 0.02\ s^{-1}$, and $K_m$ values for the LPXTG and the Gly5 nucleophile of $7.33 \pm 1.01$ mM and $196 \pm 64$ μM, respectively. In the absence of the nucleophile SaSrtA works as a protease that hydrolyze the sorting motif with a $k_{cat} = 0.086 \pm 0.015\ s^{-1}$ (Frankel et al., 2005).

Since the characterization of SaSrtA, the *in vitro* enzymatic activity of several other sortases has been investigated. However, none of them has shown to be as active as SaSrtA which catalyzes transpeptidation ~20–500-fold faster than other characterized sortases (Jacobitz et al., 2017).

Due to the low reaction rate and long incubation time required for reaction product analysis, sequence specificities of most sortases have been barely determined. Apart from SaSrtA, for which the substrate specificity was experimentally determined in detail, (Ryan G. Kruger et al., 2004) recognition sequences of other sortases are mainly predicted by bioinformatics means.

Moreover, as the composition of the peptidoglycan cell wall differs from strain to strain, sortases from different species are expected to have a different specificity with respect to the nucleophile substrate that resolve the thioacyl intermediate. For instance, sortase A from *Streptococcus pyogenes* (SpSrtA) was shown to accept dialanine as nucleophile, the simplest form of cross-bridge subunits in the peptidoglycan of *S. pyogenes* (Kang et al., 2011), while sortases from Bacillus species, which were shown to attach proteins to the diaminopimelic acid cross-bridges in the cell wall (Marraffini and Schneewind, 2007), are expected to accept this molecule *in vitro*.

## 1.6 Sortases as protein engineering tools

The demonstration that sortase A from *S. aureus* could break a peptide bond within the LPXTG motif and then reform a new bond with an incoming oligo-glycine nucleophile *in vitro* (Ton-That et al., 2000) paved the way for the development of sortases as valuable tools for protein engineering. The transpeptidation reaction catalyzed by sortases, also referred to as "sortagging" (Popp et al., 2007), has attracted increasing attention and has been exploited to site-specifically link fluorescent dyes, carbohydrates and other moieties to protein substrates and to the surface of cells (Antos et al., 2017, 2016). Sortase-mediated transpeptidation reactions have also been used for protein-protein ligation (Levary et al., 2011), protein immobilization on solid supports (Chan et al., 2007; Raeeszadeh-Sarmazdeh et al., 2015) and peptide and protein cyclization (Antos et al., 2009b; Zhang et al., 2015).

The majority of sortagging applications use sortases to modify proteins of interest either at the C or at the N-terminus. For C-terminal labeling target proteins carrying the LPXTG motif at their C-terminal are reacted with oligo-glycine-modified probes in presence of the sortase enzyme. Conversely, for N-terminal labeling, target proteins contain at least one glycine residue at the N-terminus and are reacted with molecular probes modified with the LPXTG motif. (**Figure 1.6)**.

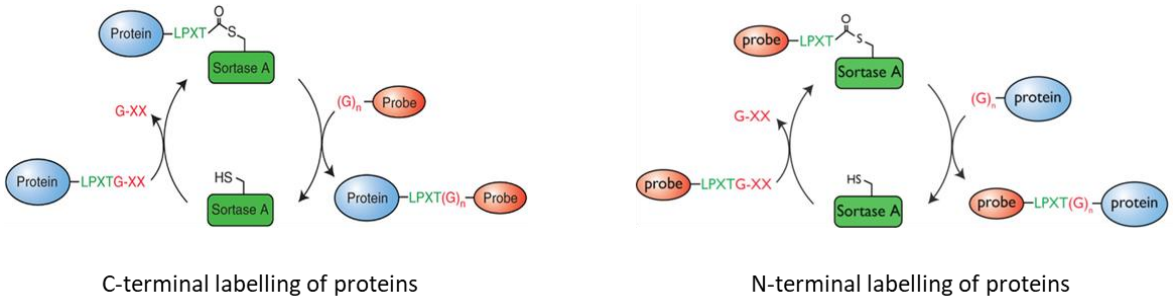


**Figure 1.6**. Schematic representation of protein labeling at the C-terminus (*left*) and at the N-terminus (*right*) using sortases. Reproduced with permission from Guimaraes *et al*. 2013 an Theile *et al*. 2013.

Site-specific conjugation of molecules has also been demonstrated to internal lysine residues of proteins by exploiting the non-canonical isopeptide ligation of SaSrtA (Bellucci et al., 2015). By using SaSrtA in combination with sortase A from *S. pyogenes* (SpSrtA) that recognizes and cleaves the LPXTA motif and accepts alanine-based nucleophiles, Ploegh and co-workers developed a strategy for the biorthogonal conjugation of two different probes to a single protein (Antos et al., 2009a).

Sortase-mediated transpeptidation proceeds site-specifically, under mild conditions and in a single step and overcomes some of the limitations associated with conventional chemical conjugation methods. For

instance, sortases have been successfully used for the site-specific conjugation of drugs to antibodies to produce antibody-drug conjugates (ADCs), a new class of biopharmaceutical drugs designed for the targeted treatment of cancer. Unlike chemical conjugation methods, the use of sortase enzymes allowed to control precisely the conjugation site and the conjugation ratio of toxins to antibodies. Sortases enabled the production of homogeneous preparations of ADCs which displayed *in vitro* cell killing activities indistinguishable from conjugates obtained through chemical conjugation methods (Beerli et al., 2015; Stefan et al., 2017).

## 1.7 Optimizing SaSrtA performance

Although the biotechnology community soon recognized the potential of the sortase-mediated transpeptidation reaction, the widespread use of sortases showed some notable limitations. The intrinsic poor enzymatic efficiency of wild type SaSrtA requires equimolar concentration of enzyme and substrate and long reaction time to achieve sufficient conjugation yields limiting its use to small-scale bioconjugates synthesis. A second limitation concerns the narrow substrate scope of SaSrtA that restricts sortagging to substrates naturally containing the LPXTG sequence or those engineered to display this motif. Still, the strong $Ca^{2+}$ dependency of SaSrtA prevents its use in low $Ca^{2+}$ concentrations conditions like in the cytoplasm of living cells or in presence of $Ca^{2+}$-chelating compounds, such as phosphate, carbonate, and ethylenediaminetetraacetic acid (EDTA).

The use of SaSrtA as a valuable tool for site-specific protein modification gained significance after the development, by directed evolution, of an enhanced version of SaSrtA. By integrating yeast display, sortase-mediated bioconjugation, and fluorescence-activated cell sorting (FACS), Liu and co-workers isolated an enhanced SaSrtA pentamutant variant (eSaSrtA) showing a 140-fold increase in activity as compared to the wild type counterpart (Irwin Chen et al., 2011). This work showed for the first time the potential of directed evolution to increase the enzymatic activity of a sortase enzyme and led to the development of additional directed evolution strategies to further improve the catalytic activity or to alter the sequence specificity of SaSrtA. Using a fluorescence resonance energy transfer (FRET)-based screening assay, Chen and co-workers identified additional beneficial mutations that resulted in a 3-fold improvement in catalytic efficiency over the pentamutant (Chen et al., 2016). Similarly, using a directed evolution approach based on a DHFR protein complementation assay, Suliman and colleagues identified SaSrtA variants with increased catalytic efficiencies (Suliman et al., 2017). More recently, a SaSrtA variant displaying improved catalytic activity and increased resistance towards the organic co-solvent DMSO was isolated (Zou et al., 2018).

The first evidence that sortase specificity could be altered originated from a domain swapping experiment in which the β6-β7 loop in SaSrtA was replaced by the homologous binding loop from SaSrtB (Bentley et al., 2007). Although at the expense of the catalytic activity, the resulting chimeric enzyme showed altered specificity in hydrolysis reactions, preferring substrates containing NPQTN over the LPETG motif. However, this variant was unable to perform transpeptidation. By randomizing the amino acid sequence of the β6-β7 loop and by using a directed evolution platform based on a phage display system, Schwarzer and co-workers were able to isolate a SaSrtA variant with a promiscuous specificity at the first residue of the sorting signal (Piotukh et al., 2011a). Some years later, the yeast display assay, used to improve the catalytic properties of the wild type SaSrtA, was applied to reprogram the sequence specificity of eSaSrtA resulting in the isolation of two orthogonal SaSrtA variants recognizing either LPXSG or LAXTG with minimal loss of activity relative to eSaSrtA (Dorr et al., 2014). More recently, the above

mentioned phage display system allowed to identify SaSrtA mutants that accept APXTG and FPXTG motifs but with a catalytic activity similar to the wild-type enzyme (Schmohl et al., 2017).

In addition to protein engineering, a complementary approach to broaden substrate scope of sortases relies on exploiting sortase homologs that are characterized of different substrate specificity. To date, apart from above mentioned sortase A from *S. pyogenes*, only few others SaSrtA homologs have been characterized that recognize sorting motifs different than LPXTG (Matsumoto et al., 2012; Nikghalb et al., 2018; Schmohl et al., 2017). Nevertheless, their use still remains hampered by the very low catalytic activity.

To allow sortase-mediated conjugation in living systems or at low calcium concentration, calcium-independent SaSrtA variants were also developed. By introducing mutations at residues of the calcium binding pocket Glu105 and Glu108, to mimic the calcium-independent equivalent sortases from *S. pyogenes* and *B. anthracis*, Nagamune and co-workers obtained a calcium-independent SaSrtA which, however, suffered from reduced catalytic activity (Hirakawa et al., 2012). By combining these two mutations with the beneficial mutation previously identified (Irwin Chen et al., 2011), Guimaraes and co-workers developed a heptamutant SaSrtA that demonstrated high catalytic efficiency in the absence of $Ca^{2+}$ (Wuethrich et al., 2014). Using a similar approach, other groups have also developed calcium-independent variants of SaSrtA and demonstrated their efficacy in various applications (Glasgow et al., 2016; Hirakawa et al., 2015; Jeong et al., 2017; Witte et al., 2015). Moreover, a calcium-independent SaSrtA variant with twelve mutations, characterized of slightly higher activity relative to the wild type SaSrtA in presence of calcium, was recently identified by a directed evolution strategy based on *in vitro* compartmentalization (IVC) (Gianella et al., 2016).

## 1.8 Directed evolution of sortases within hydrogel microcompartments

In the last years, several efforts have been made to improve the activity and to alter the specificity of sortase enzyme through a variety of directed evolution strategies. However, apart from SaSrtA, *in vitro* evolution of other sortase enzymes have not yet been reported.

Although the yeast surface display assay developed by Liu and co-workers was successfully applied for directed evolution of SaSrtA (Irwin Chen et al., 2011), the relative low number of enzyme molecules displayed on the cell surface (up to 100.000) might be insufficient to generate a readily detectable output signal when sortases with lower catalytic activity than SaSrtA are assayed. In addition, the single turnover nature of the yeast display system does not allow for output signal amplification thereby limiting the sensitivity of the assay and, consequently, the capability to detect and evolve poorly active sortases.

To improve the assay sensitivity and achieve a downward extension of the dynamic range of the screening system, one possibility is to increase the amount of the enzyme assayed during the screening procedure. If microtiter plate-based screening assays are employed, this can be easily achieved by expressing the protein of interest in the cytoplasm of proliferating cells in liquid cultures and by performing the enzymatic reaction in cell lysates. However, screening platforms that rely on the use of microtiter plates require a significant investment in terms of money, time, and space and although advancements have been made, the throughput of these methods is typically limited to $10^3$–$10^4$ variants per screen.

A more powerful method, that enable selection of enzymes for multiple-turnover at high-throughput, relies on the use of artificial microcompartments. Compared to robotic microtiter plate-based systems, directed evolution platforms that rely on microcompartments allow the screening of libraries with a 1.000 fold-increase in speed and 1-million-fold reduction in volume (Agresti et al., 2010). Compartmentalization into artificial microcompartments enables the linkage of the genotype (the nucleic acid sequence that encodes the catalysts) and the phenotype (the optical readout that originates from catalysis), an essential feature of any directed evolution strategy.

The potential of miniaturized reaction within artificial compartments for directed evolution of catalysts was first demonstrated by Tawfik and Griffiths who introduced the term "*in vitro* compartmentalization*"* (IVC) (Tawfik and Griffiths, 1998). In IVC, members of a library are spatially separated into water-in-oil emulsion droplets with volumes as small as a femtoliter, where ach droplet acts as an independent microreactor. Typically, protein catalysts produced by cells or *in vitro* translation are co-compartmentalized with a fluorogenic substrate whose conversion and specific retention allow the faithful analysis and selection of catalysts with improved functional properties. Directed evolution campaigns that rely on the use of bulk water-in-oil emulsions were initially developed and applied for the evolution of DNA polymerases (Ghadessy et al., 2001), β-galactosidase (Mastrobattista et al., 2005) or thiolactonases (Aharoni et al., 2005). However, the polydispersity of these emulsions made it difficult to carry out quantitative assays and to control single cell or individual DNA molecule compartmentalization. To overcome this limitations microfluidics-based technologies, that allow to generate emulsion droplets with uniform size, were implemented and incorporated into *in vitro* evolution assays to screen for peroxidase, arylsulfatase

and cellulase activities (Agresti et al., 2010; Kintses et al., 2012; Ostafe et al., 2014). A microfluidic device was employed by Hollfelder and co-workers to screen for phosphotriesterase activity from single cell lysates compartmentalized within emulsion droplets containing agarose and alginate (Fischlechner et al., 2014). The stepwise deposition of the polymers poly-allylamine hydrochloride (PAH) and poly-styrene sulfonate (PSS) (known as layer-by-layer assembly) on the surface of the droplets, yielded robust microspheres that were suitable for fluorescence-activated cell sorting (FACS) and that were characterized of a size-selective shell. Unlike emulsion droplets, the semipermeable nature of the shell enables gel-shell beads to exchange buffer or small exogenous molecules facilitating for instance the execution of multistep reactions or the execution of reactions that require external substrate supply.

Although directed evolution platforms using microdroplets have been integrated with different protein expression systems like *in vitro* transcription and translation (Fallah-Araghi et al., 2012), cell display (Agresti et al., 2010; Irwin Chen et al., 2011), cell secretion (Beneyton et al., 2017) and cell lysis (Kintses et al., 2012), screening procedures based on cells typically involve the compartmentalization and the analysis of a single cell. To date, only few examples of cell proliferation within emulsion droplets are reported in literature (Beneyton et al., 2014; Wang et al., 2014). Although the low solubility of oxygen in the oil phase of the emulsion droplets to support aerobic cell growth can be overcome by the use of fluorinated oils, proliferation of single cells within emulsion droplets rely on the limited amount of growth medium contained in the aqueous phase of the droplet that prevents high cell density cultivations.

An alternative strategy to encapsulate and cultivate single cells without limitations of oxygen or nutrients supply rely on the use of hydrogel microdroplets. Hydrogels are three-dimensional networks of hydrophilic polymer in which water is the dispersion medium. Due to their many advantageous features, hydrogels have attracted increased attention in the scientific community and have been used for many biological and biomedical applications including drug delivery, single molecule and cell analysis and tissue engineering (Ahmed, 2015; Peppas et al., 2006). Among the polymers used to prepare hydrogels, alginate has received much attention in literature and has been widely used for cell encapsulation (Goh et al., 2012; Rathore et al., 2013). Alginate is a naturally occurring anionic polymer isolated from brown algae that enables the formation of hydrogels in the presence of divalent cations like $Ca^{2+}$. The porosity of the alginate gel allows the diffusion of nutrients to support cell growth and reagents to perform reactions but prevents the diffusion of cells or colonies that remain immobilized within the alginate hydrogel matrix.

Cell encapsulation using alginate can be carried out under very mild conditions and is therefore suitable for cellular screening applications that require single cells surviving and proliferating. In addition, the mechanical strength of alginate hydrogels enables the accumulation of a large number of cells without affecting hydrogels stability. To date, several technologies have been developed that allow to encapsulate single cells within uniform alginate microspheres at high-throughput (Leong et al., 2016) and, depending on the particle size, clone processing technologies such as FACS (fluorescence activated cell sorter) or COPAS (complex object parametric analysis and sorting) have been used for particles analysis and sorting.

# 2 Aim of the work

Over the last decades, there has been an increasing demand for technologies that allow the specific incorporation of novel functionalities in proteins useful for a wide range of applications.

While early methods of protein modification relying on the reactivity of either lysine, cysteine or other residues on the target protein still have a widespread utility, the development of chemoenzymatic technologies for the site-specific protein modification represented a breakthrough in this field as allow to overcome limitations associated with conventional chemical ligation methods (Rabuka, 2010; Rashidian et al., 2013)

Sortases are a class of enzymes that are responsible for the covalent attachment of secreted proteins to the cell wall of Gram-positive bacteria. Over recent years, the transpeptidation reaction catalyzed by sortases, and in particular by sortase A from *S. aureus* (SaSrtA), has been extensively studied and it has seen an increasing use in the construction of novel protein derivatives as well as to perform demanding conjugation processes. Several strategies have been developed that allow optimizing sortase performance and to expand the range of substrates compatible with sortase-based approach. However, at present, the vast majority of the protocols rely on the use of the well-characterized sortase A from *S. aureus* (SaSrtA) and on evolved variants thereof.

Although evolved versions of SaSrtA have clearly shown enhanced reaction rates over the wild-type enzyme, recent studies have suggested that are not optimal for all applications. For instance, it was shown that the wild-type SaSrtA gives higher overall yields in the ligation of GFP to polystyrene beads as compared to evolved versions (Heck et al., 2014a). In another study, the pentamutant SaSrtA was seen more prone to higher levels of side products (Heck et al., 2014b). Efforts to broaden substrate scope has led to the directed evolution of few SaSrtA variants with altered specificity and to the identification of naturally occurring SaSrtA homologs that also prefer alternative sorting sequence over the canonical LPXTG motif. However, while these evolved sortases have yet to see widespread use, sortase A homologs suffer again of poor catalytic efficiency.

Due to their inherent low activity, sortases from classes other than class A are not currently used for sortagging applications and with the exception of SaSrtA other sortases have not been evolved. This can be likely attributed to the fact that directed evolution strategies developed so far are not sensitive enough to detect the activity of poorly active sortases.

In this context, the aim of this thesis was to identify novel sortase enzymes that would further expand the use of sortase-based ligation methods and to develop a directed evolution strategy compatible with sortases with low activity.

# 3 Results and discussion

## 3.1 Identification and characterization of novel sortase enzymes

### 3.1.1 Sampling sortase diversity

With the goal to expand the number of available sortase variants that can be used for protein engineering applications such as in biorthogonal conjugation of antibody-drug conjugates, the natural diversity of sortases was explored. Seven sortases from classes with a predicted recognition sequence different from the LPXTG of SaSrtA, including one member of the non-yet-characterized class F, were selected as target enzymes for *in vitro* transpeptidation activity analysis (**Table 3.1**). Depending on the specificity and the activity of the newly identified sortases, *in vitro* evolution to improve their activity should be performed. Sortase B and sortase D1 from *Bacillus anthracis* (BaSrtB and BaSrtD respectively) with putative recognition sequences NPXTG and LPXTA respectively were chosen because their structure was determined and therefore expression of soluble enzyme was previously known. Two additional class D2 sortases, sortase D from *Clostridium perfringens* (CpSrtD) and sortase D from *Clostridium acetobutylicum* (CaSrtD) were chosen because in various clostridia, sortase-like proteins have been identified, but none of them was characterized until October 2014 (Leeuwen et al., 2014). The first of the two selected class E sortases, sortase E from *Streptomyces coelicolor* (ScSrtE2), is responsible in this organism for aerial hyphae development and has been shown to cleave LAXTG-containing peptides *in vitro* (Andrew Duong et al., 2012). The second selected class E enzyme (MkSrtE) is the single sortase-like protein found in the archaeon *Methanopyrus kandleri* and represents one of the few identified but not-yet-characterized sortases from non-Gram-positive bacteria. As *M. kandleri* is a hyperthermophile and a thriving halophile, the potential transpeptidation activity of MkSrtE at high temperature and high salt concentrations makes this enzyme very attractive as it would further expand the scope of sortase-mediated ligations. The class F sortase was selected from *Propionibacterium acnes (PaSrtF)* because in its genome a single sortase gene is annotated and because a previous study provided indirect evidence that a sortase is active in this organism (Lodes et al., 2006). Class C sortases were not taken into consideration because, similar to class A enzymes, members of this class recognize proteins with sorting signals that contain the consensus LPXTG (Comfort and Clubb, 2004).

### 3.1.2 Recombinant expression and purification

Prior to gene synthesis, amino acid sequences of target sortases were subjected to an *in silico* analysis with *Predict protein*, *Phobius*, *Signal P* and *TM pred* to delineate signal peptide sequences and to identify transmembrane regions. Genes encoding for the putative soluble domain were codon optimized for expression in *Escherichia coli*, custom-synthetized and subsequently cloned into an expression vector to yield proteins with a 3C protease cleavage site and a histidine tag at the C-terminus.
Following expression analysis in a small-scale test, recombinant target sortases were expressed in four liters' cultures and subsequently purified by metal affinity chromatography. An overview of selected sortases along with their purification results is given in **Table 3.1**.

**Table 3.1**: Overview of selected sortases and relative purification results; red letters in the sorting motif indicate positions differing from the SaSrtA motif LPXTG where the X in third position designates no preference for a specific amino acid sidechain.

| Name | RefSeq | Class | Organism | Full length protein (aa) | Predicted specificity | Structure | Recombinant protein (aa) | Yield (mg/L of culture) |
|---|---|---|---|---|---|---|---|---|
| *BaSrtB$_{\Delta 37}$* | NP_846988.1 | B | *B. anthracis* | 254 | NPXTG | Yes (2004) | 217 (38-254) | ~ 40 |
| *BaSrtD$_{\Delta 24}$* | NP_847260.1 | D1 | *B. anthracis* | 198 | LPXTA | Yes (2012) | 174 (25-198) | ~ 45 |
| *CpSrtD$_{\Delta 22}$* | WP_003458327.1 | D2 | *C. perfringens* | 187 | LPXTA | Yes (2015) | 165 (23-187) | ~ 60 |
| *CaSrtD$_{\Delta 23}$* | NP_346846.1 | D2 | *C. acetobutylicum* | 194 | LPXTA | No | 171 (24-194) | --- |
| *CaSrtD$_{\Delta 66}$* | | | | | | | 128 (67-194) | --- |
| *ScSrtE$_{\Delta 157}$* | NP_628038.1 | E | *S. coelicolor* | 352 | LAXTG | Yes (2016) | 195 (158-352) | --- |
| *ScSrtE$_{\Delta 193}$* | | | | | | | 159 (194-352) | --- |
| *MkSrtE$_{\Delta 24}$* | NP_613445.1 | E | *M. kandleri* | 162 | LAXTG | No | 138 (25-162) | --- |
| *PaSrtF$_{\Delta 34}$* | WP_002530979.1 | F | *P. acnes* | 217 | LPXTG | No | 183 (35-217) | ~ 5 |

Three of the selected sortases namely BaSrtB$_{\Delta 37}$, BaSrtD$_{\Delta 24}$ and CpSrtD$_{\Delta 22}$, showed good solubility and were purified with high yield (≥ 40 mg per liter of culture) and purity (> 95%) by using an identical purification strategy (**Figure 3.1**). By contrast, the remaining sortases exhibited very low solubility and could not be purified. In the attempt to improve their solubility, a series of solubility studies were carried out using different expression strains in combination with different expression conditions and several extraction buffers. Moreover, additional variants of CaSrtD$_{\Delta 23}$ and ScSrtE $_{\Delta 157}$ consisting of the conserved domain only, were constructed by removing the N-terminal linker segment that connects the catalytic domain to the putative transmembrane anchor (CaSrtD$_{\Delta 66}$ and ScSrtE$_{\Delta 193}$ respectively). Although under

certain conditions protein solubility was improved, $MkSrtE_{\Delta 66}$ and the two length variants of CaSrtD appeared quite unstable and were lost during the purification procedure (E. Calà and M. Castiglione master thesis). Unexpectedly, in contrast to two other studies, in which the purification and the crystallization of a four amino acid shorter variant at the N-terminus ($ScSrtE_{\Delta 161}$, residues $Thr^{162}$-$Ser^{352}$) were reported (Andrew Duong et al., 2012; Michele D. Kattke et al., 2016), in our hands $ScSrtE_{\Delta 157}$ (residues $Gln^{158}$-$Ser^{352}$) showed very low solubility and could not be isolated under similar conditions. Same results were observed with the shorter variant $ScSrtE_{\Delta 193}$.

Positive outcomes were instead obtained with $PaSrtF_{\Delta 34}$. In this case, increased ionic strength significantly improved the solubility of the enzyme that was isolated and subjected to preliminary activity analysis. Later on, having realized the potential of this sortase, the purification procedure of PaSrtF was further optimized. Total purification yield was improved by using a C-terminal twin streptavidin tag while satisfactory purity was achieved by performing, in addition to affinity chromatography, a step of ion exchange chromatography (**Figure 3.2**).

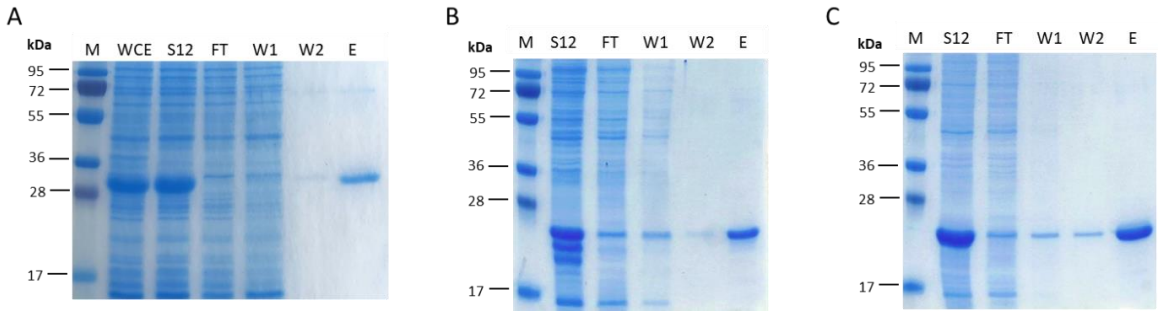


**Figure 3.1.** SDS-PAGE analysis of BaSrtB (**A**), BaSrtD (**B**) and CpSrtD (**C**) purification by metal affinity chromatography. M: Protein Ladder; WCE: whole cell extract; S12: Clarified cell lysate at 12,000*g*; FT: Flow through; W1: Column wash with 10 mM imidazole; W2: Column wash with 20 mM imidazole; E: Eluate

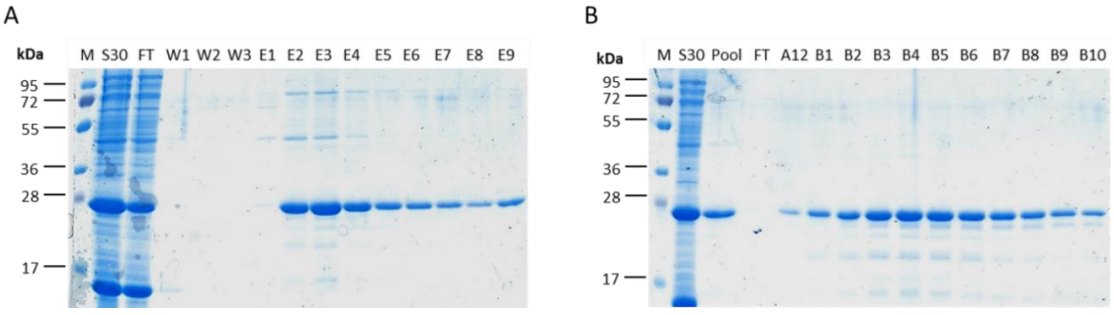


**Figure 3.2.** SDS-PAGE analysis of PaSrtF purification by affinity chromatography (**A**) followed by anion exchange chromatography (**B**) M: Protein Ladder; WCE: Whole cell extract; S12: Clarified cell lysate at 30,000*g*; FT: Flow through; W1-W3: Washes; E1-E9: Elution fractions; Pool: Pool of elution fractions E2-E9 from A; A12-B10: Elution fractions.

### 3.1.3 Activity and specificity analysis of BaSrtB, BaSrtD and CpSrtD

Part of the results discussed within this section are the cumulative work of the authors Chasper Puorger, Salvatore Di Girolamo and Georg Lipps and have been published in 2017 (Puorger et al., 2017). RP-HPLC, LC/MS and relative data analysis were performed by Dr. Chasper Puorger.

Following purification, the activity of BaSrtB, BaSrtD and CpSrtD was analyzed through a high performance liquid chromatography (HPLC)-based assay. As depicted in **figure 3.3 A**, FITC-labeled recognition peptides, specific for different classes of sortases, were individually mixed with a biotinylated GGGK nucleophile and the transpeptidation reaction started by the addition of each of the purified sortase enzyme. By determining with reverse phase-HPLC (RP-HPLC) the transpeptidation product yields of each reaction, the activity of target sortases was estimated in comparison to the evolved variant of the well-characterized sortase A from *S. aureus* (eSaSrtA) (**Table 3.2)**. Among the purified sortases, only BaSrtB, reacted with the class B specific peptide substrate DNPXTGDE, yielded sufficient amounts of transpeptidation product that allowed the subsequent determination of its sequence specificity. By contrast, only trace amount of products was detected when BaSrtD and CpSrtD were reacted with their putative recognition peptides making their sequence specificity determination impossible.

**Table 3.2.** Overview on the product yield for the different sortases as determined with RP-HPLC

| Substrate peptide / Sortase | **LPXTGE** (class A substrate) | **DNPXTGDE** (class B substrate) | **KLPXTASN** (class D substrate) | **ALAXTGS** (class E substrate) |
|---|---|---|---|---|
| **eSaSrtA** (class A, 5 µM[a]) | +++++ (1h[b]) | - | - | ++++ (24h[b]) |
| **BaSrtB** (class B, 50 µM[a]) | - | ++ (24h[b]) | +/- (24h[b]) | n. d. |
| **BaSrtD** (class D-1, 50 µM[a]) | - | - | + (24h[b]) | n. d. |
| **CpSrtD** (class D-2, 50 µM[a]) | - | - | - | +/- (24h[b]) |

+++++: >60 % product; ++++: 30 – 60 % product; +++: 10 – 30 % product; ++: 5 – 10 % product; +: < 5% product; +/-: trace amounts of product; -: no activity found; n. d.: not determined
[a] Enzyme concentrations used in the reactions; [b] Reaction time

Sequence specificity of BaSrtB was determined by using a newly developed liquid chromatography-mass spectrometry (LC-MS)-based method. The method relies on reacting mixtures of FITC-labeled recognition peptides with one randomized position at a time and the biotinylated GGGK nucleophile in presence of the designated sortase as described above. Following the reaction, biotinylated transpeptidation products are isolated from the reaction mixture with streptavidin-coated magnetic beads and analysed via LC-MS (**Figure 3.3**).

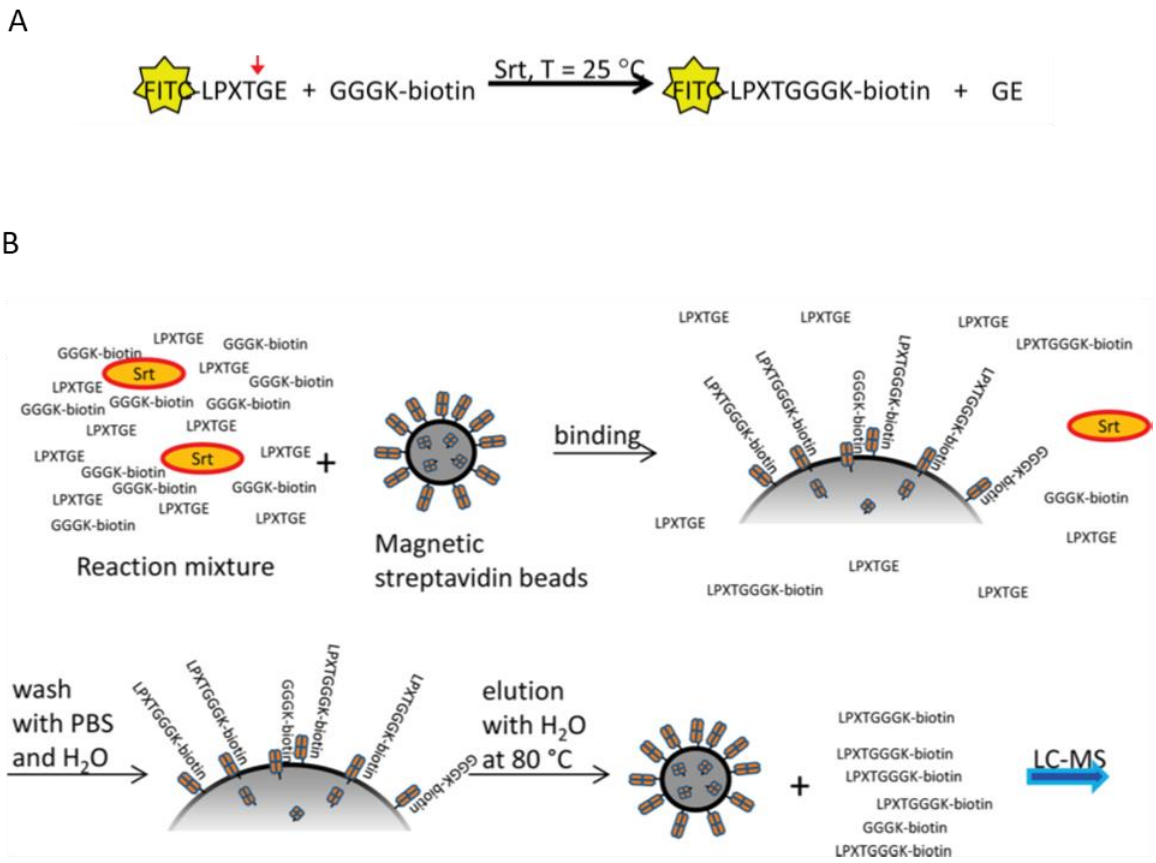


**Figure 3.3.** Overview of the method for sequence specificity determination using recognition peptide libraries. (**A**) *In vitro* transpeptidation reaction scheme for RP-HPLC analysis. The X in the substrate peptide designates one of the 20 amino acids (**B**) Depiction of the transpeptidation product isolation procedure used to obtain samples for LC-MS analysis (Puorger et al., 2017)

For method development, the highly active eSaSrtA was employed. The LC-MS analysis of the transpeptidation products obtained by reacting mixture of recognition peptides with individual variable positions and the biotinylated nucleophile in presence of eSaSrtA allowed to identify which sequences from the mixture are preferentially recognized by this sortase (**Figure 3.4 A**). The results were in good agreement with previously published data (I. Chen et al., 2011; Ryan G. Kruger et al., 2004) demonstrating the validity of the. Once established for the eSaSrtA the method was successfully applied to determine the sequence specificity of BaSrtB (which was found about $10^4$-fold less active than eSaSrtA) (**Figure 3.4 B**), and, as discussed below, of PaSrtF (**section 3.1.5**).

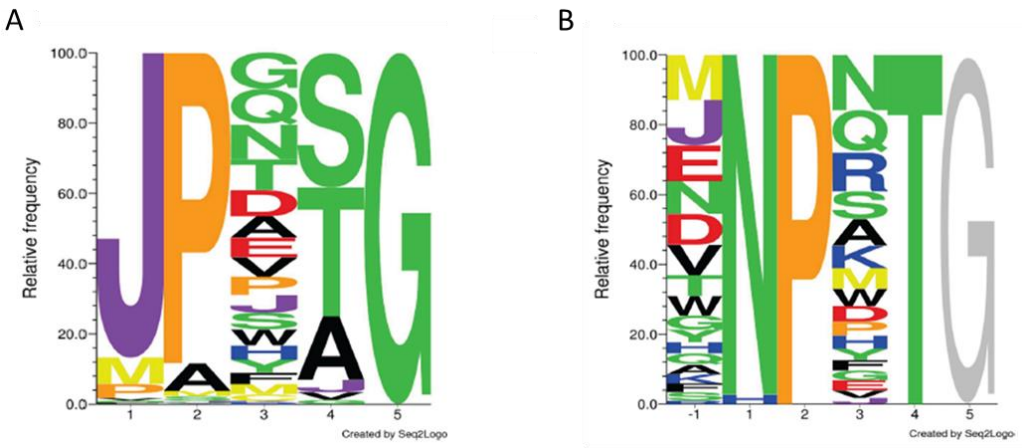


**Figure 3.4.** Logo representations of the sequence specificity of (**A**) eSaSrtA and (**B**) BaSrtB. Both sortases show no specificity at position 3, while the other positions are more stringent. Uncharged polar amino acids are colored green, basic amino acids blue, hydrophobic amino acids black, and acidic amino acids red; proline is colored orange, and cysteine and methionine are colored yellow. J (purple) represents isoleucine and leucine, which could not be distinguished in the LC−MS analysis because of their identical masses. Glycine at position 5 in the recognition sequence of BaSrtB is colored gray since it could not be determined directly because of the low rate of substrate turnover (Puorger et al., 2017).

Besides elucidating for the first time the detailed sequence specificity of a non-class A sortase, we showed that BaSrtB catalyzes a transpeptidation reaction *in vitro* and that it can accept oligo-glycine-modified molecules as nucleophile. For this reason, BaSrtB was selected as the first valuable target for directed evolution purposes. By contrast, due to the limited product formation, BaSrtD and CpSrtD were no further characterized nor considered as targets for directed evolution.

### *3.1.4* Structure determination of sortase D2 from *C. perfringens*

As the class D1 sortase from *B. anthracis* (BaSrtD) was the sole class D member for which the molecular structure was reported (Scott A. Robson et al., 2012), the structure determination of the sortase D2 from *C. perfringens* (CpSrtD) was attempted by the research group of Prof. Dr. Timm Maier (Biozentrum, University of Basel) using X-ray crystallography. The structure of the protein was successfully determined at 2.3 Å resolution. Unexpectedly, the crystal structure of CpSrtD was published by Suryadinata *et al.* (Suryadinata et al., 2015). Nevertheless, our protein model was very similar to the published CpSrtD model. As shown in **figure 3.5**, the only notable difference concerns the conformation of the β3-α4 loop (residues 106-116) that cause the different orientation of the conserved histidine residue (His109).

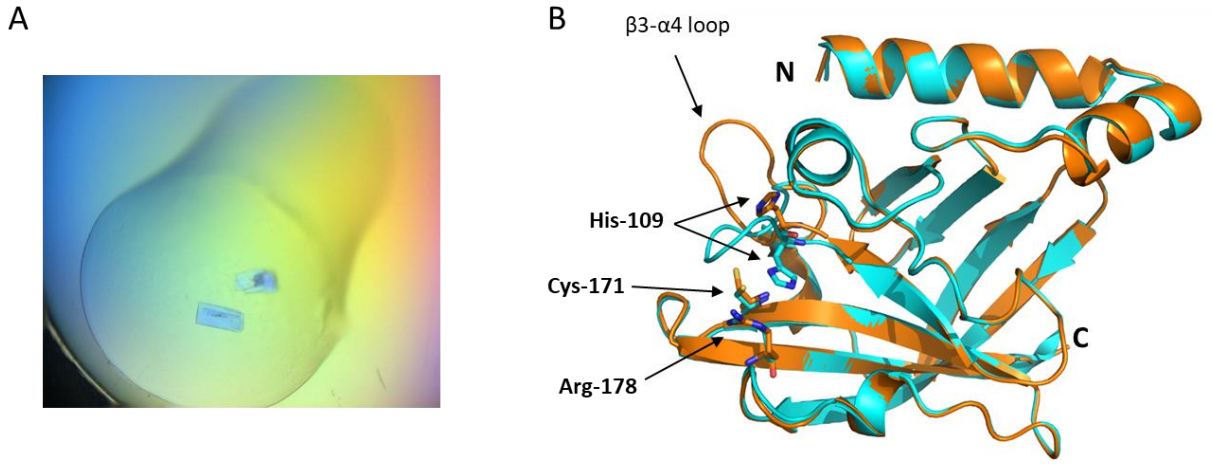


**Figure 3.5. (A)** CpSrtD protein crystals. **(B)** Superposition of the published *Cp*SrtD structure (blue; PDB entry 4d70) and the CpSrtD structural model as determined in this work (orange). The only notable difference concerns the conformation of the β3-α4 loop.

### 3.1.5 Characterization of sortase F from *Propionibacterium acnes*

The results discussed within this section are the cumulative work of the author Salvatore Di Girolamo, Chasper Puorger, Mara Castiglione, Maren Vogel, Rémy Gebleux, Manfred Briendl, Tamara Hell, Roger Beerli, Ulf Grawunder, Georg Lipps and have been published in 2019 (Di Girolamo et al., 2019).
RP-HPLC, LC/MS and relative data analysis were performed by Dr. Chasper Puorger.

While biochemical analysis and structures have been reported for at least one member of class A, B, C, D and E sortases, at present, class F enzymes remained to be studied.
Genome analysis of the completely sequenced type strain *P. acnes* KPA171202 (Brüggemann et al., 2004) revealed that, in this Gram-positive bacterium, only a single sortase gene is annotated. According to the conserved domain database of the NCBI, the sortase gene encodes for a sortase that belongs to the class F subfamily. Since a previous study provided indirect evidence that in *P. acnes* a sortase enzyme is active (Lodes et al., 2006) and since data from an RNA-sequencing experiment showed that the gene is expressed under normal growth conditions, an in-depth characterization of this sortase was performed.
The analysis of the amino acid sequence of PaSrtF with *SignalP* (Petersen et al., 2011) allowed to delineate a 24 amino acid long signal peptide suggesting that the sortase is, as expected, targeted to the secretory pathway. Unlike other sortases, PaSrtF lacks the hydrophobic region that should anchor the protein to the cell membrane. We suggest that, in this sortase, the signal peptide is not cleaved but the enzyme remains attached to the membrane by the hydrophobic core of the signal peptide. C-terminal to the signal peptide is a region expected to be unordered which may constitute a flexible linker that connects the conserved catalytic domain (residues 65-215) to the bacterial cell membrane. For recombinant protein production, the signal peptide and ten residues from this flexible linker were omitted. The resulting PaSrtF variant ($PaSrtF_{\Delta 34}$) was purified and subsequently subjected to biochemical characterization.
In order to identify the sorting motif preferred by PaSrtF a **gel-based conjugation assay** was set up. A panel of FITC-labeled peptides carrying sorting motifs recognized by different sortase classes were incubated with an N-terminally hexa-glycine-modified protein serving as nucleophile (Gly6-AlgQ2, see **section 3.2.3.1** for details) in presence of the purified PaSrtF. Following SDS-PAGE, the gel was scanned with a fluorescence scanner to verify the presence of fluorescent transpeptidation products. As can be seen in **figure 3.6**, only the peptide carrying the sortase A/C motif LPXTG was transferred to the protein serving as nucleophile demonstrating catalytic activity of PaSrtF towards the class A sorting motif.

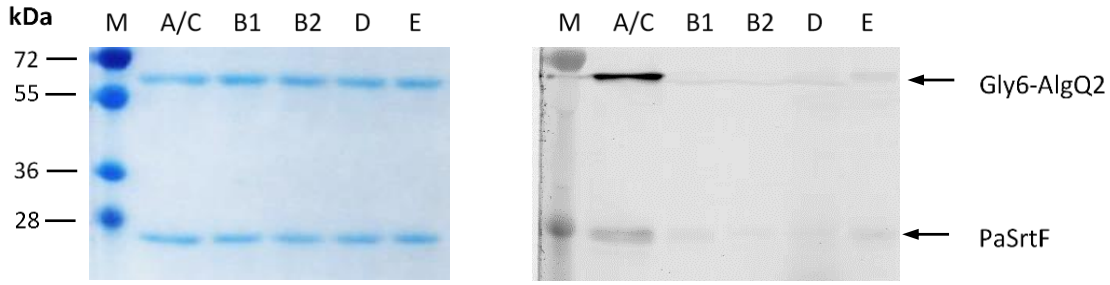


**Figure 3.6.** PaSrtF recognizes the LPXTG sorting motif for transpeptidation. Recombinant PaSrtF (10 µM) was mixed with 10 µM Gly6-AlgQ2 and 10 µM of each FITC-labeled recognition peptide and incubated for 6 hours at 25 °C in 50 mM sodium phosphate, pH 8.5 and 500 mM NaCl, 5 mM DTT. The formation of transpeptidation products was analyzed by SDS-PAGE gel fluorescence scanning (right panel). Equal protein loading was assessed by staining the gel with Coomassie (left panel). Lane M designates the protein ladder. The peptide substrates were from left to right LPXTGE (sortase A/C substrate), DNPNTGDE (sortase B substrate 1), ENPXTNAGT (sortase B substrate 2), KLPXTASN (sortase D substrate), and ALAXTGSE (sortase E substrate).

Next, by using FITC-LPXTGE peptides, the **gel-based conjugation assay** was employed to determine the pH optimum of PaSrtF reaction in the pH range from 4 to 12. As can be seen in **figure 3.7**, similar to SrtA from *S. aureus*, PaSrtF is most active at a slightly alkaline pH between 8 and 9. The outcome was in excellent agreement with the results obtained by analyzing initial rates of the reactions with RP-HPLC (**Figure 3.8 A**). Moreover, analysis of the product yield after 24 hours, showed highest product formation at slightly lower pH (between 7 and 8) probably due to the partial inactivation of PaSrtF at basic pH during prolonged incubation times (**Figure 3.8 B**).

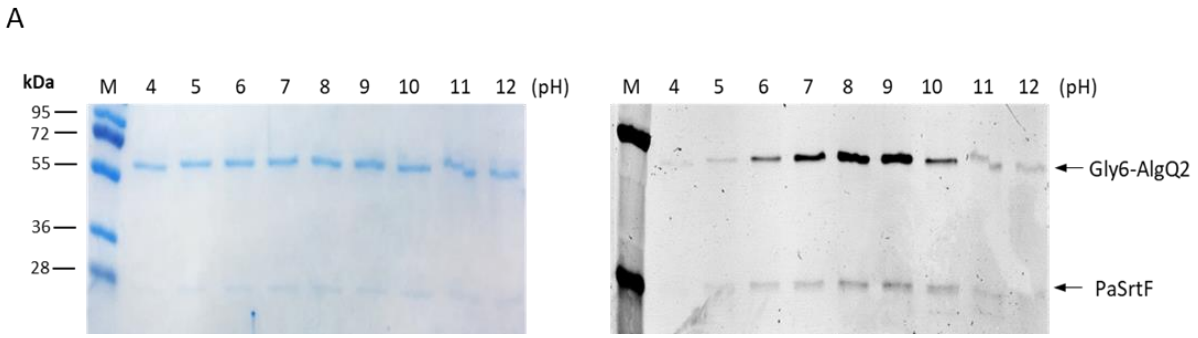


**Figure 3.7.** PaSrtF is most active between pH 8 and 9. The activity of PaSrtF was measured at different pH values in a 0.2 M boric acid/0.05 M citric acid/0.1 M phosphate buffer system (Carmody, 1961) supplemented with 500 mM NaCl. Reactions were carried out with 2.5 µM enzyme, 10 µM FITC-LPXTGE and 10 µM Gly6-AlgQ2 for 6 hours at 25 °C.

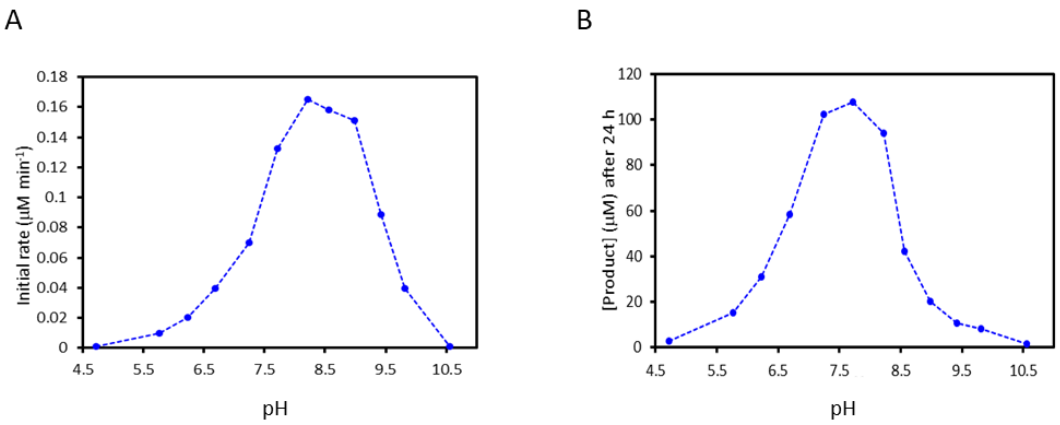


**Figure 3.8.** (**A)** Initial rates of transpeptidation assay carried out with 5 µM PaSrtF, 250 µM FITC-LPQTGE and 1 mM GGGK-biotin, analyzed with RP-HPLC. (**B**) Analysis of amounts of transpeptidation products after 24 hours.

Similarly, the **gel-based conjugation assay** served to evaluate the influence of the ionic strength on PaSrtF activity. Surprisingly, PaSrtF prefers high salt concentrations with the highest activity found between 0.5 and 1 M NaCl (**Figure 3.9**). Interestingly, at salt concentration higher than 1 M NaCl another nucleophile, possibly a degradation product of the Gly6-AlgQ2 protein, was preferentially labeled over the whole protein. Similar behavior was observed when the NaCl dependence of PaSrtF activity was analyzed with RP-HPLC. The outcome confirmed that PaSrtF remains active even at 3 M NaCl and that it less active at NaCl concentration below 500 mM. In addition, comparable product yields between 0.75 and 3 M NaCl after 24 hours, suggest that the enzyme is stabilized at high salt concentration during long reaction times (data not shown). Hence, the high salt tolerance of PaSrtF would potentially broaden the scope of sortagging approaches.

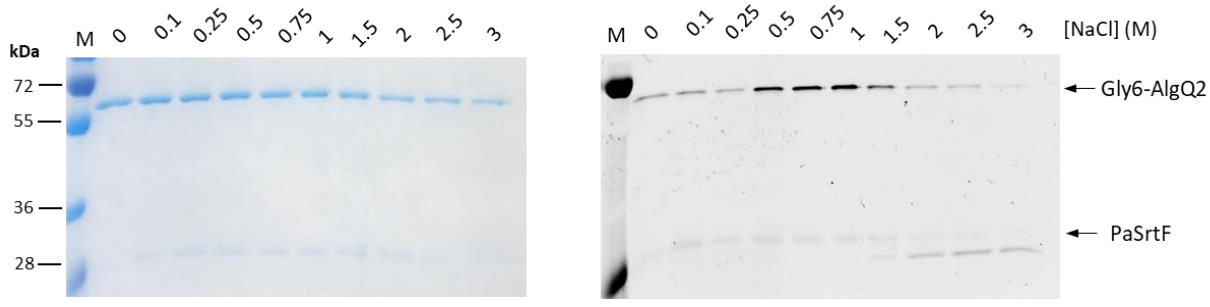


**Figure 3.9.** PaSrtF activity at different ionic strengths. PaSrtF shows highest activity between 0.5 and 1 M NaCl. The NaCl concentration was varied between 0 and 3 M in 50 mM sodium phosphate, pH 8.5, 5 mM DTT. The gel-based conjugation assay was carried out with 2.5 µM enzyme, 10 µM FITC-labeled recognition peptide and 10 µM Gly6-AlgQ2 after 6 hours incubation at 25 °C.

Previous studies have shown that SaSrtA is strongly activated by calcium ions (Ilangovan et al., 2001; Naik et al., 2006). More recently, the activity of CpSrtD was found enhanced in presence of magnesium (Suryadinata et al., 2015). At present, the above-mentioned enyzmes are the only two reported sortases whose activity is modulated by metal ions.

To evaluate whether metal ions have a stimulatory effect on PaSrtF activity, a number of bivalent cations such as $Zn^{2+}$, $Mg^{2+}$, $Ni^{2+}$, $Ca^{2+}$ and $Mn^{2+}$ were screened using a **FRET-based cleavage assay**. The assay makes use of a peptide carrying the LPXTG motif, labeled with the fluorophore-quencher pair EDANS-Dabcyl (*SrtA substrateII, Anaspec*). When the peptide is cleaved by the sortase, the fluorophore-quencher pair is broken up causing an increase in fluorescence that can be continuously monitored by using a fluorescence reader. As can be seen in **figure 3.10**, none of the screened metal ions stimulated PaSrtF activity compared to the "cation-free" reaction (reaction performed without additional bivalent ions) suggesting that PaSrtF activity is independent of bivalent ions. This, would enable the direct use of SrtF for *in vivo* and cell-based applications. Interestingly, as previously described also for CpSrtD (Suryadinata et al., 2015), PaSrtF is strongly inhibited by the presence of zinc ions.

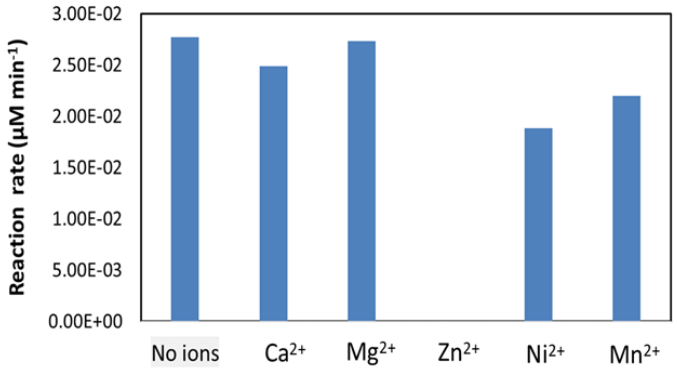


**Figure 3.10.** PaSrtF activity measured in presence of different metal bivalent cations (10 mM). Reaction rates were determined by measuring reactions of 5 µM PaSrtF with 20 µM of the quencher-fluorophore peptide and 2 mM Gly3 in a fluorescence spectrophotometer in 50 mM Tris-HCl, 500 mM NaCl, pH 8.5 at 25 °C for 1 hour.

To determine the optimal temperature at which PaSrtF achieves maximal transpeptidation activity, the **FRET-based cleavage assay** was performed at different temperatures. The results showed a broad temperature optimum around 25 °C with a significant decline of the activity above 40 °C (**Figure 3.11**)

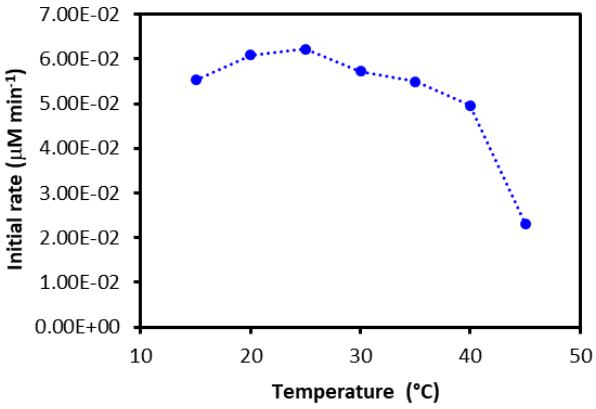


**Figure 3.11.** PaSrtF activity measured in the temperature range from 15 to 45 °C. Rates were determined by measuring reactions of 5 µM PaSrtF with 20 µM quencher-fluorophore peptide and 2 mM Gly3 in a thermostatized cuvette in a fluorescence spectrophotometer in 50 mM Tris-HCl, 500 mM NaCl, pH 8.5.

Next, the detailed sequence specificity of PaSrtF was determined by using the LC-MS-based method as described above for BaSrtB. As shown in **figure 3.12**, compared to eSaSrtA, PaSrtF is less strict on the amino acid residue at the first position but it has a clearer preference for proline at position 2 and for threonine at position 4. As for SaSrtA, PaSrtF has no preference at position 3 where all amino acids except Proline were found. For position 5 no product formation was observed with the corresponding peptide mixture. However, since peptides with a glycine at position 5 were used for investigation of all other positions, glycine is at least one of the most probable amino acids at this position.

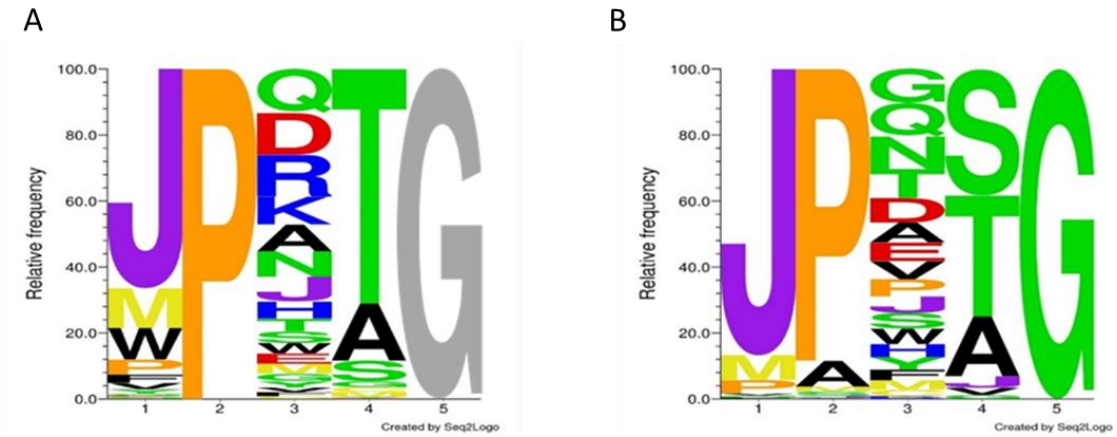


**Figure 3.12.** Comparison of the sortase specificity of PaSrtF (**A**) and eSaSrtA (**B**). The sortase specificity was investigated by incubating the sortases with peptide mixtures with one position variable at a time. Transpeptidation products were isolated and the identity of the variable amino acid at a given position was determined by LC-MS. The letter J stands for Leucine and Isoleucine, which are not distinguishable by mass.

Very important, determination of the Michealis-Menten kinetics parameters with RP-HPLC showed that $k_{cat}$ of PaSrtF (0.06 $min^{-1}$) is comparable to $k_{cat}$ of the wild type SaSrtA ($k_{cat}$ = 0.04 $min^{-1}$) making PaSrtF the first naturally occurring characterized sortase enzyme with an activity similar to the most thoroughly used wild type SaSrtA. Compared to the wild type SaSrtA, PaSrtF has a significantly lower $K_m$ value for the LPXTG-peptide (0.26 mM versus 7.6 mM) and a 10-fold higher $K_m$ value for the nucleophile (2.3 mM versus 0.14 mM) (**Figure 3.13**).

| | $k_{cat}$, $min^{-1}$ | $K_{m\ LPQTG}$, mM | $k_{cat}/K_{m\ LPQTG}$, $M^{-1}\ s^{-1}$ | $K_{m\ GGGK\text{-}biotin}$, mM |
|---|---|---|---|---|
| **PaSrtF** | 0.06 | 0.26 | 3.85 | 2.3 |
| **SaSrtA** | 0.04 | 7.6 | 0.088 | 0.14 |

**Figure 3.13.** Michaelis-Menten parameters determined for SrtF from *P. acnes* and for SrtA from *S. aureus.*

To investigate the utility of the newly identified PaSrtF for protein engineering, a site-specifically conjugated antibody-drug conjugate (ADC) was prepared by *NBE therapeutics AG* using a similar approach to the one previously described for eSaSrtA (Beerli et al., 2015; Stefan et al., 2017). Determination of the drug content by RP-HPLC revealed that PaSrtF is capable to generate highly homogeneous ADCs, which, in a cell-killing assay have shown similar potency and specificity to ADCs developed using eSaSrtA.
All together, these results make the newly identified PaSrtF a powerful alternative to the most frequently used SaSrtA for sortase-mediated ligations applications. Moreover, PaSrtF represented an ideal target for our directed evolution campaign.

### 3.1.6 Analysis of sortase F length-variants

Although PaSrtF$_{\Delta 34}$ was purified and characterized, purification of this variant was quite challenging because of the low protein solubility. With the goal to optimize and improve PaSrtF purification and understand whether the flexible linker that connects the conserved domain to the bacterial cell membrane is important for the enzymatic activity, two additional PaSrtF variants were analyzed: PaSrtF$_{\Delta 47}$ and PaSrtF$_{\Delta 60}$ obtained by further extending the deletion of the N-terminal region. A graphical representation of PaSrtF variants architecture is given in **figure 3.14**.

Similar to PaSrtF$_{\Delta N34}$, both SrtF$_{\Delta 47}$ and SrtF$_{\Delta 60}$ required high ionic strength (500 mM NaCl) for soluble extraction and were purified following the same protocol described for PaSrtF$_{\Delta N34}$.

After purification, a **gel-based conjugation assay** was performed to evaluate the activity of PaSrtF$_{\Delta N47}$ and PaSrtF$_{\Delta 60}$ in comparison to PaSrtF$_{\Delta 34}$. As shown in **figure 3.15**, while PaSrtF$_{\Delta 34}$ and PaSrtF$_{\Delta N47}$ displayed similar activities, PaSrtF$_{\Delta 60}$ appeared about 70 % then less active than PaSrtF$_{\Delta 34}$. Consistent results were obtained by determining the total product yields with RP-HPLC (data not shown).

Although further investigations are required, these preliminary results indicate that the conserved domain alone may be not sufficient to achieve efficient transpeptidation and that residues of the flexible linker may play a role on binding the substrate peptide.

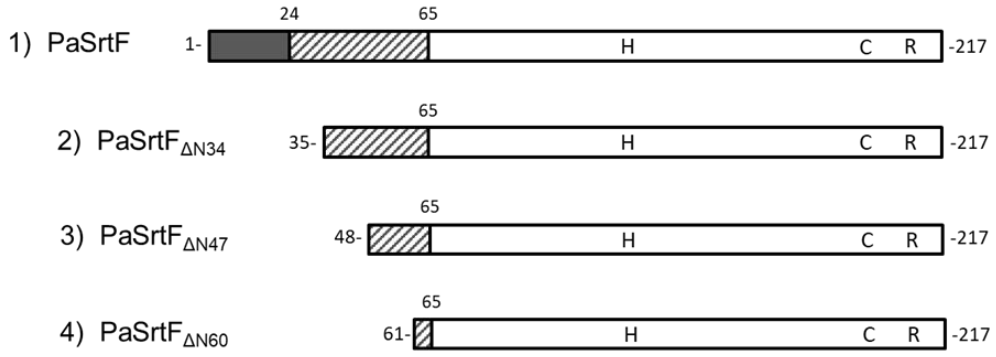


**Figure 3.14.** Graphical representation of the architecture of the full-length PaSrtF (1), PaSrtF$_{\Delta N34}$ (2), PaSrtF$_{\Delta N47}$ (3) and PaSrtF$_{\Delta N60}$ (4) showing the position of the conserved histidine (H124), cysteine (C195) and arginine (R208) residues within the conserved domain (residues 65-217). The N-terminal signal peptide and the flexible linker that connect the conserved domain to the bacterial cell membrane are depicted as a gray and striped box respectively.

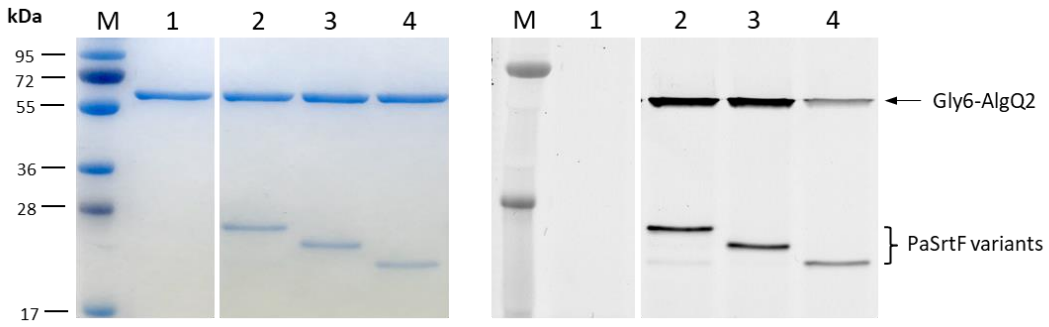


**Figure 3.15.** Gel-based conjugation assay of PaSrtF length-variants. Recombinant PaSrtF variants (2.5 µM) were mixed with 10 µM Gly6-AlgQ2 and 50 µM fluorescent peptide substrate and incubated for 3 hours at 25 °C in 50 mM sodium phosphate, pH 8.5 and 500 mM NaCl. The extent of the transpeptidation reaction was analyzed by SDS-PAGE gel fluorescence scanning (right panel) and quantified with *imageJ*. Equal protein loading was assessed by staining the gel with Coomassie (left panel). Lane M designates the protein ladder; Lane 1 negative control (No sortase); Lane 2: reaction with $PaSrtF_{\Delta 34}$; Lane 3: reaction with $PaSrtF_{\Delta 47}$; Lane 3: reaction with $PaSrtF_{\Delta 60}$;

### 3.1.7 Construction and analysis of a chimeric sortase

The development of a chimeric enzyme from two functionally related proteins has proved to be an effective strategy for improving or altering its activity and to gain valuable information on the structure-function relationship of the parent proteins. For instance, in a previous work, the construction of a chimeric sortase by domain swapping, allowed to get insights on how sortases enzymes discriminate between their substrates (Bentley et al., 2007). The replacement of the β6-β7 loop in sortase A from *S. aureus (*SaSrtA*)* with the corresponding loop from the sortase B from the same organism (SaSrtB) yielded a loop-swapped sortase A able to cleave NPQTN peptide substrates with a specificity profile change compared to SaSrtA by a factor of over 700,000. However, the chimeric enzyme was unable to perform transpeptidation onto the pentaglycine molecule used as nucleophile.

In this work, with the goal to alter the sequence specificity of the highly active eSaSrtA, a chimeric sortase was constructed and investigated. Driven by the structure similarity between class A and class D1 sortases (S. A. Robson et al., 2012), we set out to create a hybrid protein (eSrtA/D) that ideally combines the high activity of eSaSrtA with the sequence specificity of BaSrtD. To this end, the SCHEMA algorithm (Voigt et al., 2002) was employed to identify fragments of parental sortases whose recombination is less likely to disrupt the three-dimensional structure of the resulting chimeric enzyme. The algorithm takes into account the 3D structures of parental proteins and generate a SCHEMA disruption profile whose minima represent crossover sites that preserve the maximum number of interactions between residues. According to the SCHEMA disruption profile for recombination of SaSrtA and BaSrtB, preferred recombination would occur at alignment position 187 and 233 **(Figure 3.16 A)**. Recombination at position 187 produces a chimeric sortase that contains the N-terminal region of eSaSrtA for residues $Gln^{59}$-$Arg^{151}$, fused to the C-terminal region of BaSrtD for residues $Thr^{143}$- $Lys^{198}$ that include the β6-β7 loop ($His^{153}$- $Pro^{166}$) which is considered the main sequence specificity determinant (S. A. Robson et al., 2012). On the other hand, the chimeric sortase obtained by recombination at position 233 generates a chimeric enzyme that do not contains the β6-β7 loop but only the disordered β7-β8 loop which may rather play a role in binding the nucleophile (S. A. Robson et al., 2012) **(Figure 3.16 B)**. For this reason, only the first chimeric variant was investigated. Primary and secondary structures of recombinant chimeric eSrtA/D are depicted in **figure 3.16 C**.

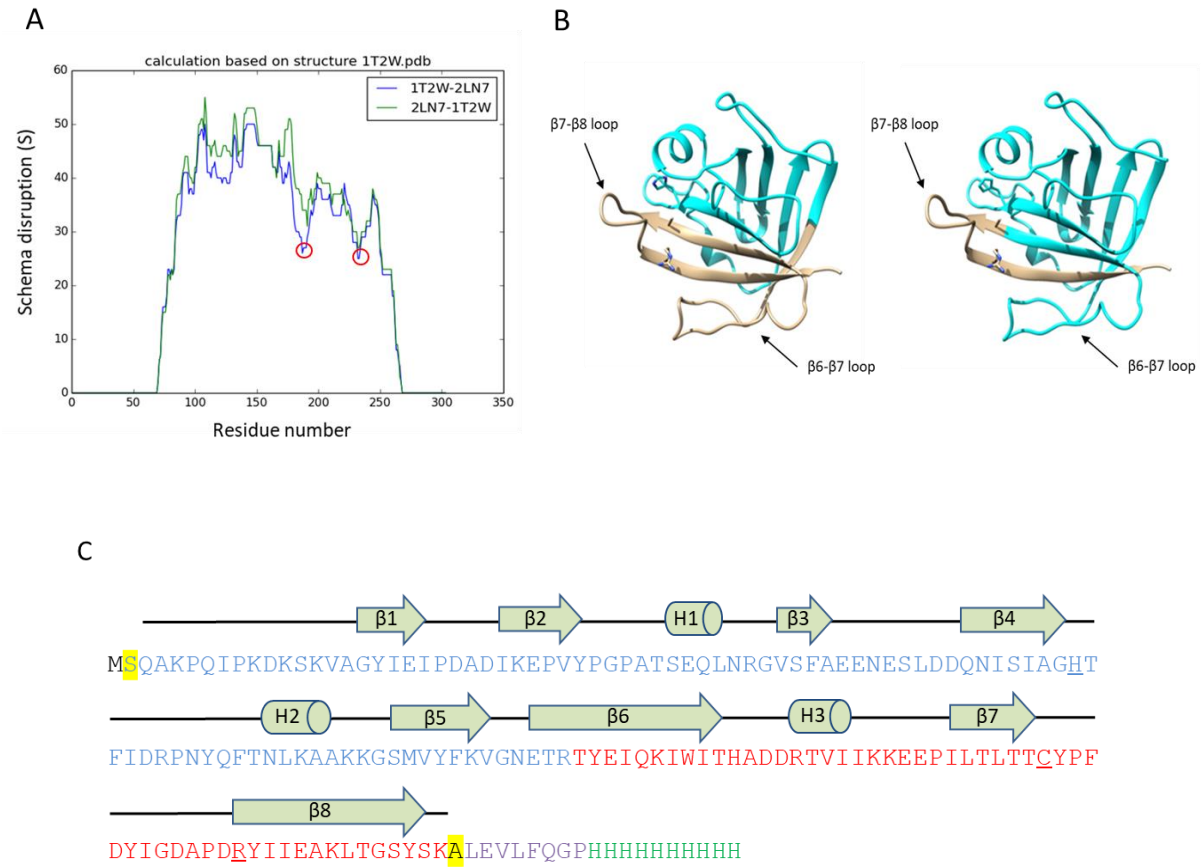


**Figure 3.16. (A**) SCHEMA disruption profile for recombination of sortase A from *S. aureus* (1T2W) and sortase D from *B. anthracis* (2LN7). Similar results are obtained when the order of proteins in the chimera is swapped (blue line and green line). Suitable recombination sites (corresponding to minima in the schema profile) are at alignment positions 187 and 233 (abscissa, red circles). (**B**) Structural model of chimeric enzymes obtained by recombination at position 187 (left) and 233 (right); Cyan: SaSrtA, Gold: BaSrtD. (**C**) Primary and secondary structures of recombinant chimeric eSrtA/D; In blue and red the eSaSrtA and BaSrtD primary sequences respectively. Conserved catalytic residues are underlined. Highlighted in yellow are the cloning scars; in violet the 3C protease cleavage site and in green the polyhystidine tag. Secondary structure elements are shown in *green* for β-strands (arrows) and helices (cylinders).

The DNA sequence encoding for the chimeric eSrtA/D, was codon optimized for expression in *Escherichia coli*, custom-synthetized and cloned into an expression vector to yield a protein with a 3C protease cleavage site and a histidine tag at the C-terminus. Although, at first, the chimeric enzyme appeared poorly soluble, a solubility study using different extraction buffers allowed to improve its solubility (**Figure 3.17 A**). Purification was performed by affinity chromatography (**Figure 3.17 B)**.

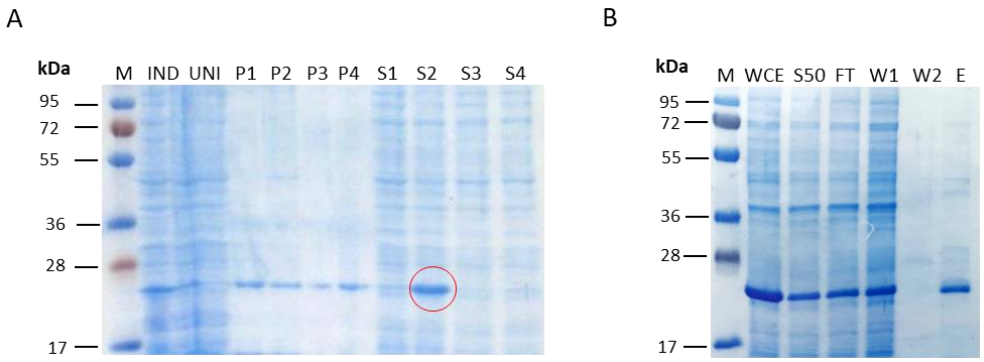


**Figure 3.17. (A)** SDS-PAGE analysis of insoluble (P) and soluble (S) fractions obtained by using different extraction buffers. Protein extraction in 50 mM Tris/HCl pH 7.5, 150 mM NaCl, 0.5 M Urea helped improving protein solubility (red circle). M: Protein Ladder, IND: Post-induction sample; UNI: Pre-induction sample; P1-P4: Insoluble fractions; S1-S4 soluble fractions. Extraction buffers were: 1) 20 mM Tris, 150 mM NaCl, 0.2% NP40 pH 7.5; 2) 50 mM Tris, 150 mM NaCl, 0.5 M Urea, pH 7.5; 3) 50 mM Tris, 2 M NaCl, pH 7.5; 4) 50 mM Tris, 150 mM NaCl, pH 7.5. **(B)** SDS-PAGE analysis of fractions from chimeric eSrtA/BaSrtD purification. M: Protein Ladder; WCE: Whole cell extract; S12: Clarified cell lysate at 50,000*g*; FT: Flow through; W1: Column wash with 10 mM imidazole; W2: Column wash with 20 mM imidazole: E: Eluate

First, to assess whether the chimeric eSrtA/D was active and showed specificity towards class D recognition substrate peptides, a **gel-based conjugation assay** was performed. The purified enzyme was incubated with the FITC-labeled peptide carrying the class D sorting motif LPXTA (KLPXTASN) in presence of the N-terminally hexa-glycine-modified protein Gly6-AlgQ2 as nucleophile (see **section 3.2.3.1** for details). As control, reactions were performed with parental enzymes eSaSrtA and BaSrtD. Unfortunately, the SDS-PAGE and gel fluorescence scanning revealed that the chimeric eSrtA/D is unable to transfer the fluorescent peptide to Gly6-AlgQ2 suggesting that the enzyme lost its transpeptidation activity (**Figure 3.18**). Next, to confirm these results and evaluate whether the chimeric eSrtA/D retained the ability to cleave the recognition peptide substrate, the formation of both cleavage and transpeptidation products was analyzed with RP-HPLC. In this case, the fluorescent peptide substrate specific for SaSrtA (FITC-LPETGE) was also tested. The HPLC analysis demonstrated the total lack of activity of the chimeric eSrtA/D (data not shown). The construction and analysis of chimeric enzymes was discontinued.

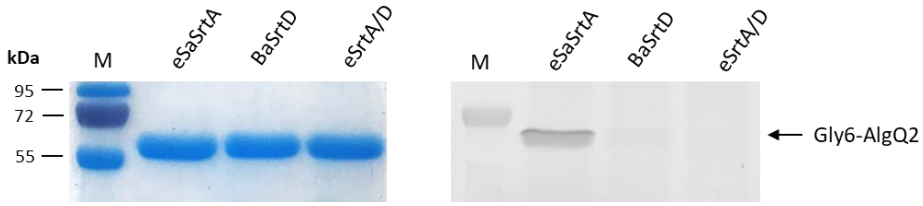


**Figure 3.18.** Gel-based conjugation assay of chimeric eSrtA/D; 10 µM chimeric sortase was mixed with 20 µM Gly6-AlgQ2 and 20 µM class D fluorescent peptide substrate (FITC-KLPNTASN) and incubated for 18 hours at 30 °C in 25 mM Tris/HCl pH 8.3, 150 mM NaCl, 10 mM $CaCl_2$. As control, reactions were performed with parental sortases: eSaSrtA (1 µM, 1 hour at 30 °C) and BaSrtD (10 µM, 18 hours, 30 °C). The formation of transpeptidation products was analyzed by SDS-PAGE gel fluorescence scanning (right panel). Equal protein loading was assessed by staining the gel with Coomassie (left panel). Lane M designates the protein ladder.

## 3.2 Establishment of a microreactor-based assay for directed evolution of sortases with low activity

With the goal to develop a directed evolution strategy compatible with sortases with low activity, the utility of a microreactor-based assay was investigated. The assay relies on the use of alginate-based microcompartments as miniature sized culture and reaction vessels suitable for high-throughput screening and sorting using the large particle flow cytometer COPAS (Complex Object Parametric Analyzer and Sorter). Compared to single-cell screening system, proliferation of cells within microcompartments, followed by cell lysis, enables a larger amount of enzyme to be assayed thereby increasing the likelihood to detect the activity of poorly active enzymes. Moreover, in comparison to traditional microtiter plate screens, the use of miniaturized cell lysate compartments in combination with COPAS provides higher throughput enabling a deeper exploration of an enzyme's sequence space in less time. Hence, microcompartments encapsulating microcolonies, here referred as microreactors, were developed and investigated as individual evolutionary units for the functional screening of sortases with enhanced activity.

As shown in **figure 3.19**, the original concept of the assay workflow consisted of different steps including cell encapsulation into polymer-based beads to spatially segregate clones carrying different enzyme sequences, cell growth, cell lysis, sortase-mediated conjugation reaction and eventually COPAS selection and genotype recovery.

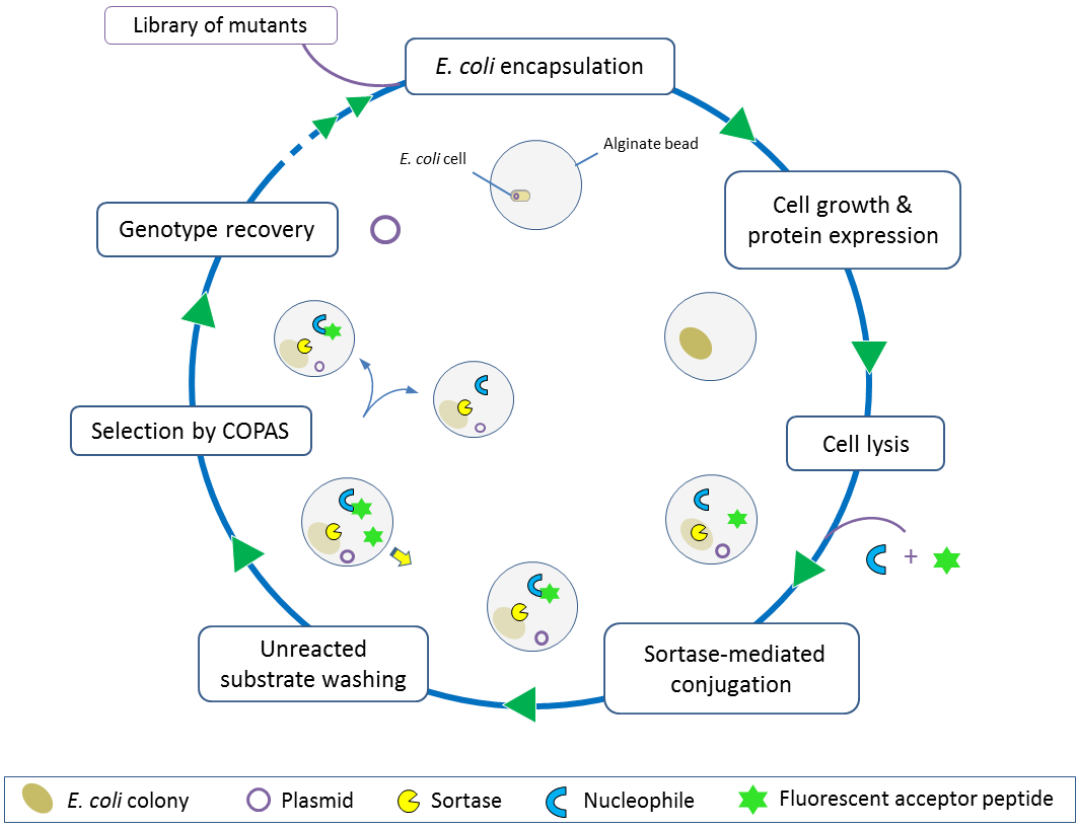

**Figure 3.19.** Workflow of the microreactor-based assay for directed evolution of sortases. Polymer-based microcompartments encapsulating *E. coli* colonies that originate from individually compartmentalized cells from a library of mutants, express a sortase variant that, upon cell lysis, is released from cells but retained inside microcompartments. Here, the sortase enzyme encounters and joins the two substrates: a fluorescent labeled recognition peptide, and an oligo-glycine-modified protein acting as nucleophile. After removal of the unreacted fluorescent substrate, retention of fluorescent transpeptidation products ensures that microcompartments harbouring the most active sortases are distinguished and isolated on the basis of fluorescence intensity using a large particle flow cytometer (COPAS). By dissolving the microcompartments, the genotype (plasmid) is recovered and if needed further randomized for a new round of evolution.

### 3.2.1 Alginate bead-based compartments as miniature sized culture vessels

Due to its unique characteristics, alginate is one of the most frequently used biomaterial in the field of cell microencapsulation. Encapsulation of living cells within alginate hydrogels can be carried out under mild and physiological conditions and is therefore suitable for applications in which cell viability is an essential requirement. In this work, three different types of alginate bead-based microcompartments were prepared and evaluated for the production of monoclonal microreactors suitable for the development of a high-throughput platform for directed evolution of low active sortases using COPAS:

1. *Gel-core alginate microbeads* (GCABs)
2. *Gel-core chitosan-coated alginate microcapsules* (GC-CAMs)
3. *Hollow-core chitosan-coated alginate microcapsules* (HC-CAMs)

*Gel-core alginate beads* (GCABs), or simply alginate beads, were prepared by extrusion dripping and external gelation as described in materials end methods. Briefly, a 3 % low viscosity alginate solution was prepared and dispersed into alginate microdroplets through the “Prilling by vibration” technique (also known as laminar-jet break-up). Alginate microdroplets, extruded through a 150 µm nozzle, were produced at a rate of 2480 Hz and ionotropically cross-linked into a gelling bath containing calcium to obtain *inhomogeneous* alginate beads, or calcium and sodium to obtain *homogeneous* alginate beads. Homogeneity refers to the distribution of the alginate concentration throughout the bead cross section and can be controlled by adjusting the concentration and ratio of gelling to non-gelling cations in the gelling solution. Production of *inhomogeneous* beads with a polymer concentration at the surface being ten times higher than the concentration in the center have been reported (Skjåk-Bræk et al., 1989). The different distribution of alginate in *inhomogeneous* and *homogeneous* alginate beads can be seen in **figure 3.20 A**.

Typically, as indicated by light microscopy and COPAS analysis (**Figure 3.20 A, B)**, uniform and monodispersed alginate beads with a diameter of about 280 and 360 µm were obtained for *inhomogeneous* and *homogenous* beads respectively. In both cases, the size distribution (calculated by COPAS as coefficient of variation) ranged between 5 and 10% **(Figure 3.20 B**). Multiplets formation was rarely detected.

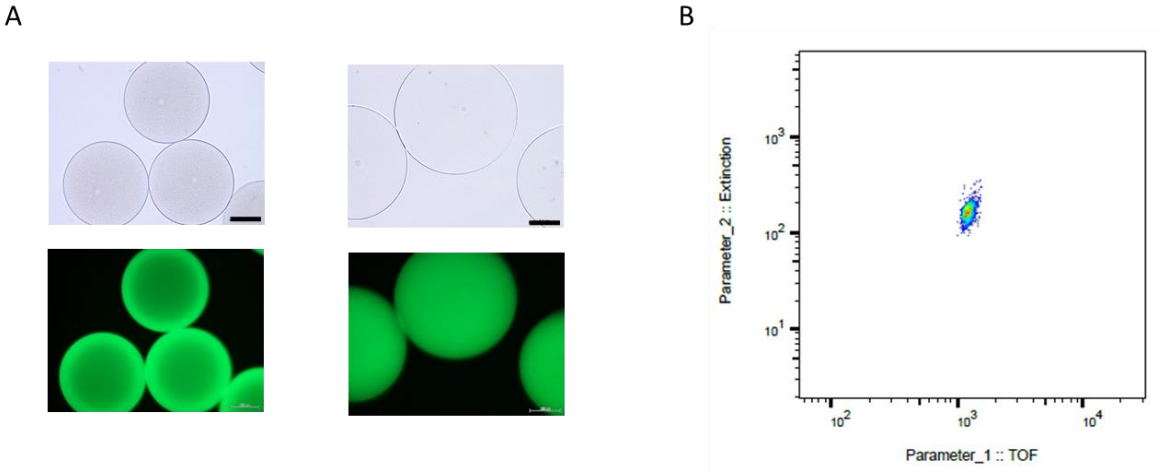


**Figure 3.20.** (**A**) Bright field and fluorescent images of *inhomogeneous* (left) and *homogeneous* (right) alginate beads. Beads loaded with the fusion protein AlgQ2-GFP (see **section 3.2.3.1** for details) show the distribution of alginate through the beads cross section. *Inhomogeneous* beads exhibit higher fluorescence intensity at the surface and lower in the centre reflecting the polymer concentration distribution. By contrast, due to the constant alginate concentration through the beads cross section, *homogeneous* beads show a constant fluorescent signal; the size bar corresponds to 100 µm. (**B**) Time-of-flight (TOF, relative estimate of the particle size) versus extinction dot-plot of COPAS-analyzed *inhomogeneous* alginate beads.

Coating alginate beads with polymers was shown to improve their mechanical resistance and chemical stability. Due to its good biocompatibility, ease of use and low price, chitosan became one of the more common polymer used as coating material (Krasaekoopt et al., 2004; Serp et al., 2000) .

Gel-core and hollow-core chitosan-coated alginate microcapsules were prepared through a modified two-stage procedure as originally outlined by Lim and Sun (Lim and Sun, 1980) (**Figure 3.21**).

The procedure comprises the formation of *gel-core alginate beads* (GCABs) as described above, followed by a membrane forming stage in which GCABs are immersed in a solution of the opposite charged polymer chitosan. Adsorption of the positively charged chitosan onto the negatively charged alginate beads surface results in the formation of *gel-core chitosan-coated alginate microcapsules* (GC-CAM) with an alginate gel core and a polyelectrolyte complex membrane of increasing thickness with increasing incubation time in the chitosan solution. Treatment of GC-CAM with a calcium-chelating agent such as sodium citrate causes the dissolution of the gel core template resulting in the production of *hollow-core chitosan-coated alginate microcapsules* (HC-CAMs).

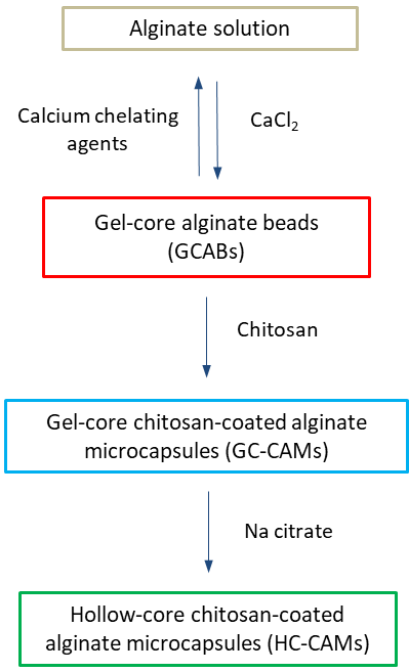


**Figure 3.21.** Alginate bead-based microcompartments production scheme. Alginate solution is dispersed in microdroplets that are ionotropically cross-linked into a gelling bath containing calcium chloride. The resulting alginate beads (GCABs) are incubated in a solution of the positively charged polymer chitosan that adsorbs onto the negatively charged alginate beads surface forming *gel-core chitosan-coated alginate microcapsules* (GC -CAMs). Treatment of GC-CAMs with sodium citrate causes the dissolution of the gel core template and leads to the formation of *hollow-core chitosan-coated alginate microcapsules* (HC-CAMs).

Previous studies have shown that long incubation times of alginate beads entrapping cells in the chitosan solution results in a lower cell survival rate (Chávarri et al., 2010; Krasaekoopt et al., 2004). For this reason, to ensure stable capsules formation while preserving cell viability, chitosan binding conditions were optimized to minimize the incubation time of alginate beads into the acidic chitosan solution. In agreement with Gåserød and colleagues (Gåserød et al., 1999, 1998) binding of chitosan was enhanced by using *homogeneous* alginate beads, by adding calcium chloride in the chitosan solution and by reducing the molecular weight of chitosan. Due to a lower alginate concentration at the surface, *homogeneous* alginate beads have a more porous and open gel structure and show higher rate of binding of chitosan in comparison to *inhomogeneous* beads (**Figure 3.22**). Similarly, the presence of calcium chloride in the chitosan solution enabled a faster adsorption of chitosan onto the alginate bead surface.

The molecular weight of the chitosan was also shown to affect both the rate and the extent of binding to the alginate beads with the smallest molecules showing a more rapid diffusion (Gåserød et al., 1998). Faster membrane formation was achieved by autoclaving the chitosan solution. The heat treatment most likely causes a reduction of the molecular weight of the chitosan used (Mw 50-190 kDa) allowing a better penetration of the chitosan molecules into the alginate gel network.

Under these conditions, stable *gel-core chitosan-coated alginate microcapsules* (GC-CAMs) with a poly-electrolyte complex membrane thickness of about 15 µm are obtained in two minutes.

When GC-CAMs were incubated in a solution of sodium citrate, the alginate core dissolved and the liquefied alginate flowed out of the capsule generating *hollow-core chitosan-coated alginate microcapsules* (HC-CAMs).

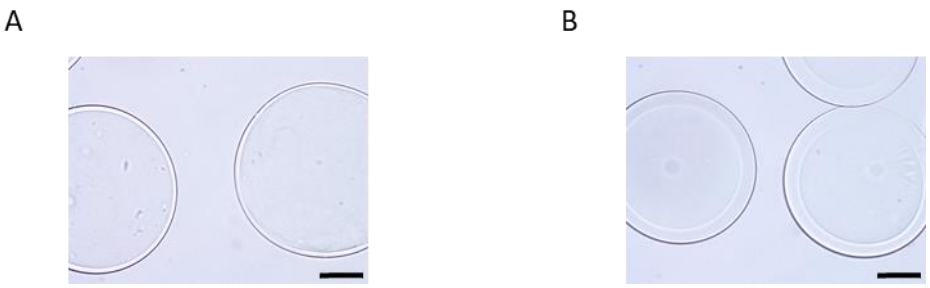


**Figure 3.22.** Effect of homogeneity degree on the binding of chitosan to the alginate beads. Shown are phase contrast images of *hollow-core chitosan-coated alginate microcapsules* obtained from *inhomogeneous* (A) and *homogeneous* alginate beads (B). Beads were coated with a 0.3% chitosan solution (not autoclaved) for 15 min then treated with 50 mM sodium citrate. Due to a lower alginate concentration at the surface, *homogeneous* beads show higher rate of binding of chitosan than *inhomogeneous* beads which result in a ticker alginate-chitosan membrane. The size bar corresponds to 100 µm.

Unlike alginate beads, chitosan-coated alginate microcapsules were found stable in absence of calcium or when exposed to either low concentrations of calcium chelating agents or high concentrations of competing ions like $Na^+$. However, all three different types of alginate bead-based microcompartments produced were mechanically quite stable and appeared intact under the microscope after COPAS analysis suggesting that they could support microbial cell growth and withstand the various external forces encountered during the whole assay.

### 3.2.2 Analysis of clones grown in alginate bead-based microcompartments

For the production of microreactors, *E. coli* cells were suspended in the alginate solution and alginate bead-based microcompartments prepared as described above. Since the encapsulation method does not allow to strictly determine the number of cells per bead, the average bead occupancy, governed by the Poisson distribution, was controlled by changing the concentration of the cell suspension. Usually, to obtain a satisfactory fraction of colonized microreactors, an average number of two cells per bead was considered.

As first step, growth of *E. coli* cells was qualitatively evaluated within GCABs. Microscopic analysis revealed that, after incubation of cells-entrapping beads in the growth-medium, cells proliferate to form colonies normally shaped as a sphere or an ellipsoid that occupy a small portion of the bead volume **(Figure 3.23 A)**. The analysis also revealed that a colony growing near the edge of the bead causes its rupture with subsequent leakage of cells to the medium. During cell encapsulation, the chance that a single cell falls in the periphery is higher than ending up in the center of the alginate bead (**Figure 3.23 B**). As consequence, growing cells in GCBs implies a high risk of cell outgrowth, making such microreactors unsuitable for the development of the assay. For this reason, GCBs-based microreactors were not further investigated.

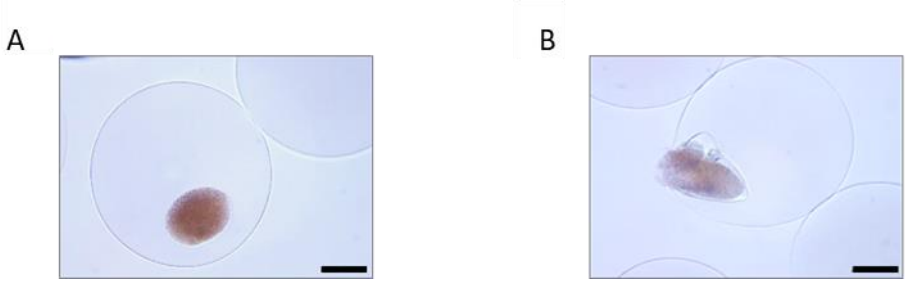


**Figure 3.23.** Microscopic analysis of gel-core alginate beads harboring a single *E. coli* colony. The size bar corresponds to 100 µm (**A**) In gel-core alginate beads, *E. coli* cells grow to form colonies shaped as a sphere or an ellipsoid that occupies only a small portion of the bead volume. (**B**) A colony growing close to the bead surface causes its rupture with subsequent leakage of cells.

Similar to cell growth within GCABs, cell growth within GC-CAMs resulted in the formation of a colony confined in a small area of the capsule. However, the presence of the polyelectrolyte membrane represented a physical barrier that prevented the rupture of the capsule when colonies grew in the bead periphery (**Figure 3.24 A**). When GC-CAM entrapping *E. coli* cells were transferred into the growth medium supplemented with sodium citrate, the alginate gel core liquefied (forming HC-CAM) and the cells proliferated to form colonies extended over the whole capsule core (**Figure 3.24 B**).

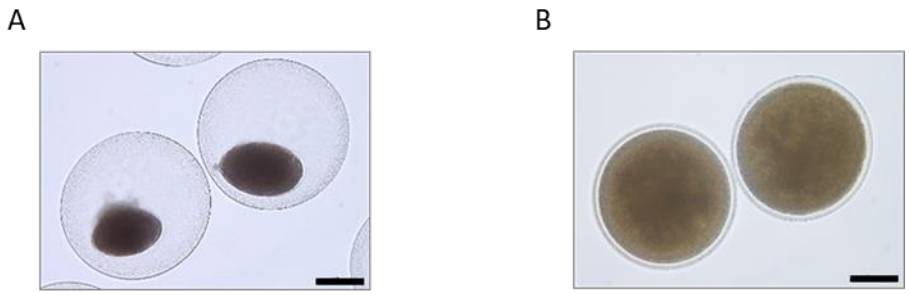


**Figure 3.24.** Microscopic analysis of gel-core (**A**) and hollow-core (**B)** chitosan-coated alginate bead-based microreactors. The presence of the chitosan-alginate polyelectrolyte complex membrane confers on capsules high mechanical strength and prevents cell outgrowth. Similar to cell growth within alginate beads, cell growth within gel-core chitosan-coated microcapsules generates colonies confined in a small area of the capsule. The addition of sodium citrate to the growth medium causes the dissolution of the alginate gel core and leads to the formation of colonies extended over the whole hollow core.

Cell survival rates, determined by comparing the number of living cells encapsulated with the number of colonies detected in microcapsules after cell growth, showed that about 80-90 % of encapsulated cells survived the encapsulation procedure demonstrating that the encapsulation method, the chitosan coating, and the sodium citrate treatment only have a minor impact on cell viability.

To evaluate whether the status of the core (gel or hollow) can affect the cell growth rate inside the microcapsules, the total number of cells grown in either gel-core or hollow-core-based microreactors was estimated through an MTT reduction assay as described by Wang and colleagues (Wang et al., 2010). The assay relies on the reduction, by the dehydrogenase system of active cells, of the water-soluble yellow dye 3-(4,5-dimethylthiazol-2-yl)-2,5-diphenyl tetrazolium bromide (MTT) to the water-insoluble purple formazan whose concentration, after dissolution in DMSO, is directly proportional to the number of metabolically active cells.

After incubation in the growth medium for 18 hours at 28 °C the estimated final biomass in microcapsules with hollow-core was twice as high as in microcapsules with a gel-core indicating that the alginate gel matrix may provide mechanical resistance against cellular growth resulting in a slightly reduced growth rate. According to the MTT assay, a single hollow-core microreactor contains up to 1.5 million cells. As, for the strain BL21, one unit of absorbance at 600 nm was found to corresponds to about 2 x $10^8$ cells/ml, a local cell density of $5\times10^{10}$ cell/ml ($OD_{600nm} \approx 250$) was calculated.

Microscopic inspection after COPAS analysis and sorting showed that cellular growth does not affect the stability of neither gel-core nor hollow-core-based microreactors making them both suitable for the development of the directed evolution assay. However, due to the variability in colony size and shape, gel-core-based microreactors provide less homogenous signals in comparison to HC-CAM-based microreactors, which might result in a reduced accuracy of the optical readout during COPAS analysis and sorting.

In addition, due to the higher specific weight, hollow-core-based microreactors provide a much better and efficient gravity-driven separation of colonized microcapsules from the empty ones allowing a considerable reduction of working volumes and sorting analysis times (**figure 3.25**).

For all the above-mentioned reasons, the hollow-core-based microreactors were preferred over the gel-core's.

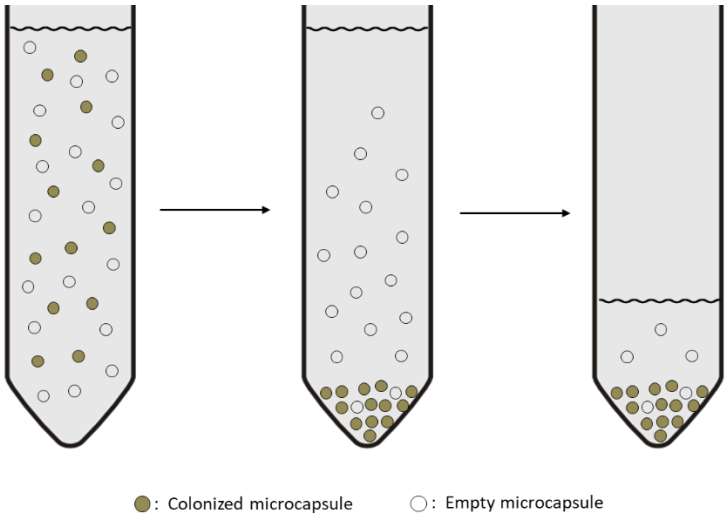


**Figure 3.25.** Scheme of gravity-driven separation of colonized and empty hollow-core microcapsules

### 3.2.3 Sortase-mediated conjugation within microreactors

While the use of microreactors enable a large amount of enzyme variants to be analyzed at a miniaturized scale, the successful application of the assay for directed evolution of low active sortases however relies on a robust and efficient sortase-mediated conjugation reaction within the microreactors. Using the well-characterized sortase A from *S. aureus (*SaSrtA*)* as a model, two different strategies were investigated with the goal to maximize the assay sensitivity and allow for detectable outputs when sortases with poor activity are assayed.

Since alginate was chosen as polymer for the production of microreactors, the first strategy relied on the use of an alginate binding protein as the nucleophilic component of the sortase-mediated conjugation that takes place within microreactors. Upon cell lysis, the intracellularly expressed sortase is expected to recognize the small and free-to-diffuse exogenous fluorescent labeled recognition peptide and attach it to the N-terminus of the oligo-glycine-modified alginate binding protein. By interacting with the alginate bead matrix, the alginate binding protein would retain the fluorescent transpeptidation products inside microreactors, ensuring a direct correlation between the sortase activity and the fluorescent output signal (**Figure 3.26**).

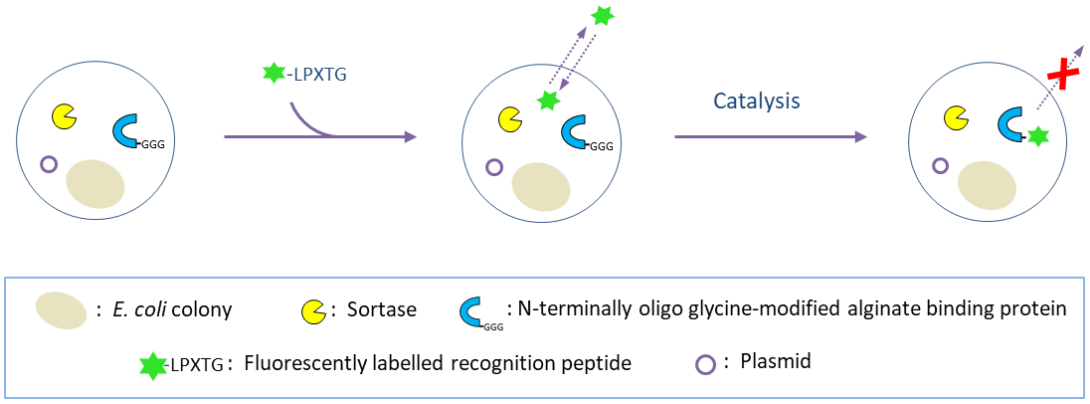


**Figure 3.26.** Scheme of the sortase-mediated conjugation reaction within microreactors based on the use of an N-terminally oligo-glycine-modified alginate binding protein. Upon cell lysis, the sortase enzyme recognizes the fluorescent labeled recognition peptide and attach it to the N-terminus of the oligo-glycine-modified alginate binding protein co-expressed along with the sortase or supplied in solution. Beyond acting as nucleophile for the sortase-mediated conjugation, the modified alginate binding protein would enable the retention of the transpeptidation products by interacting with the alginate contained in microreactors.

Distinct from the first strategy, the second strategy requires only two reaction components and relies on the expression of a sortase enzyme harboring a glycine tag at its N-terminus. It has been suggested that, in such a fusion construct, the N-terminus can access the active site in an intramolecular fashion and, due to the increased local substrate concentration, improve the sortase-mediated conjugation reaction rate (Amer et al., 2016; Piotukh et al., 2011b). In this case, in absence of a specific retention mechanism, transpeptidation products retention would be ensured by coating microreactors with a selective membrane made of the polyelectrolytes poly-allylamine hydrochloride (PAH) and poly-styrene sulfonate (PSS) (**Figure 3.27)**. Microreactors with controlled permeability would allow the low molecular weight fluorescent recognition peptide (≈ 1 kDa) to diffuse inside and take part in the sortase-mediated conjugation reaction while would prevent the higher molecular weight transpeptidation products (≈ 20 kDa) from diffusing out.

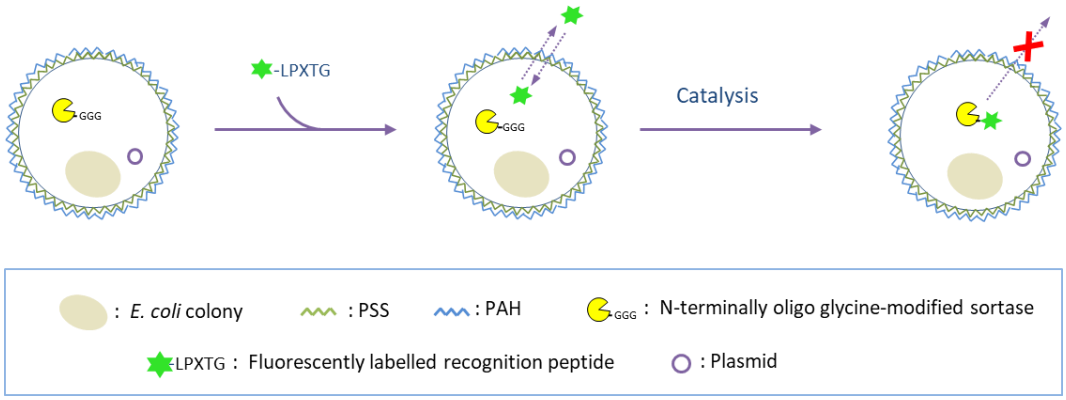


**Figure 3.27.** Scheme of the sortase-mediated conjugation within PSS-PAH-coated microreactors based on the use of an N-terminally oligo-glycine modified sortase. Upon cell lysis, the N-terminally oligo-glycine-modified sortase captures the fluorescent labeled recognition peptide through an intramolecular transpeptidation reaction. Transpeptidation products retention is ensured by the presence of a selective polyelectrolyte shell that surrounds microreactors.

Because of the lower affinity of SaSrtA for the recognition peptide substrate as compared to the oligo-glycine nucleophile, the assay was formatted so that the fluorescent labeled recognition peptide substrate is supplied exogenously. By lowering the concentration of the peptide provided during each round of the directed evolution experiment, this format would allow to increase the evolutionary pressure and select for variants with improved peptide recognition capabilities and thus with higher catalytic efficiencies.

### 3.2.3.1 Conjugation and product capture strategy based on AlgQ2

In this work, three putative alginate-binding proteins were selected and investigated as the nucleophilic component of the sortase-mediated conjugation reaction within microreactors.

The first one, AlgQ2 from *Sphingomonas* species, was selected because its structure was previously determined (Momma et al., 2002) and because it was shown to specifically bind alginate (Momma et al., 2005). However, due to its size, AlgQ2 showed low expression rate, especially when co-expressed with the sortase enzyme. For this reason, two smaller putative alginate binding protein domains were probed as alternative to AlgQ2: (i) the C-terminal carbohydrate-binding domain of AlgX (AlgX-C) from *Pseudomonas aeruginosa* involved in the biosynthesis of alginate (Riley et al., 2013) and (ii) the carbohydrate-binding motif (CBM) of the "sugar binding protein" from *Bacteroides thetaiotamicron* that in addition carries an Alginate Lyase domain.

In view of using the alginate binding proteins as nucleophiles in the sortase-mediated conjugation reaction, 5 glycine residues were introduced at the N-terminus of the amino acid sequences used for gene synthesis. As the cloning method used in this work introduces a serine residue after the N-terminal methionine (considered to be removed by the expression host enzyme *methionine amino peptidase* (Frottin et al., 2006), the "cloning scar" serine residue must be changed into another glycine residue in order to obtain alginate binding proteins with a glycine tag at the N-terminus.

First, to evaluate the alginate binding ability of these three putative alginate binding proteins, the corresponding genes were overexpressed in *E. coli* fused at the C-terminal with GFP. Unfortunately, among them, only the fusion construct AlgQ2-GFP was expressed in soluble form and could be purified through affinity chromatography.

To analyze the alginate-binding ability of AlgQ2, *homogeneous* alginate microbeads were prepared and incubated with the purified AlgQ2-GFP (87 kDa). As negative control, alginate microbeads were incubated either with GFP (30 kDa) or with a similar size protein also fused to GFP (VvGT5-GFP, 79 kDa) which should not display any alginate binding ability. Since the average pore size diameter for a 3 % alginate gels was found to be about 15 nm (Li et al., 1996), AlgQ2-GFP, with an estimated Stokes radius of approximately 3.8 nm (Erickson, 2009) is expected to diffuse out from alginate beads after washing unless it is retained through interaction with alginate. Fluorescence microscopy analysis revealed that only alginate beads incubated with AlgQ2-GFP retain fluorescence demonstrating that AlgQ2 indeed has alginate binding properties (**Figure 3.28**).

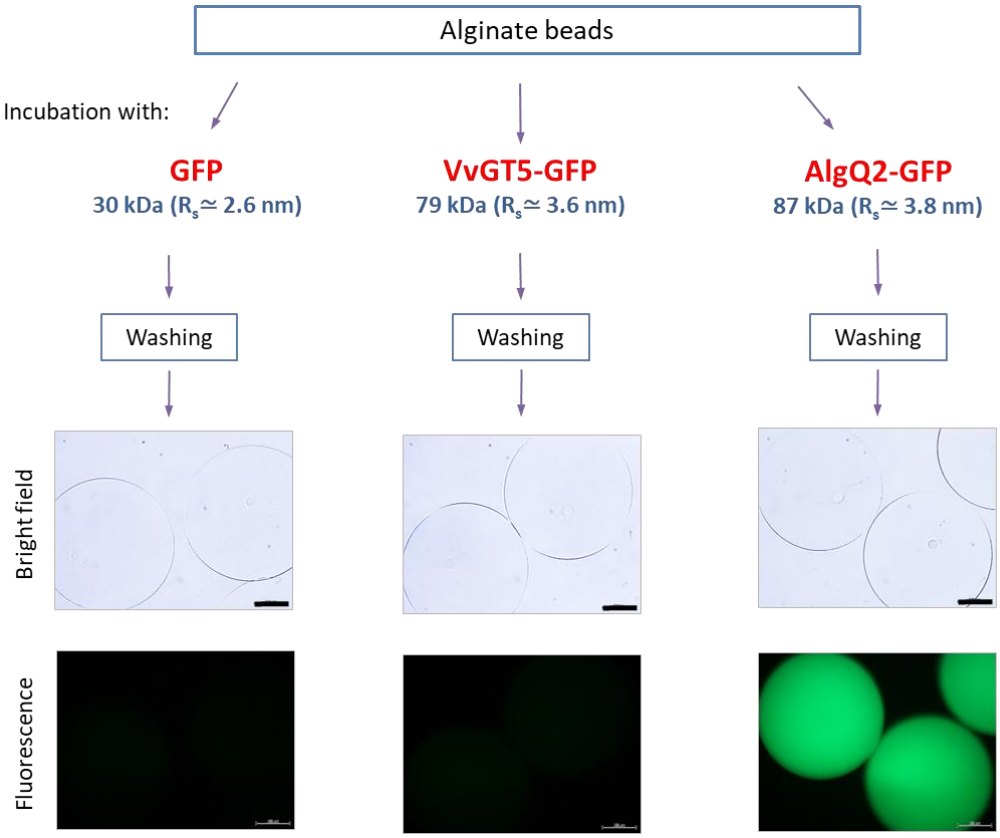


**Figure 3.28.** AlgQ2 displays alginate beads binding properties. About 2000 *homogeneous* alginate beads were incubated with 500 nM of either GFP, VvGT5-GFP or AlgQ2-GFP in 25 mM Tris/HCl pH 8.0, 10 mM $CaCl_2$ for 30 minutes then washed with the same buffer overnight. Shown are the beads in bright field and as fluorescence images (Exposure time 1/500s). Only alginate beads incubated with AlgQ2-GFP retain fluorescence. Molecular weight and Stokes radius ($R_s$) are reported for each protein. The size bar corresponds to 100 µm.

Next, to establish whether the N-terminally oligo-glycine-modified AlgQ2 would work as nucleophile in a sortase-mediated conjugation reaction, sequence encoding for Gly5-AlgQ2 was transferred in an expression vector (p7XC3H) yielding AlgQ2 with the N-terminus SGGGGG (Ser-Gly5-AlgQ2). After, as mentioned above, the "cloning scar" serine was changed into another glycine residue to yield AlgQ2 with six glycine at its N-terminus (Gly6-AlgQ2). Upon expression and purification, Gly6-AlgQ2 was incubated with the FITC-labeled peptide substrate bearing the recognition motif LPXTG in presence of the enhanced version of sortase A (eSaSrtA) (**Figure 3.29 A**)**.** After separation of reaction components by SDS-PAGE, the fluorescence scan of the gel revealed the presence of a strong linkage between the fluorescent peptide and Gly6-AlgQ2 but not with either BSA or Ser-Gly5-AlgQ2 used as negative controls (**Figure 3.29 B**). Beyond showing that Gly6-AlgQ2 works as nucleophile in the sortase-mediated conjugation and it is therefore suitable for the development of the microreactor-based assay, this experiment confirmed the importance of the presence of the N-terminal glycine residue to achieve efficient conjugation.

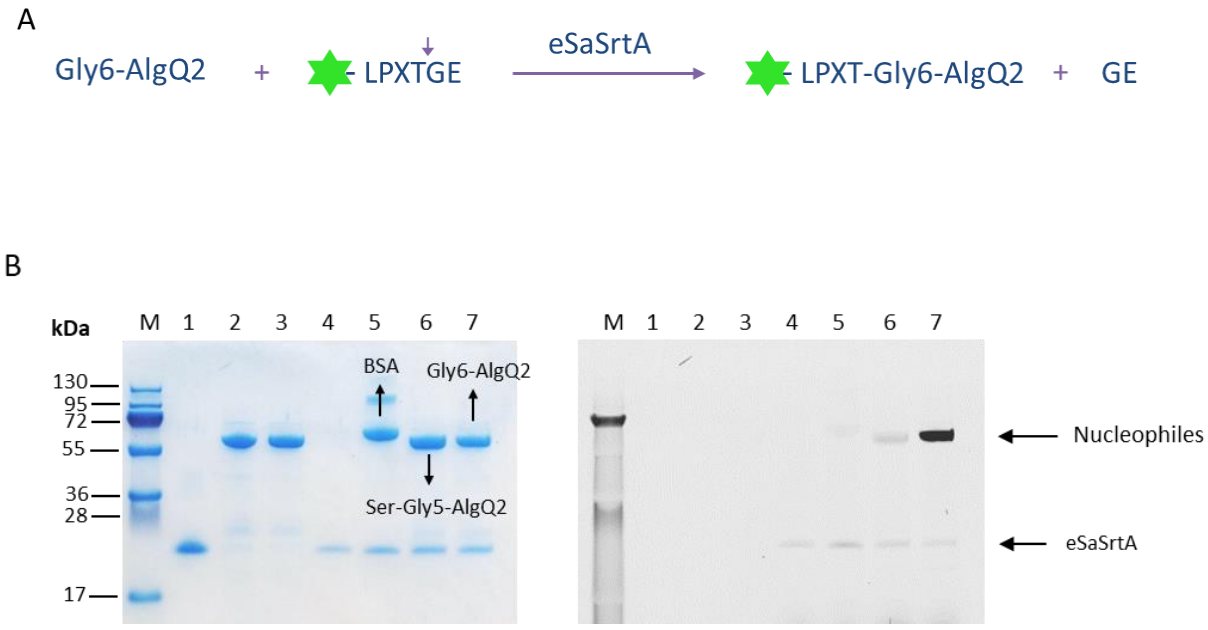


**Figure 3.29:** AlgQ2 acts as a nucleophile in a sortase-mediated conjugation reaction. (**A**) Reaction scheme for the sortase-mediate conjugation of the fluorescent recognition peptide to the N-terminally oligo-glycine modified AlgQ2. (**B**) Gel-based conjugation assay; eSaSrtA (1 µM) was mixed with 2 µM FITC-LPXTGE and 2 µM of either Gly6-AlgQ2, bovine serum albumin (BSA) or Ser-Gly5-AlgQ2 in 25 mM Tris/HCl pH 8.2, 150 mM NaCl, 10 mM $CaCl_2$ and incubated in for 1 hour at 30 °C. The formation of transpeptidation products was analyzed by SDS-PAGE gel fluorescence scanning (right panel). Equal protein loading was assessed by staining the gel with Coomassie (left panel). Lane 1: eSaSrtA alone; lane 2: Gly6-AlgQ2 alone; Lane 3: No eSrtA; lane 4: No Gly6-AlgQ2; lane 5: reaction with BSA; lane 6: reaction with Ser-Gly5-AlgQ2; lane 7: reaction with Gly6-AlgQ2.

#### 3.2.3.1.1 Sortase-mediated conjugation within alginate beads

A requirement for the use of microreactors for directed evolution purposes is that the sortase enzyme, released from colonies upon cell lysis, retains activity in the environment of the alginate bead matrix and efficiently catalyzes the conjugation of the fluorescent labeled recognition peptide to the N-terminally oligo-glycine modified molecule. The capability of eSaSrtA to conjugate the fluorescent peptide to Gly6-AlgQ2 within alginate beads was therefore examined. To this end, *homogeneous gel-core alginate beads* (GCABs) were prepared and incubated with recombinant eSaSrtA and Gly6-AlgQ2 for protein loading. After washing the alginate beads to remove unbound proteins, the reaction was initiated by the addition of FITC-LPXTGE. Following one-hour incubation, beads were washed to remove unreacted substrate peptides thereby terminating the reaction. As the fluorescent recognition peptides linked to Gly6-AlgQ2 were supposed to remain inside the alginate beads, fluorescent beads were expected if the sortase-mediated conjugation reaction takes place. As revealed by fluorescence microscopy analysis, high fluorescent signals were obtained with beads loaded with both Gly6-AlgQ2 and eSaSrtA incubated with the fluorescent specific peptide (**Figure 3.30 A1**). Conversely, beads loaded only with Gly6-AlgQ2 or beads loaded with both proteins but incubated with a fluorescent labeled peptide not recognized by eSaSrtA (FITC-NPNTG) appeared not fluorescent demonstrating that the reaction is dependent both on the SaSrtA activity and on its substrate specificity and that the fluorescent recognition peptide can freely diffuse through the alginate bead matrix. (**Figure 3.30 A2, A3**). In addition, SDS-PAGE analysis of the bead samples followed by fluorescence scanning of the gel confirmed the linkage between Gly6-AlgQ2 and the fluorescent recognition peptide proving the feasibility of the sortase-mediated conjugation reaction within the alginate bead environment (**Figure 3.30 B**)

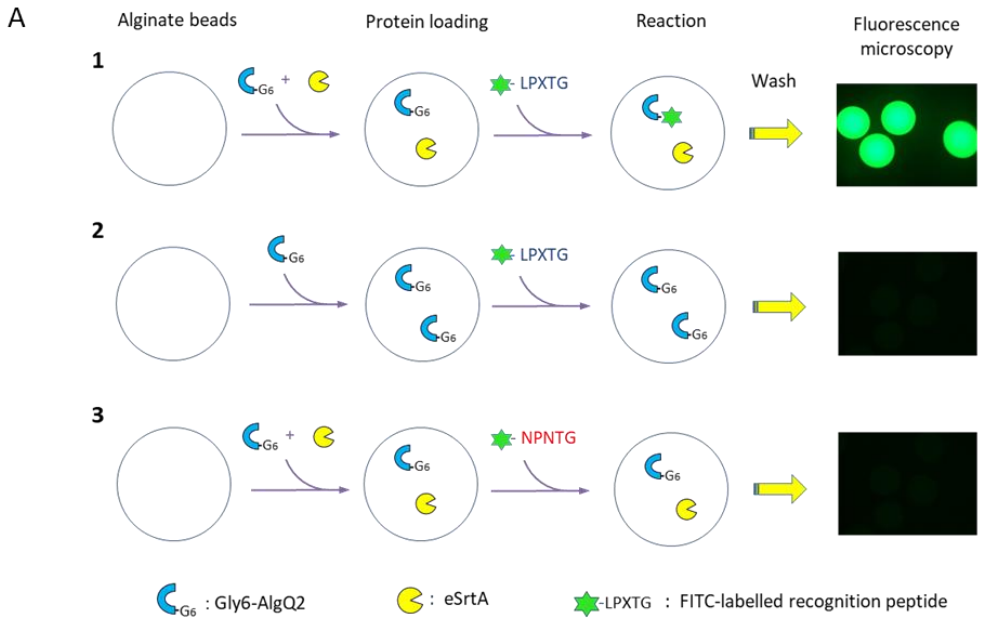

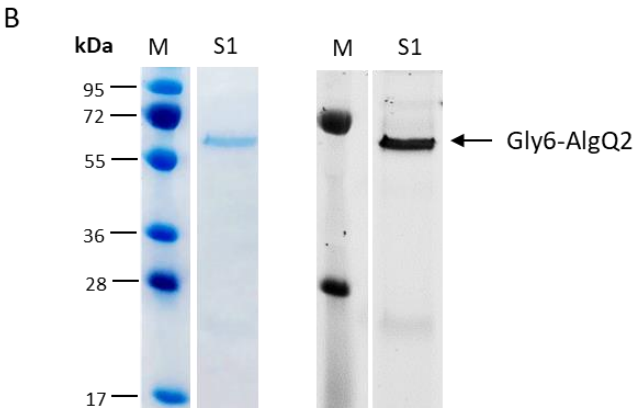


**Figure 3.30. (A)** SaSrtA-mediated conjugation within alginate beads. (**1**) About 1000 alginate beads were incubated with 2 µM eSaSrtA and 8 µM Gly6-AlgQ2 for 30 min then washed to remove unbound proteins. The reaction was initiated by adding 10 µM FITC-LPXTGE. After 1 hour incubation at 30 °C, beads were washed to remove unreacted peptide and then analyzed by fluorescence microscopy (Exposure time 1/50s). Beads loaded with Gly6-AlgQ2 only (**2**) or reacted with the class B-specific peptide FITC-DNPNTGDE (**3**) were used as negative controls. (**B**) Coomassie staining and fluorescence scan of the SDS-PAGE gel of the bead sample 1 (S1) depicted in A1 showing the linkage between SaSrtA and the fluorescent recognition peptide.

When alginate beads loaded only with eSaSrtA were incubated with FITC-LPXTGE, fluorescent beads were observed (**Figure 3.31 A**). Interestingly, the fluorescence analysis by SDS-PAGE/fluorescence scanning, revealed a linkage between the fluorescent peptide and the eSaSrtA itself (**Figure 3.31 B)**.

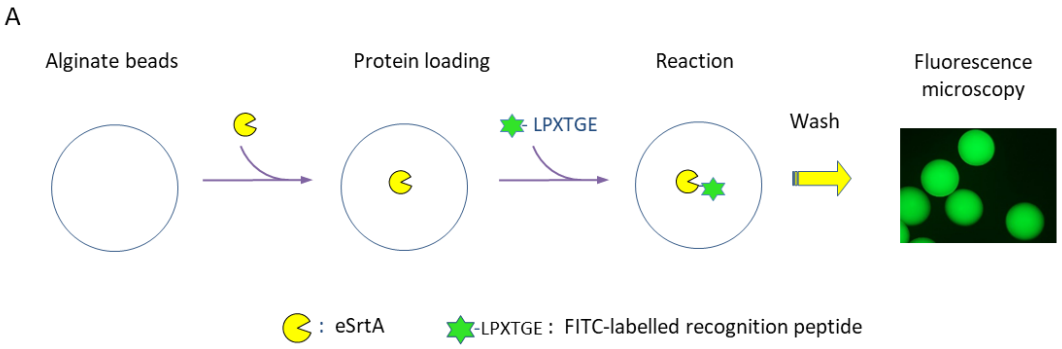

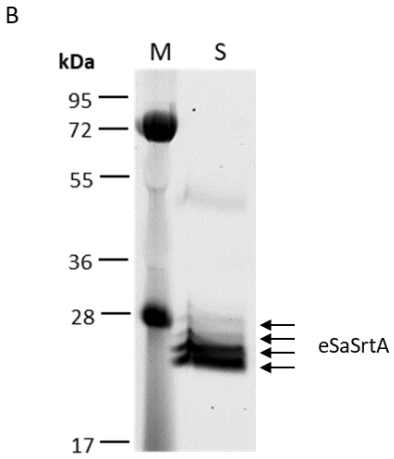


**Figure 3.31. (A)** About 1000 alginate beads were incubated with 2 µM eSaSrtA for 30 min then washed to remove unbound protein. After 1-hour incubation with 10 µM FITC-LPXTGE at 30 °C, beads were washed to remove unreacted peptide and then analyzed by fluorescence microscopy (Exposure time 1/50s). (**B**) Fluorescence scan of the SDS-PAGE gel of the bead sample (S) depicted in A1 showing the linkage between SaSrtA and the fluorescent recognition peptide.

Previous studies have reported that in absence of a dedicated nucleophile SaSrtA forms a stable thioacyl intermediate with the recognition peptide substrate (Bellucci et al., 2015; Dasgupta et al., 2011). However, the progressive upshift of the band corresponding to SaSrtA along with a decreasing fluorescence intensity, strongly suggested that one or more fluorescent peptides have been linked to the SaSrtA molecule. As SaSrtA was shown to transfer LPXT motifs to the ε amino-group of lysine residues through a non-canonical isopeptide ligation (Bellucci et al., 2015; McConnell et al., 2018) it is likely that, in addition to the thioacyl intermediate, species in which one or more the fluorescent peptides are linked to exposed lysine residues of the SaSrtA protein can be formed.

To confirm this hypothesis and evaluate the occurrence of stable thioacyl intermediates formation, SaSrtA was reacted with FITC-LPXTGE in absence of Gly6-AlgQ2 and the resulting fluorescent SaSrtA product subsequently purified from the excess of fluorescent peptide by using a desalting column (**Figure 3.32 A**). When the fluorescent SaSrtA product was incubated for 18 hours in absence of nucleophile, a slightly reduction of the fluorescent signal was observed in comparison to samples incubated for one hour (**Figure 3.32 B**). This reduction, which, correspond to about 30 and 17 % of the total product in presence and in absence of calcium respectively, is most likely associated to the resolution of the thioacyl intermediate by the hydrolysis side reaction. As consequence, the remaining fluorescent product might therefore consist of SaSrtA possibly linked to one or more fluorescent peptide molecule at lysine residues level.

Notably, no fluorescent signal reduction was observed when Gly6-AlgQ2 was added to enforce the thioacyl intermediate resolution further confirming that in addition to the thioacyl intermediate, stable linkages between fluorescent peptides and lysine residues of SaSrtA may occur through an intermolecular isopeptide ligation.

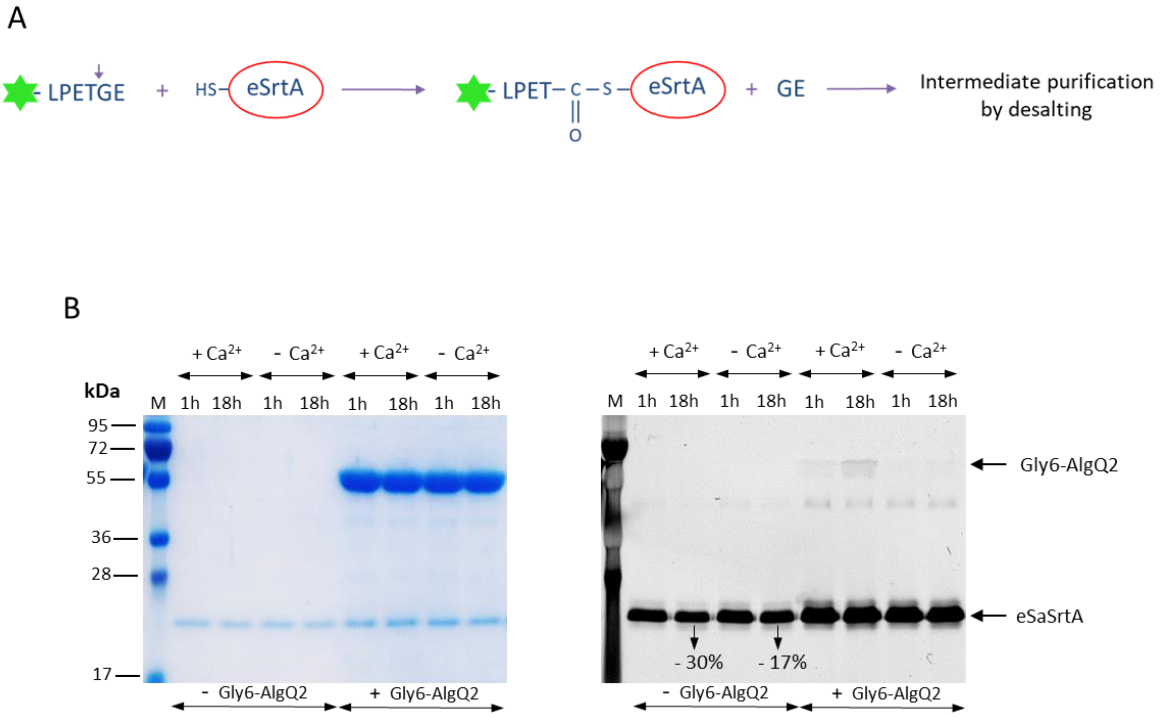


**Figure 3.32.** (**A**) Reaction scheme for thioacyl intermediate formation and purification. Recombinant eSaSrtA was incubated with FITC-LPXTGE in absence of nucleophile and the resulting fluorescent product purified from the fluorescent peptide by using a desalting column (**B**) The purified product (2 µM) was incubated in 25 mM Tris/HCl pH 8.2, 150 mM NaCl for 1 or 18 hours, with or without $CaCl_2$ (10 mM), and in the absence or in presence of the nucleophile Gly6-AlgQ2 (8 µM). Intermediate-solving reactions were analyzed by SDS-PAGE gel fluorescence scanning (right panel). Band signal intensities were quantified with *ImageJ*. Fluorescent signals were normalized to total protein loading assessed by staining the gel with Coomassie (left panel).

### 3.2.3.1.2 Analysis of the fusion protein Gly6-AlgQ2-eSaSrtA

With the goal to reduce the diffusion of eSaSrtA from alginate beads and enhance the sensitivity of the sortase-mediated conjugation assay within alginate beads, the fusion protein Gly6-AlgQ2-eSrtA was constructed by linking the C-terminus of the Gly6-AlgQ2 alginate binding protein with the N-terminus of the eSaSrtA enzyme via a GSGS linker.

When alginate beads, loaded with the purified Gly6-AlgQ2-eSrtA (without any further nucleophile addition) were incubated with FITC-LPXTGE for one hour, alginate beads appeared highly fluorescent. The analysis of the beads content by SDS-PAGE and fluorescence scanning revealed a linkage between the construct Gly6-AlgQ2-eSrtA and the FITC-labeled recognition peptide and raised the question whether the conjugation reaction occurs intra or inter-molecularly (**Figure 3.33**).

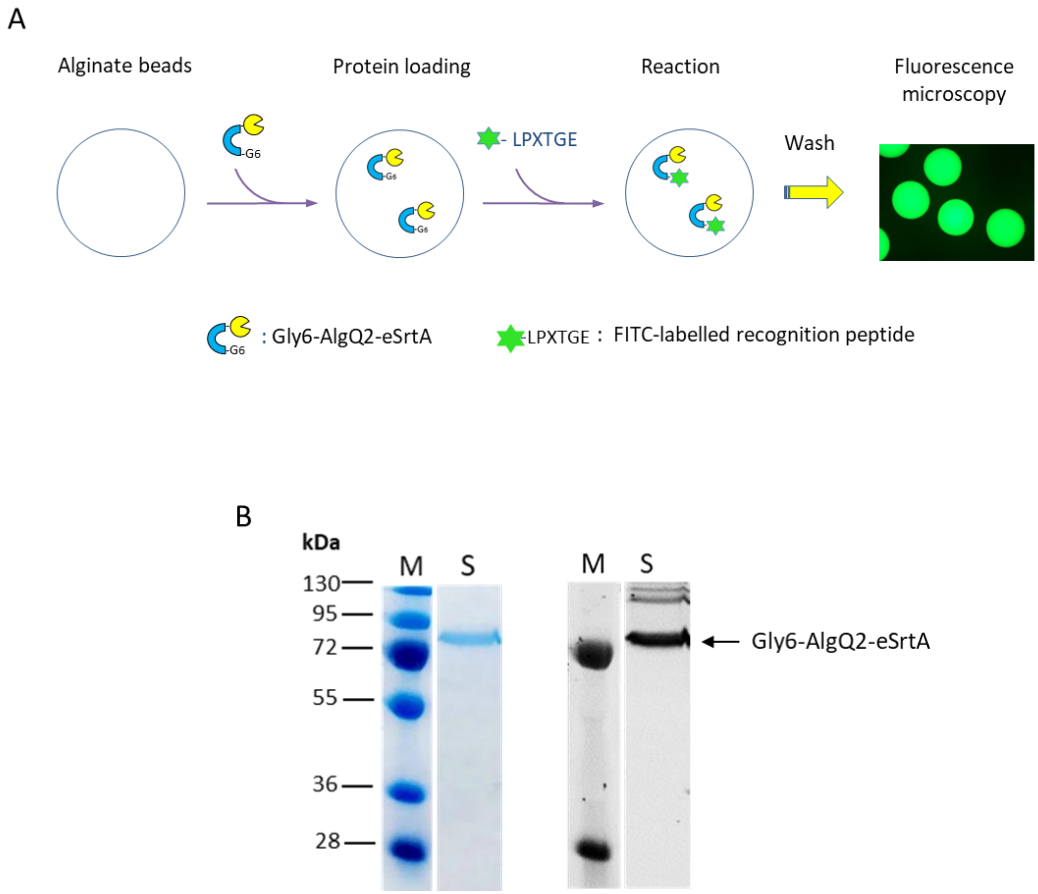


**Figure 3.33.** (**A**) About 1000 alginate beads were incubated with 2 µM Gly6-AlgQ2-eSrtA for 30 min then washed to remove unbound protein. After 1 hour incubation with 10 µM FITC-LPXTGE at 30 °C, beads were washed to remove unreacted peptide and analyzed by fluorescence microscopy (Exposure time 1/50s). (**B**). Coomassie-staining and fluorescence scan of SDS-PAGE gel of the bead sample (S) depicted in figure A showing the linkage between Gly6-AlgQ2-SrtA and the fluorescent recognition peptide.

To establish whether the conjugation reaction occurs intra or inter-molecularly, a **gel-based conjugation assay** was set up in which Gly6-AlgQ2-eSrtA was reacted at three different concentrations (10, 1 and 0.1 µM) with an excess of the fluorescent substrate peptide (FITC-LPXTGE) and subsequently analysed by SDS-PAGE for fluorescence quantification (**Figure 3.34 A)**. When, after 2 and 10 min incubation, equal amounts of Gly6-AlgQ2-eSrtA were analysed by SDS-PAGE and gel fluorescence scanning, comparable amounts of labeled protein were observed for the three reactions (**Figure 3.34 B)**. If the intermediate resolving step of the reaction is rate-limiting and occurs intermolecularly, we would expect a 100-fold lower fluorescent signal intensity for the reaction at the lowest protein concentration (0.1 µM) compared to the reaction at the highest protein concentration (10 µM) as observed for the unmodified SaSrtA (**see figure 3.38 B**). Still, as shown in **figure 3.35**, in comparison to the reaction performed with equimolar concentration of Gly6-AlgQ2 and eSaSrtA (10 µM), the reaction performed with Gly6-AlgQ2-eSrtA showed increased reaction rate therefore suggesting that Gly6-AlgQ2-eSrtA labels itself intramolecularly. These results were in agreement with a recent study by Amer and colleagues who showed that in a fusion construct involving SaSrtA the glycine tag at the N-terminus can access the enzyme active site in an intramolecular fashion (Amer et al., 2016). As suggested in this study, the presence of the oligo-glycine nucleophile substrate and the sortase enzyme within the same polypeptide might improve the reaction rate by increasing the effective nucleophile concentration in proximity of the active site of the enzyme.

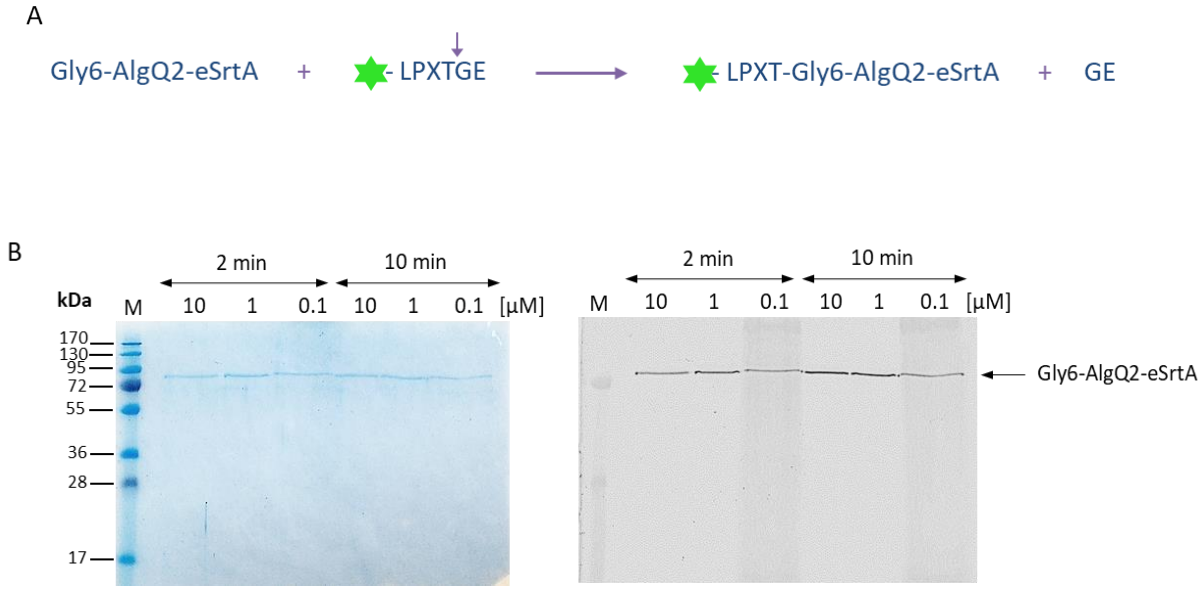


**Figure 3.34. (A)** Reaction scheme for the fusion Gly6-AlgQ2-eSrtA-mediated conjugation **(B)** Gel-based conjugation assay; the fusion protein Gly6-AlgQ2-SrtA was incubated at three different concentrations (10, 1 or 0.1 µM) in 25 mM Tris/HCl pH 8.2, 150 mM NaCl, 10 mM $CaCl_2$ with an excess of FITC-LPXTGE (40 µM) for 2 and 10 minutes. Equal amounts of Gly6-AlgQ2-eSrtA (3 pmol) from each reaction were analyzed by SDS-PAGE gel fluorescence scanning (right panel). Equal protein loading was assessed by staining the gel with Coomassie (left panel). Comparable amounts of labeled protein detected for the three reactions suggest that Gly6-AlgQ2-eSrtA labels itself intramolecularly.

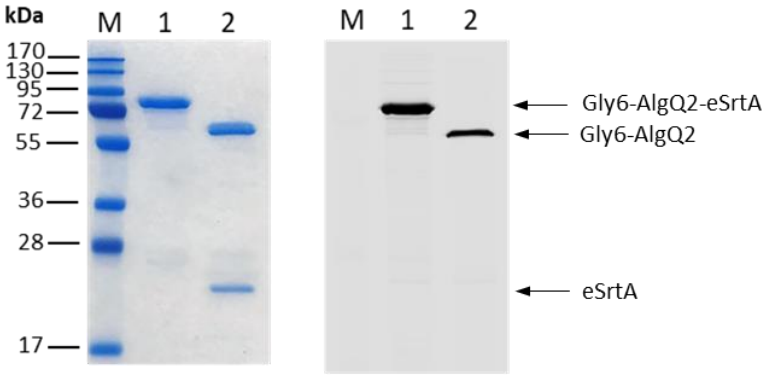


**Figure 3.35. (A)** Comparison of the eSrtA-mediated conjugation performed with 10 µM Gly6-AlgQ2-eSrtA (lane 1) or 10 µM of Gly6-AlgQ2 and 10 µM eSaSrtA (lane 2) for 5 minutes.

Beyond providing improved reaction rates, the use of fusion construct Gly6-AlgQ2-eSrtA set the stage for a new two-components conjugation platform that allows to overcome limitations associated with the supply of the oligo-glycine nucleophile substrate within microreactors. For instance, when Gly6-AlgQ2 was co-expressed with the wild type SaSrtA, very poor expression yields were observed for both proteins making co-expression an inadequate approach for the nucleophile supply (**Figure 3.36)**. Since even lower expression yields would be expected when Gly6-AlgQ2 is co-expressed with the construct Gly-AlgQ2-eSrtA (needed to prevent the diffusion of the sortase enzyme from microreactors), the use of the fusion construct Gly6-AlgQ2-SrtA was preferred over the use of the two separate proteins for the validation of the strategy based on the use of the alginate binding protein AlgQ2. However, while the use of two separate proteins would allow for multiple turnover kinetics the use of the fusion protein Gly6-AlgQ2-SrtA limits the reaction to single turnover.

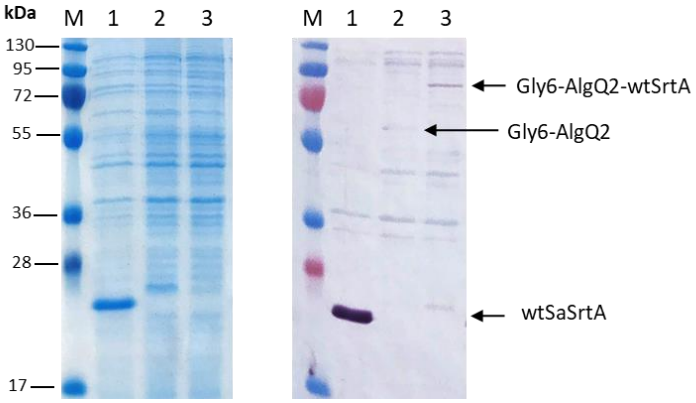


**Figure 3.36.** SDS-PAGE (left) and Western blot analysis (right) showing expression yields of SaSrtA alone (lane 1), SaSrtA and Gly6-AlgQ2 (lane 2) and Gly6-AlgQ2-SrtA (lane 3) in *E. coli* BL21. Protein expression was achieved by the addition of 0.5 mM IPTG to exponential growing cells for 18 hours at 28 °C. Lane M designates the ladder.

### 3.2.3.2 Conjugation strategy based on N-terminally oligo-glycine-modified sortases

Inspired by the intramolecular conjugation mechanism observed with Gly6-AlgQ2-SrtA and by the previously described phage-display assay by Schwarzer and co-workers (Piotukh et al., 2011b), five glycine residues were added at the N-terminus of the wild type sortase A (G5-SrtA), and the ability of this construct to capture the fluorescent substrate peptide by an intramolecular reaction was subsequently evaluated.

Interestingly, when G5-SrtA was overexpressed in *E. coli* a significant reduction in protein expression was observed in comparison to the unmodified sortase A. In the attempt to explain this observation, the length of the sequence at the amino terminus was varied between one, two or three glycine residues (to achieve G1-SrtA, G2-SrtA and G3-SrtA respectively) and the expression-activity relationship of these modified sortases was analysed through the **gel-based conjugation assay**. Whole cell extracts (WCE) were incubated with the FITC-LPETGE and subsequently analysed by SDS-PAGE and fluorescence scanning (**Figure 3.37**). As can be seen in the Coomassie-stained gel, the presence of one or more glycine residues at the N-terminus of SaSrtA results in a notable reduction of protein expression with G5-SrtA showing the lowest expression yield. However, the fluorescence scan of the gel revealed a massive improvement of the fluorescent signal intensity for single or multiple glycine-modified SaSrtA as compared to the unmodified enzyme.

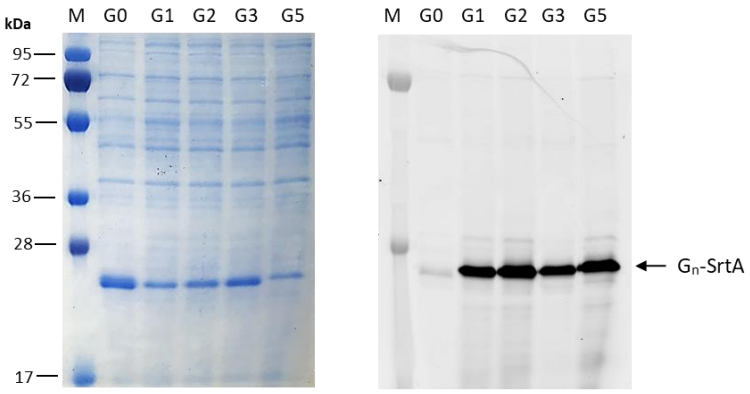


**Figure 3.37** Expression-activity relationship of wild type unmodified (G0) and N-terminally glycine-modified SaSrtA (G1-G5). Whole cell extracts (WCE) in 25 mM Tris/HCl pH 8.2, 150 mM NaCl, 10 mM $CaCl_2$ of *E. coli* cultures expressing SaSrtA variants were incubated with FITC-LPETGE for 3 hours at 30 °C and subsequently analysed by SDS-PAGE (left) and fluorescence scanning (right). The addition of one (G1) or more (G2, G3, G5) glycine residues at the N-terminus of SaSrtA causes a protein expression reduction. However, in comparison to wild type SaSrtA (WT), N-terminally glycine-modified SaSrtA variants show improved reaction rates.

To establish whether the observed reactions occur intra or inter-molecularly, the wild type SaSrtA with a single glycine at its N-terminus (G-SrtA) was purified and a **gel-based conjugation assay** was performed as described above for the fusion protein Gly6-AlgQ2-eSrtA (**section 3.2.3.1.2**). Similarly, when G-SrtA was incubated at at three different concentrations with an excess of the fluorescent substrate peptide and an equal amount of protein were analysed by SDS-PAGE followed by fluorescence scanning of the gel, comparable amounts of labeled protein were observed for the three reactions (**Figure 3.38 A)**. Similar to what observed for Gly6-AlgQ2-eSrtA, the linkage of the fluorescent peptide to the amino-terminal glycine of the enzyme seems to occur intramolecularly. In support of this assumption is the different labeling behaviour observed with the unmodified eSaSrtA. In this case, the amount of protein labeled was proportional to the protein concentration (**Figure 3.38 B**). However, it is not clear how, in absence of a flexible linker, the amino group of the glycine at the N-terminus reaches the active site of the enzyme (**Figure 3.38 C**).

As for the fusion construct Gly6-AlgQ2-eSrtA, the use of a N-terminally oligo-glycine-modified sortase allows for a two-component sortase-mediated conjugation platform that facilitate the execution of the microreactor-based assay. Moreover, due to the higher expression yield of G-SrtA as compared to Gly6-AlgQ2-eSrtA, the assay based on the use of an N-terminally oligo-glycine-modified sortase is expected to provide higher sensitivity.

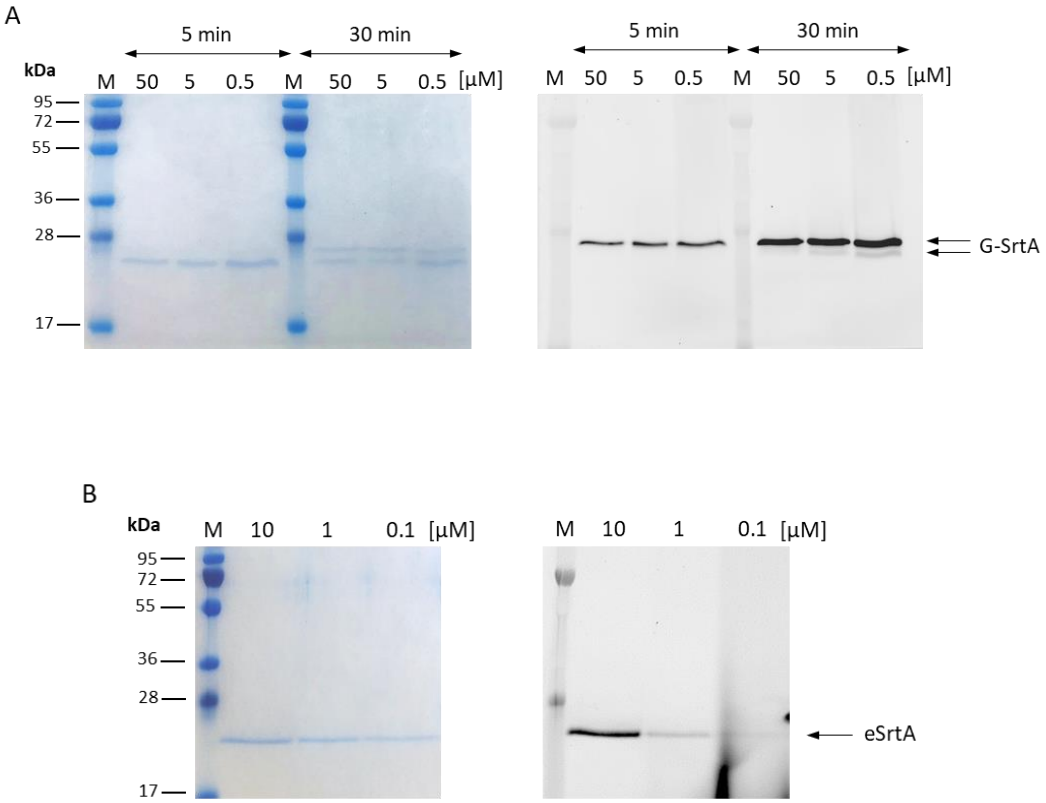

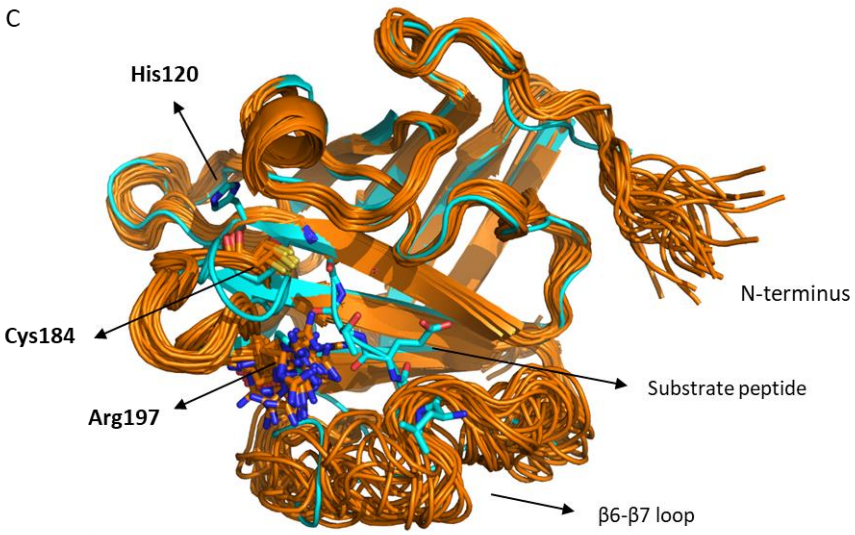


**Figure 3.38.** G-SrtA intramolecular labeling evaluation. (**A**) Gel-based conjugation assay; G-SrtA was incubated at three different concentrations (50, 5 or 0.5 µM) with FITC-LPETGE (200 µM) in 25 mM Tris/HCl pH 8.2, 150 mM NaCl, 10 mM $CaCl_2$ for 5 and 30 minutes at 30 °C. Equal amounts of G-SrtA (10 pmol) from each reaction were analyzed by SDS-PAGE gel fluorescence scanning (right panel). Equal protein loading was assessed by staining the gel with Coomassie (left panel). Similar to Gly6-AlgQ2-SrtA, comparable amounts of labeled protein detected for the three reactions suggest that G-SrtA labels itself intramolecularly. The conjugation of the fluorescent peptide to the amino-terminal glycine of G-SrtA causes the upshift of the band corresponding to G-SrtA. (**B**) Gel-based conjugation assay as in A performed with the unmodified eSaSrtA for 5 minutes showing that the amount of labeled protein is proportional to the protein concentration. (**C**) The NMR-derived structural ensemble of $SaSrtA_{\Delta N59}$ in complex with the peptide substrate shows the reduced flexibility of its N-terminal region and raise the question of how the glycine residue at the N-terminus of G-SrtA reaches the active site.

### 3.2.4 Layer-by-layer coating to control capsule permeability

Although the use of an N-terminally oligo-glycine-modified sortase would represent an alternative to the use of the fusion Gly6-AlgQ2-sortase, this approach requires a different mechanism for preventing the enzyme and the relative fluorescent transpeptidation product to escape microreactors. To this end, inspired by the work of Hollfelder and co-workers, we decided to investigate the utility of a layer-by-layer (LBL) coating technique. LBL assembly of thin films made of polyelectrolytes of opposite charges onto template particles has been used to affect the permeability of microcapsules (Antipov and Sukhorukov, 2004), (Price et al., 2010). Among the polyelectrolyte coating pairs used, the pair PSS and PAH (poly-styrene sulfonate and poly-allylamine hydrochloride respectively; **figure 3.39 C**) is one of the most studied and has been successfully applied to produce stable and semipermeable microcapsules for high-throughput purposes with a molecular weight cut-off ranging from 2 to 6 kDa (Fischlechner et al., 2014; Mak et al., 2008). Consequently, by using PSS and PAH for the coating, the fluorescent recognition substrate peptide with a molecular weight of about 1 kDa should be able to diffuse inwards and outwards from microreactors while molecules with a molecular weight above the cut-off value should remain encapsulated. To test this, GFP-expressing HC-CAM-based microreactors were used as templates for the sequential deposition of PSS and PAH and, upon cell lysis, analyzed for their capability to retain the GFP (30 kDa). As can be seen in **figure 3.39 A** microreactors coated with one layer of either PSS or PAH were found highly permeable to GFP while microreactors coated with one layer of PSS and one layer of PAH already retained 99% of GFP as compared to uncoated microreactors. When PAH was deposited as first layer followed by PSS more than 60% of GFP was found in solution indicating that efficient layer-by-layer coating of chitosan-alginate microcapsules requires the interaction between the negatively charged PSS and the positively charged chitosan (**Figure 3.39 B)**. Interestingly, when a PSS solution without calcium chloride was used for coating (PSS*), only 10 % of the GFP was retained inside microreactors suggesting that, as previously reported for chitosan, the presence of calcium chloride possibly improves the deposition of PSS by increasing the porosity of the chitosan-alginate complex membrane.

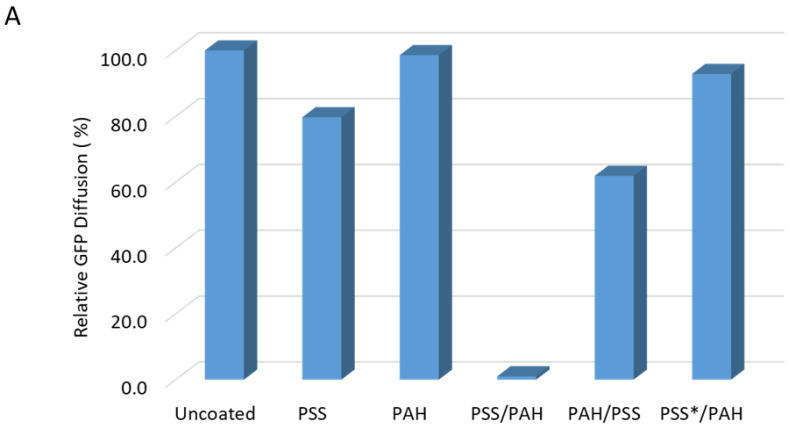

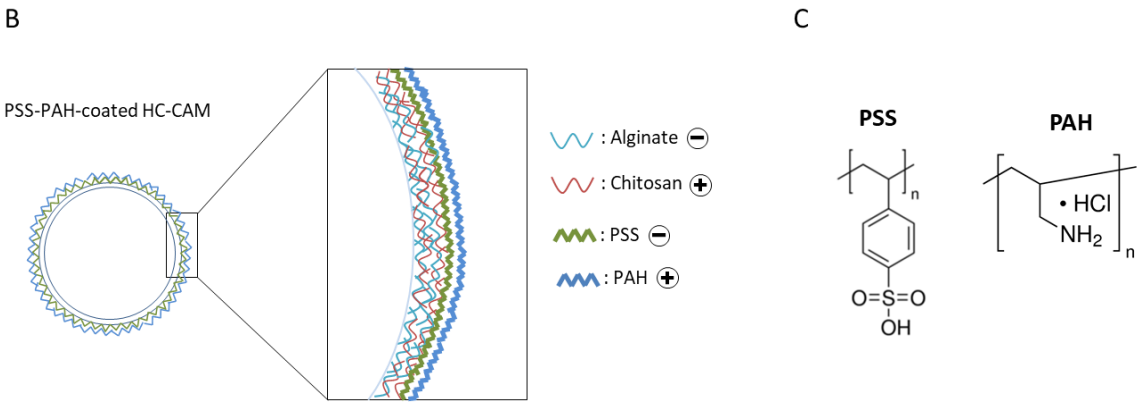


**Figure 3.39.** (**A**) Analysis of PSS-PAH coating on capsule permeability. GFP-expressing HC-CAM-based microreactors were differently coated using the coating pair PSS and PAH and, upon cell lysis, evaluated for their capability to retain the GFP. Microreactors coated with one layer of PSS followed by one layer of PAH (PSS/PAH) retained 99% of GFP as compared to uncoated microreactors. Assembly of the PSS-PAH shell is impaired when a PSS solution without $CaCl_2$ (PSS*) is used. (**B**) Schematic illustration of PSS-PAH-coated HC-CAM. (**C**) Chemical structures of PSS and PAH.

### 3.2.5 Encapsulated cell lysis optimization

In order to make the fluorescent labeled recognition peptide accessible to the intracellularly expressed sortase enzyme, a cell lysis step is required before the sortase-mediated conjugation reaction can take place in microreactors. Disruption of encapsulated cells was achieved by treating microreactors with BugBuster (Merck Millipore), a mixture of non-ionic detergents capable of cell wall and membrane perforation. To determine the appropriate BugBuster concentration to obtain efficient cell lysis, microreactors lacking the PSS/PAH coating were treated with different concentrations of the detergents mixture and cell viability was evaluated through the MTT reduction assay (see **section 3.2.2** for details).

According to the MTT assay results, about 97% of encapsulated cells were not viable after treatment with 0.25 X BugBuster for 30 minutes (**Figure 3.40 A**). Equivalent results were obtained with PSS/PAH-coated microreactors, indicating that the presence of the shell does not affect cell lysis efficiency (data not shown).

To ensure that the MTT assay outcome correlates with an efficient cell lysis, the release of GFP from GFP-expressing microreactors was also analysed. As shown in **figure 3.40 B**, after treatment with 0.25 X BugBuster for 5 and 30 minutes, microreactors released only about 17 and 29 % of GFP respectively. Although most of the cells appeared dead after treatment with 0.25 X BugBuster, the release of GFP was not efficient suggesting that cells were not completely lysed. On the other hand, when microreactors were treated with 0.5 X BugBuster about 82 % of the GFP was already present in the supernatant after 5 minutes incubation and about 93 % after 15-30 minutes. No significant improvement was observed at higher detergent concentration.

A

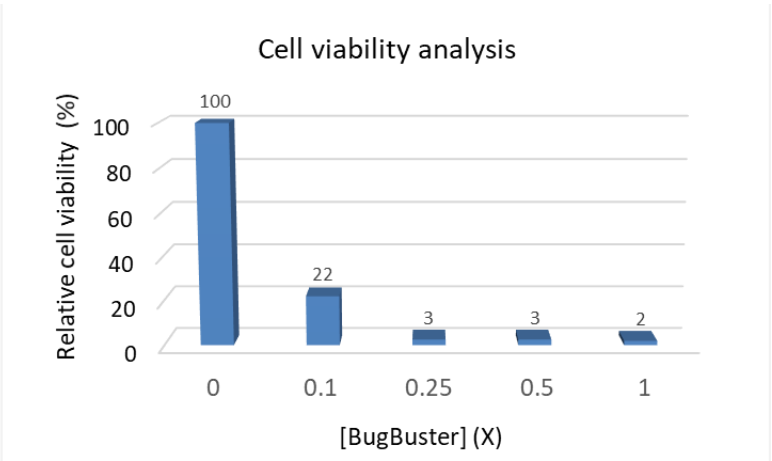

B

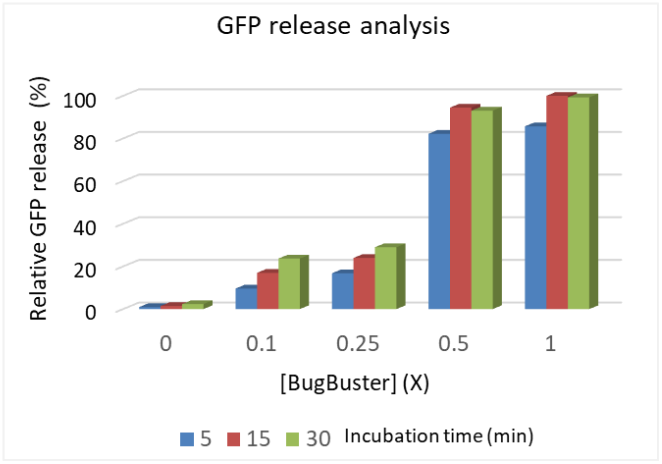


**Figure 3.40.** Effect of BugBuster concentration on cell lysis. (**A**) Cell viability determination through the MTT reduction assay at increasing BugBuster concentrations. (**B**) Analysis of the relative GFP released in the supernatant from GFP-expressing microreactors at increasing BugBuster concentrations.

In addition to BugBuster, the benefit of using the commercial autolytic strain XJb (DE3) to improve cell lysis efficiency was also analysed. In this strain, the arabinose-induced expression of the bacteriophage λ endolysin is supposed to weaken the cell wall allowing higher cell lysis efficiency. As shown in **figure 3.41**, GFP-expressing microreactors prepared using this strain released in the supernatant about 97 % of GFP after treatment with 0.2 X BugBuster. By contrast, GFP-expressing microreactor prepared using the standard expression strain BL21 (DE3) released about four fold less protein at the same conditions. Although the autolytic strain alone cannot be used as alternative to the chemical cell lysis, it allows to considerably reduce the amount of BugBuster needed.

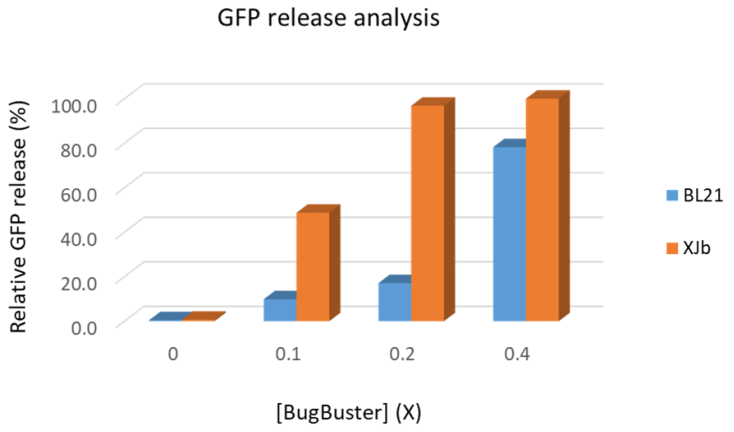


**Figure 3.41.** Analysis of the GFP release in the supernatant from microreactors harboring GFP-expressing BL21 or XJb at increasing BugBuster concentrations.

### 3.2.6 Unreacted fluorescent substrate peptide washing optimization

With the aim to detect even minimal fluorescence intensity changes between samples, the reduction of the fluorescent background after incubation of microreactors with the fluorescent substrate peptide was highly desirable. In order to achieve an efficient removal of unreacted fluorescent substrate peptides, a series of detergents were screened for their capability to break up electrostatic and hydrophobic interactions that may occur between the fluorescent recognition peptide substrate and the cellular or capsule components.

In a preliminary screen, microreactors expressing the inactive sortase A (SaSrtA-C184G) were treated with BugBuster for cell lysis and, after washing, incubated with the fluorescent labeled peptide FITC-LPXTGE. Upon removal of the supernatant, microreactors were incubated with a washing solution containing one of the detergents selected for the screen. Three non-ionic (Tween 20, TritonX-100, IGEPAL CA630) and one zwitterionic detergents (Zwittergent 3-14) were used because unlike ionic detergents are considered to be "mild" thereby allowing proteins to retain their native structure and function. Following washing steps without detergents, microreactors were examined for the residual fluorescence by fluorescence microscopy. The results of this screen showed that efficient peptide removal is possible by using washing solutions containing 0.1% Triton-X 100 or Zwittergent 3:14.

To confirm these results and to further optimize peptide washing conditions, microreactors expressing either Gly6-AlgQ2-SrtA or the inactive Gly6-AlgQ2-SrtA-C184G were reacted with FITC-LPXTGE and subsequently washed with Triton-X 100 or Zwittergent 3:14 before COPAS analysis. In addition, the influence of the ionic strength and the pH of the washing solution was evaluated.

By calculating the ratio between the median value of the green fluorescent signal of the wild type and the inactive population respectively, the extent of the fluorescence intensity change between the two populations was determined for each condition. The results have shown that higher ratios, and therefore best washing conditions to reduce the fluorescence background, are obtained with Triton X-100 or Zwittergent 3:14 at pH 10 (**figure 3.42**). These conditions were found optimal for both uncoated and PSS-PAH-coated microreactors.

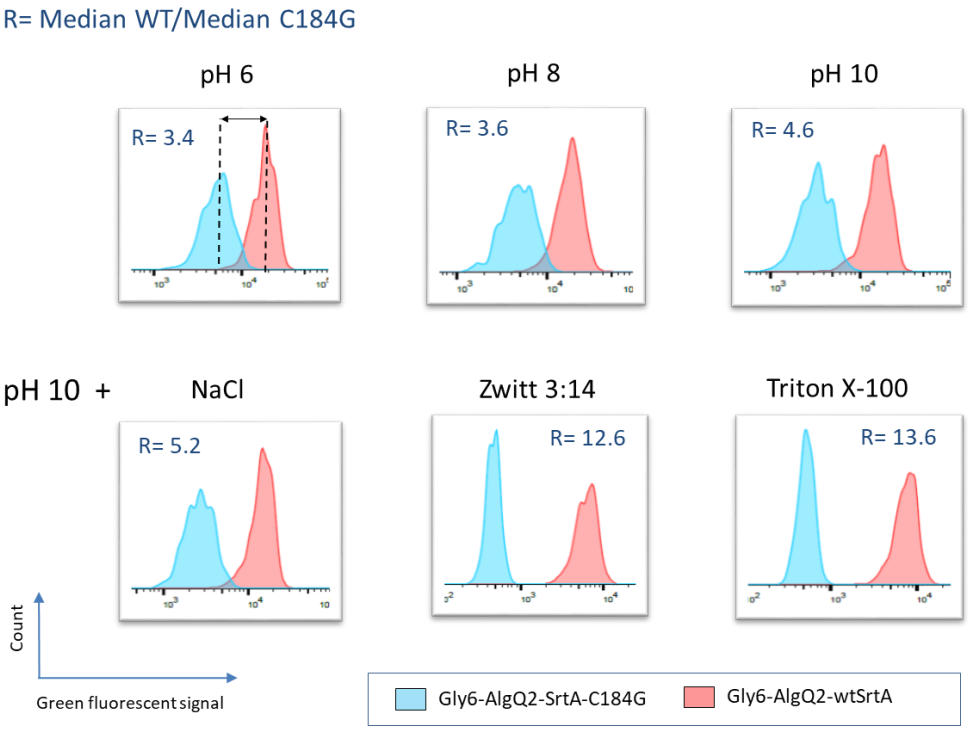


**Figure 3.42.** Unreacted peptide washing analysis; microreactors expressing either Gly6-AlgQ2-SrtA or the inactive Gly6-AlgQ2-SrtA-C184G were reacted with 50 µM FITC-LPETGE for 18 hours at 30 °C and subsequently washed three times with either 25 mM MES pH 6, 25 mM Tris/HCl pH 8 or 25 mM Glycine pH 10 for 5 minutes. Washing at pH 10 was also performed in presence of either 1 M NaCl, 0.1% Zwittergent 3-14 or 0.1% Triton X-100. Following COPAS analysis, the ratio (R) between the median value of the green fluorescent signal for microreactors expressing the wild type and the inactive SaSrtA was calculated for each condition. Higher ratios, and therefore best washing conditions were obtained at pH 10 in presence of Triton X-100 or Zwittergent 3:14. Shown are overlays of histograms of microreactors analyzed with COPAS.

### 3.2.7 Fluorescence normalization with Propidium Iodide

With the goal to precisely screen for sortase mutants with higher activity, the green fluorescent signal developed by the sortase activity should be normalized for the amount of sortase assayed within each microreactor. Supposing that the expression of the mutant enzymes remains approximately constant, the amount of enzyme assayed within microreactors will be proportional to the number of lysed cells that can be quantified by using propidium iodide (PI), a red fluorescent DNA intercalating agent that cannot cross the membrane of live cells. Once bound to DNA, its fluorescence is enhanced 20-30 fold and with a fluorescence emission maximum at 617 nm can be used in combination with FITC to quantify the lysed biomass within each microreactor during COPAS analysis and sorting (**figure 3.43**).

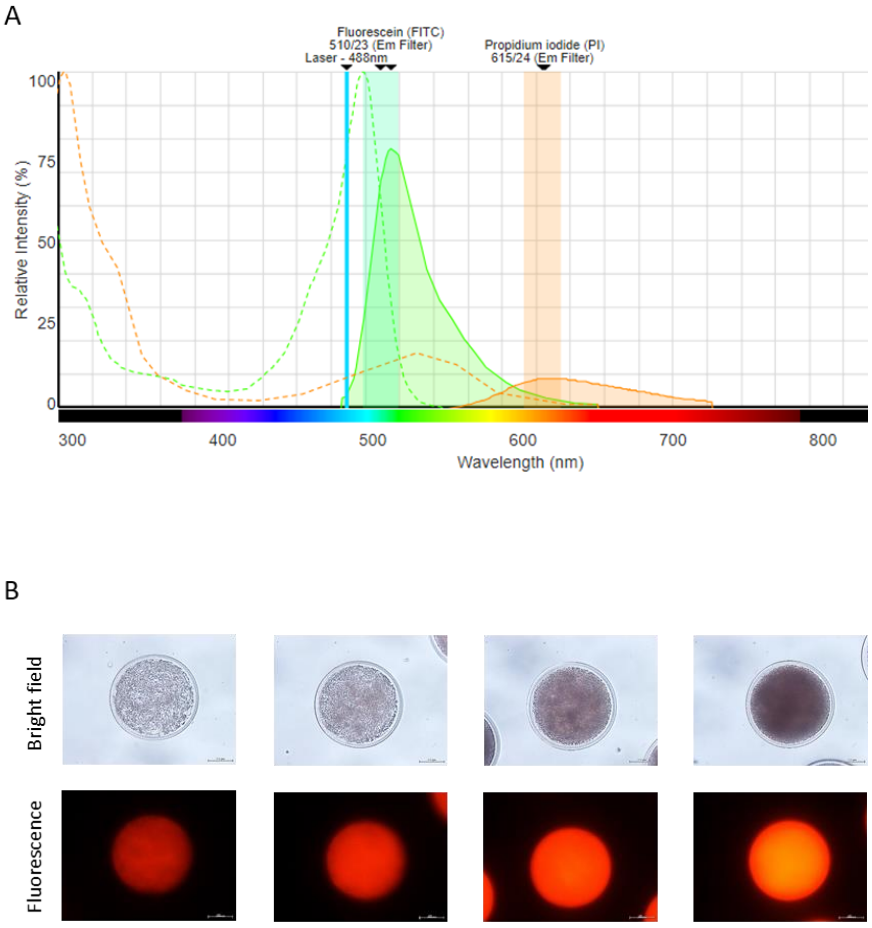


**Figure 3.43.** (**A**) Excitation and emission spectra simulation of Fluorescein isothiocyanate (FITC) and propidium iodide (PI). FITC and PI emission spectra overlap can be corrected by COPAS through fluorescence compensation (**B**) Bright field (upper panel) and fluorescence microscopy analysis (lower panels) of microreactors incubated with propidium iodide after BugBuster treatment showing that at increasing cell densities (from left to right) correspond increasing red fluorescence signals. The size bar corresponds to 100 µm.

### 3.2.8 Genotype recovery from individual microreactors

The recovery of the genotype from individual microreactors was possible using two alternative strategies: PCR and electroporation. In both cases, microreactors were dissolved to make the plasmid accessible. While dissolution of uncoated microreactors was simply achieved by treatment with NaHCO3 (MA Xiao-Jun, 2004), dissolution of PSS-PAH-coated microreactors required a short treatment with a solution of NaOH (pH ≥ 12) to deprotonate the polycation PAH and disassemble the polyelectrolyte complex shell (Déjugnat and Sukhorukov, 2004).

As can be seen in **figure 3.44**, amplification of the gene of interest from the plasmid was possible from microreactors at each phase of the assay workflow (untreated, lysed, reacted, washed). However, no amplification product was observed when a dissolved empty bead, taken from the reaction mixture, was used as template for PCR reaction showing that microreactors do not exchange the plasmids between microreactors during the whole assay duration.

Although PCR is very sensitive and would allow to amplify few DNA molecules, direct transformation of the plasmid into the expression strain would simplify the assay workflow. When electrocompetent BL21 cells were electroporated, up to 500 transformants were obtained from a single uncoated microreactor. Possibly, due to complexation of the plasmid with the polycation PAH, slightly lower transformation efficiencies (up to 150 CFU) were achieved by using individual PSS-PAH-coated microreactors.

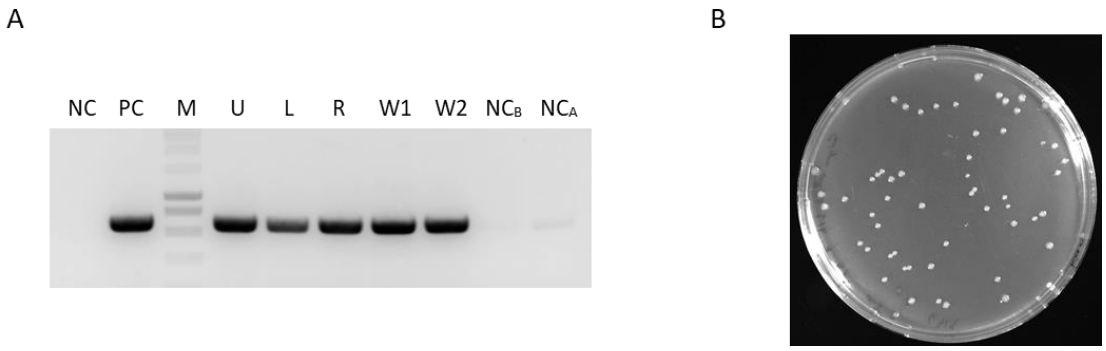


**Figure 3.44.** Genotype can be recovered from a single microreactor by PCR or electroporation (**A**) Agarose gel electrophoresis of PCR reactions performed using as template a single microreactor from each phase of the assay workflow. NC: Negative control (No template), PC: Positive control, M: DNA Ladder, U: Untreated microreactor, L: Lysed microreactor, R: Reacted microreactor, W1: Microreactor after 1 hour peptide washing, W2: Microreactor after 2 hours peptide washing, $NC_B$: Not-colonized microreactor before treatments, $NC_A$: Not-colonized microreactor after treatments. (**B**) LB agar plate showing transformants obtained after electroporation into *E. coli* BL21 of an aliquot of a single dissolved PSS-PAH-coated microreactor.

## 3.2.9 Validation of the microreactor-based assay

Following the optimization of the various steps of the assay, the complete procedure was tested using uncoated microreactors expressing the Gly6-AlgQ2-SrtA and PSS-PAH-coated microreactors expressing the construct G-SrtA.

### 3.2.9.1 Validation of the assay with Gly6-AlgQ2-wtSaSrtA

To assess the functionality of the assay with Gly6-AlgQ2-SrtA, the ability of the intracellularly expressed fusion protein to capture exogenous fluorescent peptide within hollow-core-based microreactors was examined. To this end, individual *E. coli* cells, harbouring the plasmid encoding either Gly6-AlgQ2-SrtA wild type or the inactive Gly6-AlgQ2-SrtA-C184G were encapsulated within hollow-core chitosan-alginate microcapsules and grown to generate microreactors expressing the respective fusion protein. Following cell lysis with BugBuster, microreactors were washed to remove excess of the detergent mixture and the sortase-mediated conjugation initiated by the addition, in the reaction buffer, of the FITC-labeled peptide carrying the recognition sequence LPETG specific for SrtA (FITC-LPETGE). After removal of unreacted substrate peptide, microreactors were analyzed by fluorescence microscopy and COPAS to evaluate the extent of reaction. The workflow of the assay is schematized in **figure 3.45 A**. As shown in **figure 3.45 B** and **C**, in comparison to microreactors expressing the inactive construct Gly6-AlgQ2-SrtA-C184G, microreactors expressing Gly6-AlgQ2-SrtA wild type exhibited high levels of fluorescence indicating a substantial conjugation and capture of the fluorescent peptide.

A

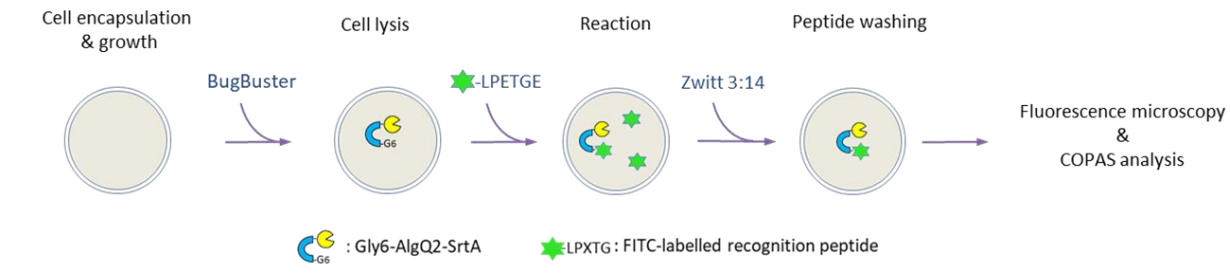

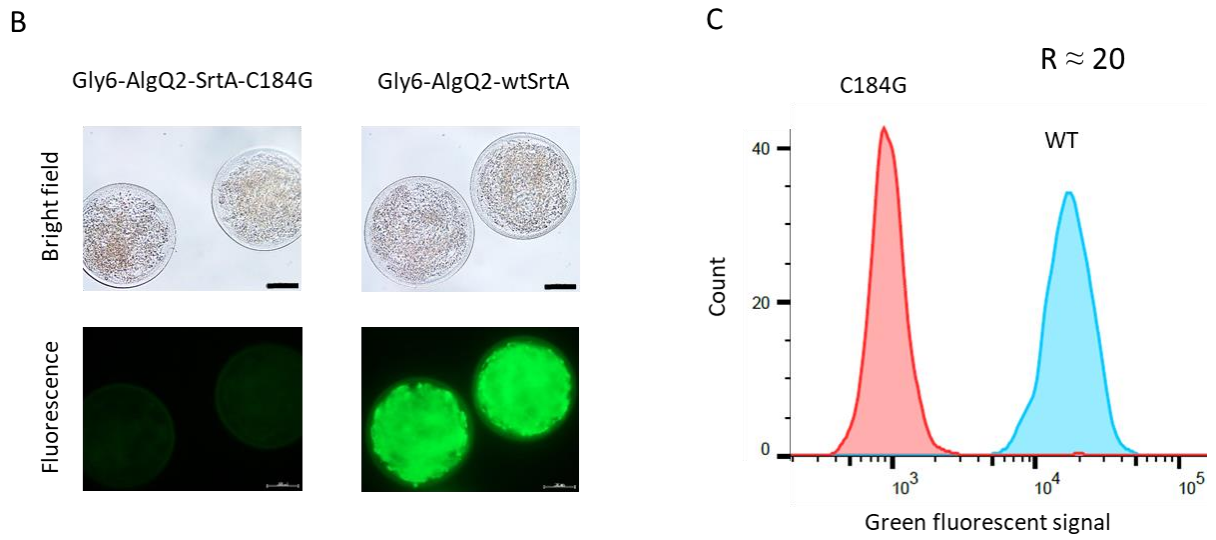


**Figure 3.45.** (**A**) Workflow of the assay performed with microreactors expressing the construct Gly6-AlgQ2-SrtA. (**B, C**) Microscope and COPAS analysis showing successful conjugation and capture of the fluorescent peptide FITC-LPETGE within microreactors expressing Gly6-AlgQ2-SrtA wild type (WT). Microreactors expressing Gly6-AlgQ2-SrtA-C184G were used as negative control. After encapsulation within HC-CAM, cells were grown in TB auto for 18 hours at 30 °C. For the reaction, microreactors were lysed in 25 mM Tris pH 8.2, 150 mM NaCl, 10 mM $CaCl_2$ and incubated in the same buffer with 10 µM FITC-LPETGE for 16 hours at 30 °C. (**B**) Bright field (upper panel) and fluorescence pictures (lower panel) of reacted microreactors. Fluorescence exposure time 1/50s; the size bar corresponds to 100 µm. (**C**) Overlay of histograms of Gly6-AlgQ2-SrtA wild type (blue) and Gly6-AlgQ2-SrtA-C184G (red) microreactors analyzed with COPAS. The ratio (R) between the median value of the green fluorescent signal of microreactors expressing the wild type and the inactive SaSrtA is given.

To confirm that the fluorescent signal originates from the Gly6-AlgQ2-SrtA-mediated intramolecular capture of the fluorescent substrate peptide, microreactors were dissolved and protein samples analyzed by SDS-PAGE and fluorescence scanning. In addition, western blot analysis was performed to verify whether the construct Gly6-AlgQ2-SrtA, by interacting through the AlgQ2 moiety with the alginate in the microreactors, is specifically retained inside microreactors (**Figure 3.46**).

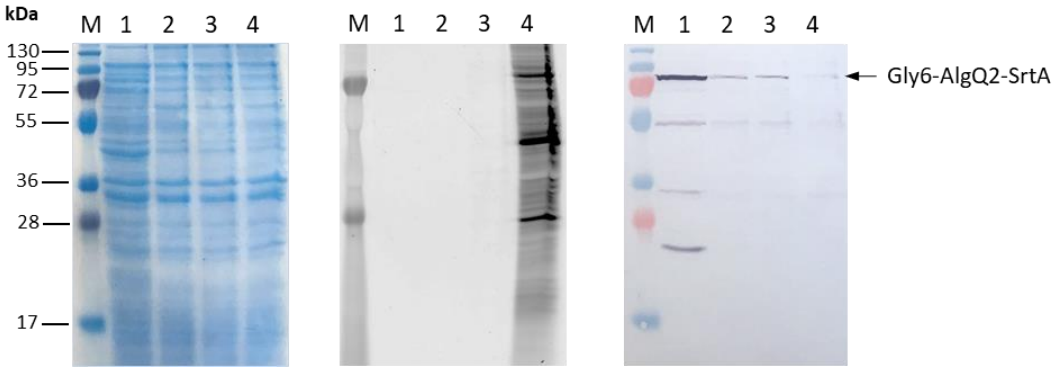

**Figure 3.46.** Coomassie-stained SDS-PAGE gel (left), fluorescence scan (middle) and western blot analysis (right) of samples of Gly6-AlgQ2-SrtA-expressing microreactors incubated without fluorescent peptide (lane2), with the class B specific peptide FITC-DNPNTGDE (lane3) and with the class A specific peptide FITC-LPETGE (lane4). The fluorescence scan shows that most of the fluorescent signal comes from unrelated *E. coli* proteins labeled by SaSrtA. The western blot analysis shows that after cell lysis and reaction (lane 2, 3, 4) the fusion protein Gly6-AlgQ2-SrtA is not retained inside microreactors as compared to untreated microreactors (lane 1). The Coomassie-stained gel confirmed equal protein loading.

Consistent with previous results, fluorescent signals were generated with microreactors expressing Gly6-AlgQ2-SrtA wild type incubated with the recognition peptide specific for SaSrtA (FITC-LPETGE, lane 4) but not in absence of recognition peptide (lane 2) or with a class B specific peptide (FITC-DNPNTGDE, lane 3). Interestingly, despite a fluorescent protein of the size of Gly6-AlgQ2-SrtA was detected in the fluorescence scan, the majority of the signal arises from unrelated *E. coli* proteins labeled by SaSrtA possibly at N-terminus glycine or exposed lysine residues. Although the labeling of *E. coli* proteins enhance the total fluorescent signal intensity thereby increasing the assay sensitivity, the directed evolution strategy based on the use of Gly6-AlgQ2-SrtA might select for variants with a reduced specificity towards the oligo-glycine acceptor substrate. In addition, as indicated by western blot analysis, considerable amount of the Gly6-AlgQ2-SrtA was found to diffuse out from reacted microreactors (lane 2, 3, 4) as compared to untreated ones (lane 1). As the release of the fusion construct was also observed from gel-core microreactors (data not shown), we thought that the release of Gly6-AlgQ2-SrtA may be independent of the presence of alginate in the capsule core. In the attempt to explain this observation, we found that the interaction between AlgQ2 and the alginate is reverted in presence of 150 mM sodium chloride normally employed during the assay. Likely, sodium ions shield the negative charges of the alginate thereby preventing electrostatic interaction with AlgQ2 (**Figure 3.47)**.

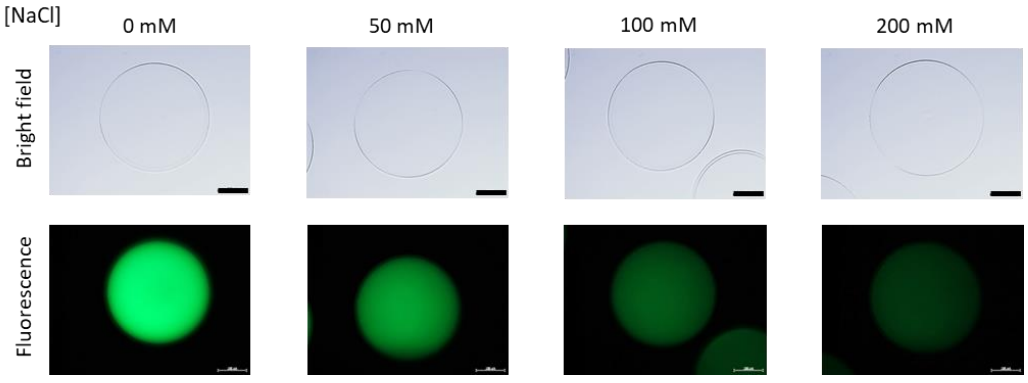


**Figure 3.47.** Binding analysis of AlgQ2 to alginate beads at increasing NaCl concentrations. About 2000 alginate beads were incubated in 25 mM Tris pH 8.0, 10 mM $CaCl_2$ with 500 nM of AlgQ2-GFP then washed for 30 min with the same buffer containing increasing NaCl concentrations. Shown are the alginate beads in bright field and as fluorescence images (Exposure time 1/500s). The size bar corresponds to 100 µm

In addition to the above-mentioned issues, when C-terminal fusion constructs with AlgQ2 were purified by affinity chromatography, a smaller protein was always co-purified (**figure 3.48 A**). On the basis of the band size, it was speculated that this second product was the result of a degradation event occurring at the C-terminal region of AlgQ2. As consequence, beyond the need of a second purification step to obtain pure fusion constructs, the putative degradation of the fusion Gly6-AlgQ2-SrtA represented an issue for the development of the microreactor-based assay as it could negatively affect the assay sensitivity.
The determination of the N-terminal sequence of this protein product (EDMAN degradation service, FGCZ, Zurich) revealed that the putative degradation event occurs in correspondence of the two consecutive methionine residues $Met^{505}$ and $M^{506}$ located within the C-terminal helix of AlgQ2 (**figure 3.48 B**).


**Figure 3.48.** (**A**) SDS-PAGE analysis of Gly6-AlgQ2-eSrtA purification showing the presence of an additional protein product in the eluate fraction (E). (**B**) AlgQ2 structural model generated with Chimera from the atomic coordinates of 1KWH (Momma et al., 2002). The C-terminal helix and the putative cleavage site are highlighted in cyan and magenta respectively.

To assess whether degradation could be avoided by removing the putative degradation site, AlgQ2 was shortened at the C-terminus by 6, 12 and 18 amino acids (meaning the partial or total removal of the C-terminal helix of AlgQ2) and the resulting AlgQ2 variants fused with eSaSrtA were purified by affinity chromatography. The SDS-PAGE analysis did not provide any evidence about the removal of this second protein product but rather showed that shortening AlgQ2 at the C-terminal impair the stability of the relative fusion proteins (**figure 3.49**).

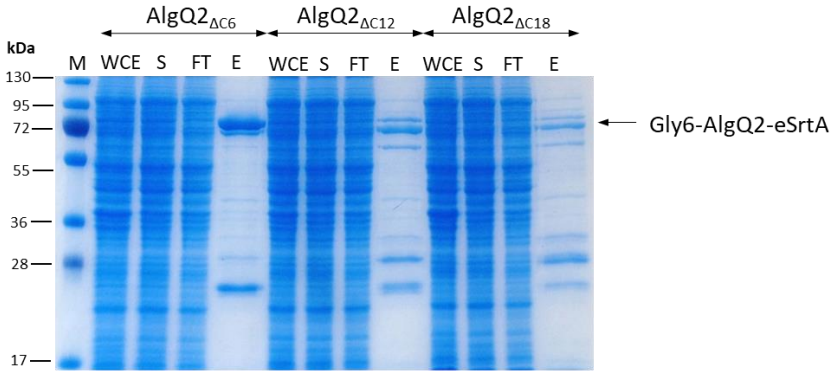


**Figure 3.49.** SDS-PAGE analysis of the purification of Gly6-AlgQ2$_{\Delta C6}$, Gly6-AlgQ2$_{\Delta C12}$ and Gly6-AlgQ2$_{\Delta C18}$ fusion constructs with eSrtA. Shortening of the C-terminus of AlgQ2 impairs the stability of the resulting fusion proteins. M: Protein Ladder; WCE: whole cell extract; S: Clarified cell lysate; FT: Flow through; E: Eluate

Next, to test whether this side product may originate from the messenger RNA translation starting from this downstream methionine, the RBS translation rate calculator (Espah Borujeni et al., 2014; Salis et al., 2009) was employed to predict the translation rate from each putative start codon of the messenger RNA encoding for AlgQ2. This tool makes use of a free energy model to calculate the total binding free energy between the ribosome and mRNA and relate the total free energy change to the mRNA's translation initiation. The analysis revealed for the start codon corresponding to the methionine 506 the third highest value of translation rate among other putative in frame start codons (the first highest being the first methionine residue downstream the promoter) therefore suggesting translation from this methionine residue. To test this hypothesis, we employed the RBS translation rate calculator to identify which silent nucleotide base substitutions upstream Met$^{505}$ and M$^{507}$ codons caused a reduction of the translation rate from these residues. For instance, when codons encoding for AlgQ2 residues Gln$^{501}$ and Val$^{502}$ were changed from CAG and GTT to CAA and GTC respectively, the predicted translation rate starting from codons encoding for Met$^{505}$ and M$^{507}$ decreased from 1208 to 24 and 39 (au) respectively. When the fusion protein Gly6-AlgQ2-eSrtA containing the above-mentioned mutations was expressed and purified using the same procedure as for the unmodified Gly6-AlgQ2-eSrtA, the presence of the small side product was drastically reduced (**figure 3.50**). Although further analysis would be required, this result clearly supported the hypothesis of protein translation from an internal methionine residue.

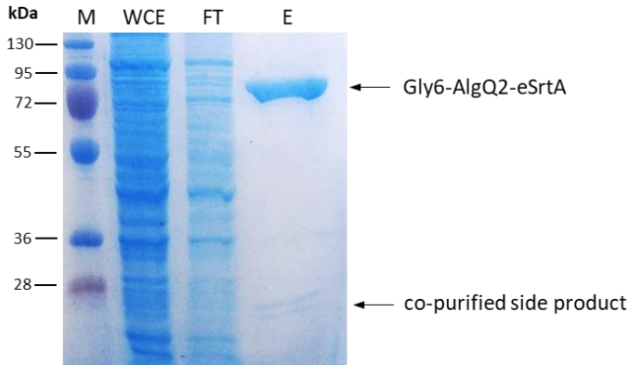


**Figure 3.50.** Purification of the fusion protein Gly6-AlgQ2-eSrtA constructed after the RBS translation rate analysis. The construct contains silent mutations in the codons codifying for the residues $Gln^{501}$ and $Val^{502}$ of AlgQ2 that are predicted to reduce the translation rate from the internal methionine 506 and 507. The SDS-PAGE analysis revealed a notable reduction of the presence of the side product. M: Protein Ladder; WCE: whole cell extract; S: Clarified cell lysate; FT: Flow through; E: Eluate

Although a significant fluorescent change was observed for microreactor expressing Gly6-AlgQ2-SrtA wild type in comparison to those expressing Gly6-AlgQ2-SrtA-C184G, the results have shown that the fusion construct and the relative fluorescent transpeptidation products are not retained within microreactors. This prevent a direct correlation between the sortase activity and the fluorescent output signal making the conjugation and product capture strategy based on the alginate binding protein AlgQ2 unsuitable for the development of the assay.

### 3.2.9.2 Validation of the assay with G-SaSrtA

To assess the functionality of the assay using the single glycine-modified SrtA (G-SrtA), microreactors expressing either G-SrtA wild type or the inactive G-SrtA-C184G were prepared and subsequently coated with a single layer of PSS and PAH. Following cell lysis, incubation with FITC-LPETGE and unreacted peptide removal, microreactors were analysed for the fluorescence. As expected, fluorescence microscopy and COPAS analysis revealed higher level of fluorescence for microreactors expressing the wild type G-SrtA as compared to those expressing the inactive enzyme demonstrating the ability of G-SrtA to capture the fluorescent substrate peptide within PSS-PAH-coated microreactors (**Figure 3.51**).

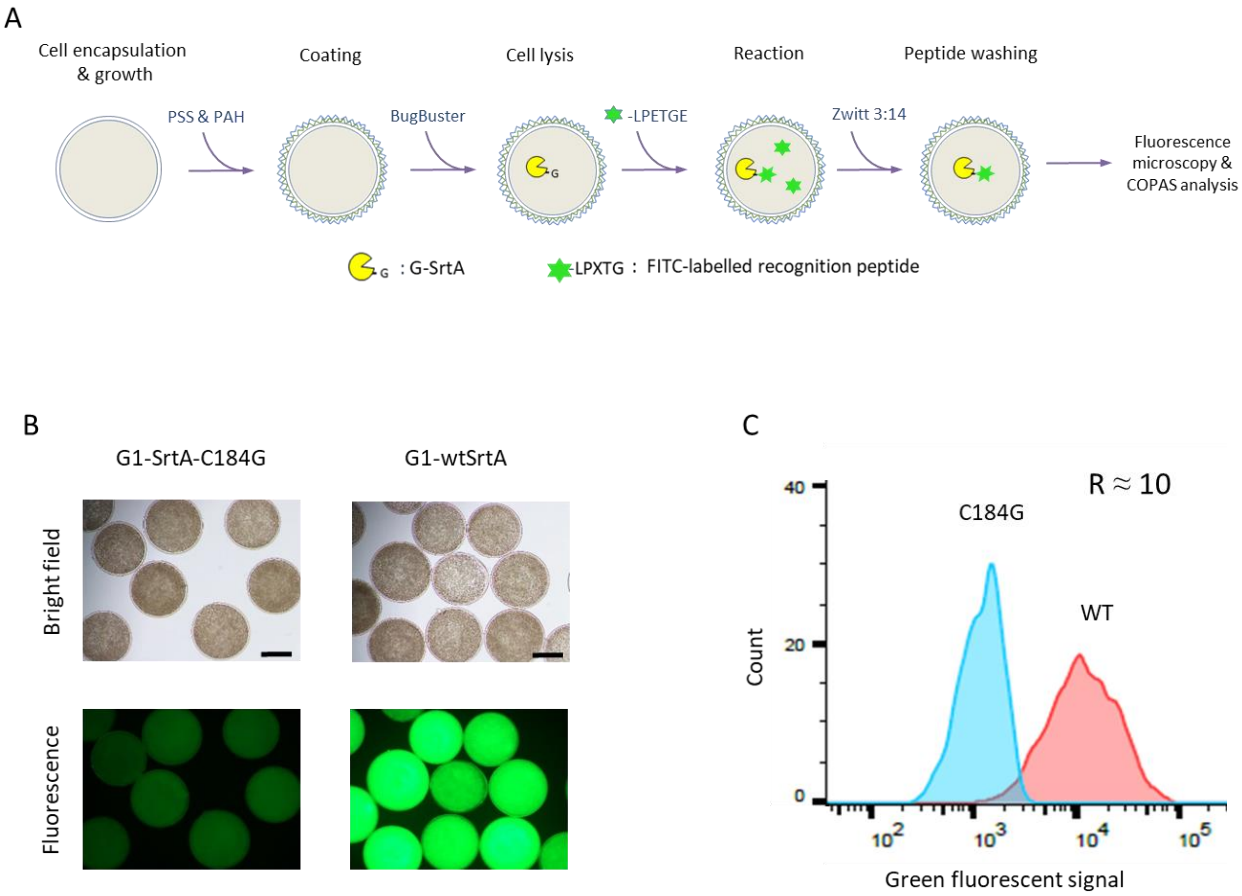


**Figure 3.51.** (**A**) Workflow of the assay performed with PSS-PAH-coated microreactors expressing the construct G-SrtA (**B, C**) Microscope and COPAS analysis showing successful conjugation and capture of the fluorescent peptide FITC-LPETGE within microreactors expressing G-SrtA wild type. Microreactors expressing G-SrtA-C184G were used as negative control. After encapsulation within HC-CAM, cells were grown in TB auto for 18 hours at 30 °C. Following PSS-PAH coating, microreactors were lysed in 25 mM Tris pH 8.2, 150 mM NaCl, 10 mM $CaCl_2$ and subsequently incubated in the same buffer with 10 µM FITC-LPETGE for 16 hours at 30 °C. (**B**) Bright field (upper panel) and fluorescence pictures (lower panel) of reacted microreactors. Fluorescence exposure time 1/50s; the size bar corresponds to 200 µm. (**C**) Histogram overlay showing fluorescence distribution of G1-SrtA wild type (red) and G1-SrtA-C184G (blue)-expressing microreactors populations analyzed with COPAS. The ratio (R) between the median value of the green fluorescent signal of microreactors expressing the wild type and the inactive SaSrtA is given.

Next, to prove that PSS-PAH-coated microreactors behave as isolated reaction compartments and efficiently retain G-SrtA during the whole application duration, microreactors were mixed in 1:10 ratio of wildtype:C184G and following PSS-PAH coating were reacted with FITC-LPETGE in the same tube. The same mixture of uncoated microreactors was used as control. The fluorescence microscopy analysis revealed that, in both mixtures, about 10% of total microreactors (those expressing G-SrtA wild type) exhibited higher level of fluorescence in comparison to the remaining 90%. However, coated microreactors displayed greater fluorescence than uncoated microreactors indicating a better retention of G-SrtA within PSS-PAH-coated microreactors (**Figure 3.52 A**). Accordingly, when reacted PSS-PAH-coated or uncoated microreactors expressing G-SrtA wild type were dissolved and analyses by SDS-PAGE and gel fluorescence scanning, the majority of G-SrtA was found to diffuse out from uncoated microreactors. On the other hand, as comparable amounts of G-SrtA were detected in both untreated (U) and reacted (R) samples, the presence of the PSS-PAH shell efficiently prevented G-SrtA from escaping coated microcapsules (**Figure 3.52 B**)

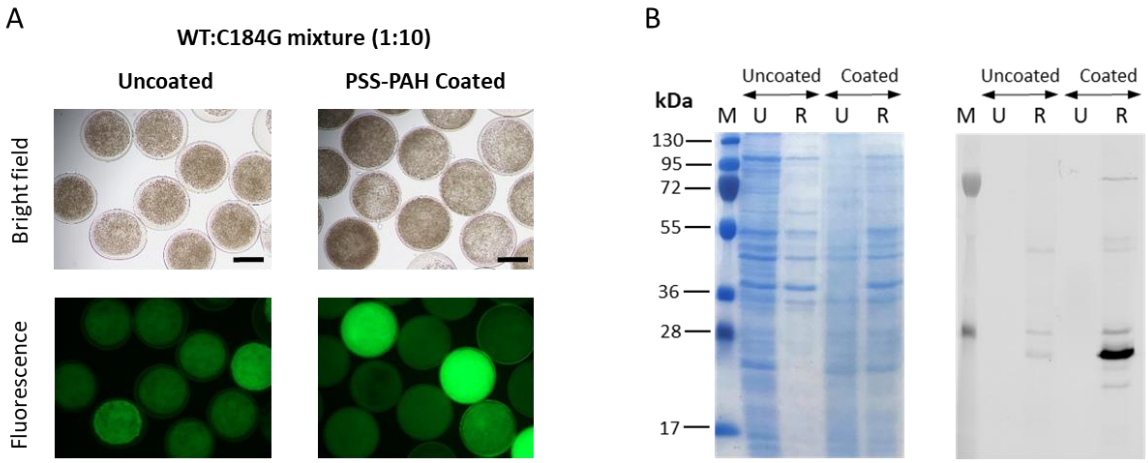


**Figure 3.52.** The PSS-PAH shell prevents the diffusion of G-SrtA. (**A**) Microscope analysis of reacted mixtures of G1-SrtA wild type (WT) and C184G-expressing microreactors in a 1 to 10 ratio. When coated, microreactors expressing G-SrtA wild type display higher level of fluorescence than uncoated microreactors demonstrating a better retention of G-SrtA.; the size bar corresponds to 200 µm. (**B**) Coomassie-stained SDS-PAGE gel and fluorescence scan of PSS-PAH-coated and uncoated G1-SrtA-expressing microreactors before any treatment (Untreated, U) and after reaction (Reacted, R). In comparison to uncoated microreactors, PSS-PAH-coated microreactors ensure the retaining of G-SrtA.

Interestingly, while the reaction performed within uncoated microreactors expressing Gly6-AlgQ2-SrtA typically led to a 20-fold increase in fluorescence intensity (see **figure 3.45 A**), the reaction performed within PSS-PAH-coated microreactors expressing G-SrtA typically showed comparable or lower fluorescence intensities. However, comparison of the total fluorescent signal obtained by reacting whole cell extracts of cultures expressing either Gly6-AlgQ2-SrtA or G-SrtA with FITC-LPETGE (**Figure 3.53**)

clearly indicate that much higher levels of fluorescence are expected for PSS-PAH-coated microreactors expressing G-SrtA than for uncoated microreactors expressing Gly6-AlgQ2-SrtA. This observation suggests that the presence of the PSS-PAH polyelectrolyte shell might hamper the proper diffusion of the fluorescent recognition peptide inside PSS-PAH-coated microreactors thereby reducing the catalytic efficiency of G-SrtA. Although further optimizations that allow to precisely control the diffusion of molecules through the polyelectrolyte shell are required, the results have shown that the microreactor-based assay that rely on this strategy can be employed for the laboratory evolution of sortases.

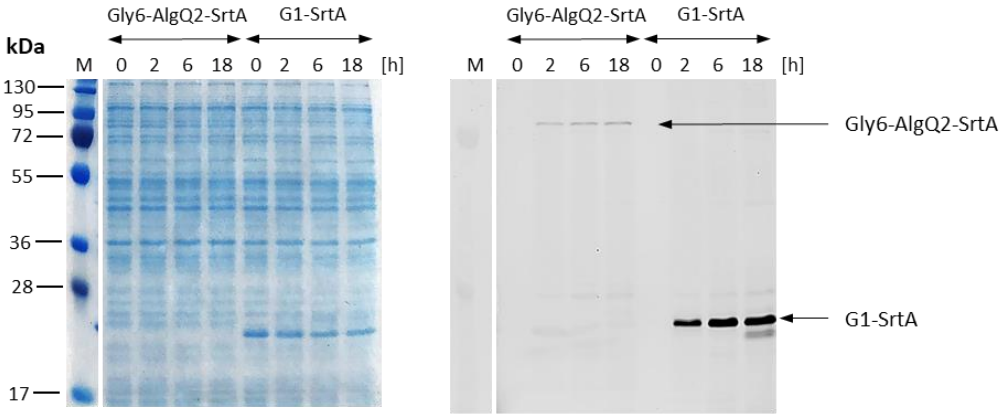


**Figure 3.53.** Comparison of Gly6-AlgQ2-SrtA and G-SrtA conjugation efficiency in whole cell extracts at different time points shows that much higher level of fluorescence and therefore higher sensitivity for the assay can be obtained using the construct G-SrtA. For the reaction, whole cell extracts were reacted with 50 µM FITC-LPETGE in 25 mM Tris/HCl pH 8.2, 150 mM NaCl, 10 mM $CaCl_2$ at 30 °C.

### 3.2.10 Microreactor-based assay with sortase B from *B. anthracis*

Once established for SaSrtA, the functionality of the microreactor-based assay was probed for sortase B from *B. anthracis*. Due to its very low activity, this sortase represents a very challenging target for directed evolution.

First, as described for SaSrtA, the fusion protein Gly6-AlgQ2-SrtB was constructed, purified and analysed for its capability to capture intramolecularly the fluorescent recognition peptide FITC-DNPNTGDE. As previously described for Gly6-AlgQ2-eSrtA (**section 3.2.3.1.2**), when Gly6-AlgQ2-SrtB was incubated at three different concentrations with FITC-DNPNTGDE, comparable amounts of labeled protein were generated independently of the protein concentration (**Figure 3.54**). Even in this case, in comparison to the reference reaction performed with equimolar concentrations of Gly6-AlgQ2 and BaSrtB (**lane Ref**), reactions performed with Gly6-AlgQ2-SrtB displayed a much higher conjugation efficiency, indicating that, similar to Gly6-AlgQ2-eSrtA, Gly6-AlgQ2-SrtB labels itself through an intramolecular reaction.

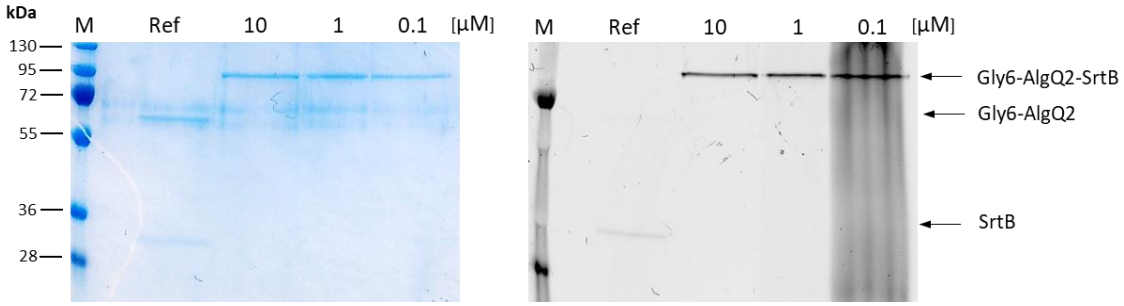


**Figure 3.54.** Gly6-AlgQ2-SrtB intramolecular labeling evaluation. The recombinant fusion protein Gly6-AlgQ2-SrtB was incubated at three different concentrations (10, 1 or 0.1 µM) with an excess of FITC-DNPNTGDE (40 µM) in 25 mM Tris/HCl pH 8.2, 150 mM NaCl, 10 mM $CaCl_2$ for 20 hours. The reaction performed with equimolar concentrations (10 µM) of Gly6-AlgQ2 and SrtB was used as reference (Ref). 3 pmol of Gly6-AlgQ2-SrtB from each reaction were analyzed by SDS-PAGE gel fluorescence scanning (right panel). Equal protein loading was assessed by staining the gel with Coomassie (left panel). Comparable amounts of labeled protein for the three reactions and higher conjugation efficiency compared to the reaction performed with separate components suggest that Gly6-AlgQ2-SrtB labels itself intramolecularly.

However, when the ability of Gly6-AlgQ2-SrtB to capture the fluorescent substrate peptide was examined within microreactors, no increase in fluorescence intensity was detected with COPAS for microreactors expressing Gly6AlgQ2-SrtB wild type as compared to microreactors expressing the inactive Gly6-AlgQ2-SrtB-C233G **(Figure 3.55)**.

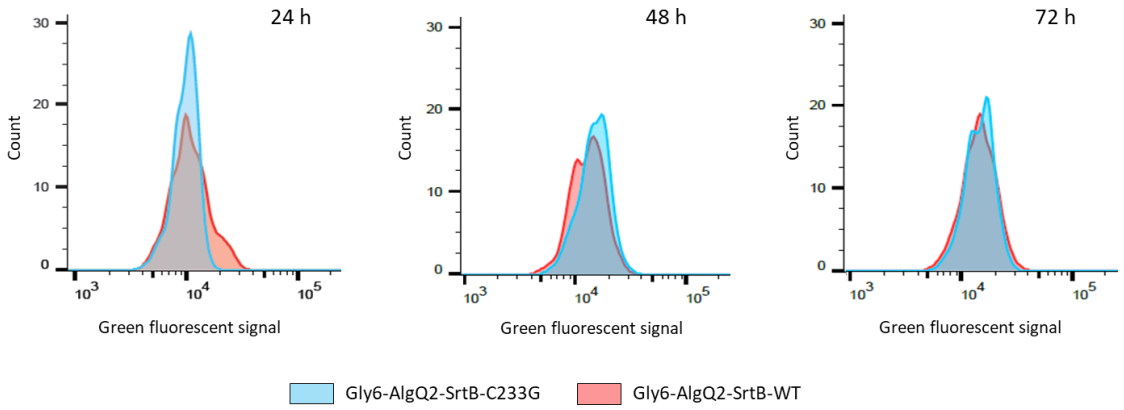


**Figure 3.55.** Histogram overlays showing fluorescence distribution of Gly6-AlgQ2-SrtB wild type (red) and Gly6-AlgQ2-SrtB-C233G (blue)-expressing microreactors populations analyzed with COPAS after 24, 48 and 72 hours reaction. No fluorescence change was detected for microreactors expressing Gly6-AlgQ2-SrtB wild type as compared to microreactors expressing the inactive Gly6-AlgQ2-SrtB-C233G.

As shown for SaSrtA, in the attempt to improve the conjugation efficiency, the N-terminus of BaSrtB was elongated by the addition of one, two or three glycine residues and the expression-activity relationship of these modified sortases was analysed. Unlike SaSrtA, no significant protein expression reduction was observed for the modified BaSrtB. However, as observed for SaSrtA, a single glycine at the N-terminus was sufficient to provide a significant reaction rate improvement (**Figure 3.56**). Although no additional experiments were performed, it is likely that, as for G-SrtA, G-SrtB labels itself through an intramolecular conjugation reaction.

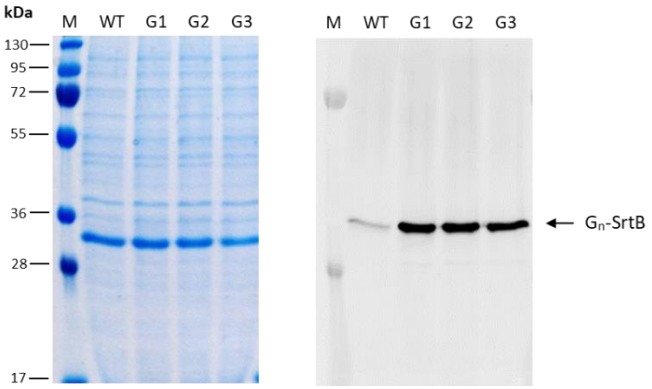


**Figure 3.56.** Expression-activity relationship of wild type and N-terminally glycine-modified BaSrtB. Whole cell extracts (WCE) of *E. coli* cultures expressing SrtB variants were incubated with 50 µM FITC-DNPNTGDE in 25 mM Tris/HCl pH 8.2, 150 mM NaCl, 10 mM $CaCl_2$ for 20 hours at 30 °C and subsequently analysed by SDS-PAGE (left) and fluorescence scanning (right). In comparison to the unmodified wild type SrtB (G0-SrtB), the presence of one (G1) or more glycines (G2, G3) at the N-terminus results in a significant reaction rate improvement. Unlike N-terminally glycine-modified SrtA, the addition of glycine residues does not cause a protein expression reduction. The conjugation of the fluorescent peptide to the amino-terminal glycine of sortases causes the upshift of the corresponding bands.

Despite the significant improvement in conjugation efficiency, when G-SrtB wild type was reacted with FITC-DNPNTGDE within PSS-PAH-coated microreactors, no change in the fluorescence intensity was detected for the population of microreactors expressing G-SrtB as compared to the population of those expressing the inactive G-SrtB-C233G (**Figure 3.57**). However, when whole cell extracts obtained by dissolving microreactors were reacted with FITC-DNPNTGDE, G-SrtB wild type appeared efficiently labeled (**Figure 3.58**). As mentioned above for the construct G-SrtA (**section 3.2.9.2**), it is possible that the low conjugation efficiency of G-SrtB within PSS-PAH-coated microreactors depends on the presence of the PSS-PAH shell that prevent the efficient supply by diffusion of the fluorescent substrate peptide. In addition, as the cell density within microreactors was calculated about 15 fold higher than in whole cell extracts, it is also possible that the proper diffusion of the fluorescent peptide inside microreactors is hampered by the high-density cell debris clump.

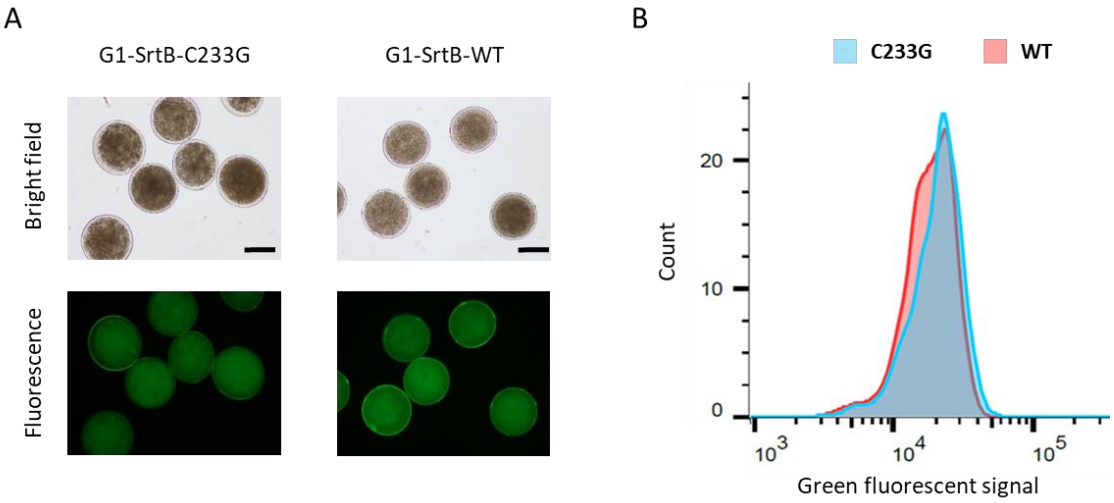


**Figure 3.57.** Microscope and COPAS analyses of reacted microreactors expressing either G1-SrtB wild type or the inactive G1-SrtA-C233G. After encapsulation within HC-CAM, cells were grown in TB auto for 18 hours at 30 °C. Following PSS-PAH coating, microreactors were lysed in 25 mM Tris/HCl pH 8.2, 150 mM NaCl, 10 mM $CaCl_2$ and incubated in the same buffer with 100 µM FITC-DNPNTGDE for 40 hours at 30 °C. (**A**) Bright field (upper panel) and fluorescence pictures (lower panel) of reacted microreactors. Fluorescence exposure time 1/50s; the size bar corresponds to 200 µm. (**B**) Histogram overlay showing fluorescence distribution of G1-SrtB wild type (red) and G1-SrtB-233G (blue)-expressing microreactors populations analyzed with COPAS. No change in the fluorescence intensity was detected for the wild type population of microreactors expressing G-SrtB as compared to those expressing the inactive G-SrtB-C233G.

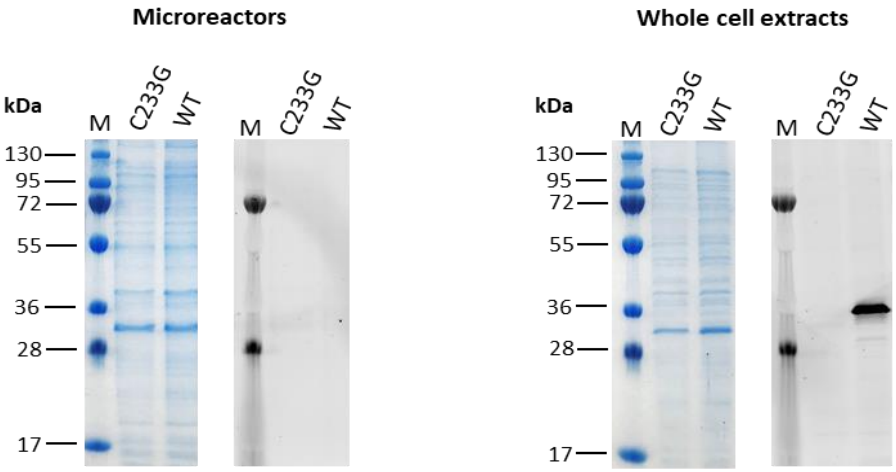


**Figure 3.58.** Conjugation efficiency of G-SrtB is much higher in whole cell extracts than in microreactors. Coomassie-stained SDS-PAGE gels and fluorescence scans of G1-SrtB-mediated conjugation reactions in microreactors (left) and in whole cell extracts obtained by sonicating about 2000 microreactors in 500 µl (right). Both microreactors and whole cell extracts were reacted with 100 µM FITC-DNPNTGDE in 25 mM Tris pH 8.2, 150 mM NaCl, 10 mM $CaCl_2$ for 16 hours at 30 °C. G1-SrtB-C233G was used as negative control.

### 3.2.11 Microreactor-based assay with PaSrtF

In addition to BaSrtB, the functionality of the assay was probed with the newly identified PaSrtF. Since PaSrtF was shown to be soluble and active only at high salt concentration and having understood that AlgQ2 is released from alginate in presence of salt thereby preventing efficient transpeptidation product retention, the sortase-mediated conjugation and product capture strategy based on the use of AlgQ2 was not investigated. Similar to SaSrtA and BaSrtB, the wild type PaSrtF was modified by the addition of one or more glycines at the N-terminus and the protein expression of these proteins analyzed by SDS-PAGE. As can be seen in **figure 3.59 A**, the addition of one glycine caused a strong reduction of protein expression, which appeared almost abolished when two or more glycine residues were present. However, the transpeptidation activity analysis of these modified proteins revealed that only G1-SrtF is able to efficiently capture the fluorescent recognition peptide to generate acceptable readouts (**Figure 3.59 B**).

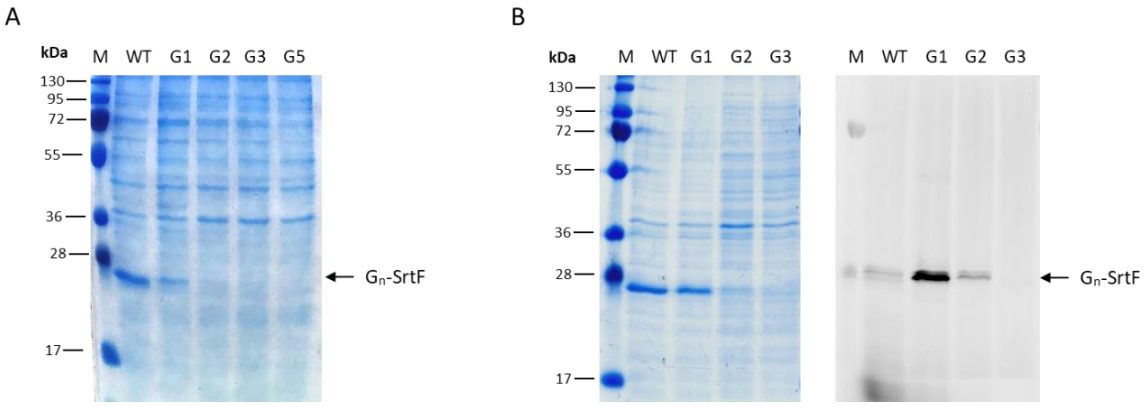


**Figure 3.59** (**A**) Expression analysis of wild type (WT) and N-terminally glycine-modified SrtF. The addition of one glycine residue (G1) at the N-terminus of SrtF causes a significant protein expression reduction. Addition of two or more glycine residues (G2-G5) almost abolish protein expression. (**B**) Expression-activity relationship of wild type (WT) and N-terminally glycine-modified SrtF. Whole cell extracts (WCE) of *E. coli* cultures expressing SrtF variants were incubated with 50 µM FITC-LPETGE in 50 mM Tris-HCl pH 7.65, 500 mM NaCl, 10 mM $CaCl_2$ for 20 hours at 25 °C and subsequently analysed by SDS-PAGE (left) and fluorescence scanning (right). In comparison to the wild type enzyme, G1-SrtF shows improved reaction rates. Because of the very low expression yield, others glycine-modified SrtF variants do not show significant transpeptidation activity.

When PSS-PAH-coated microreactors expressing G-SrtF wild type were reacted with FITC-LPETGE, they appeared more fluorescent than microreactors expressing the inactive G-SrtF homologue (C195G) demonstrating the suitability of the assay for directed evolution of PaSrtF (**Figure 3.60**).

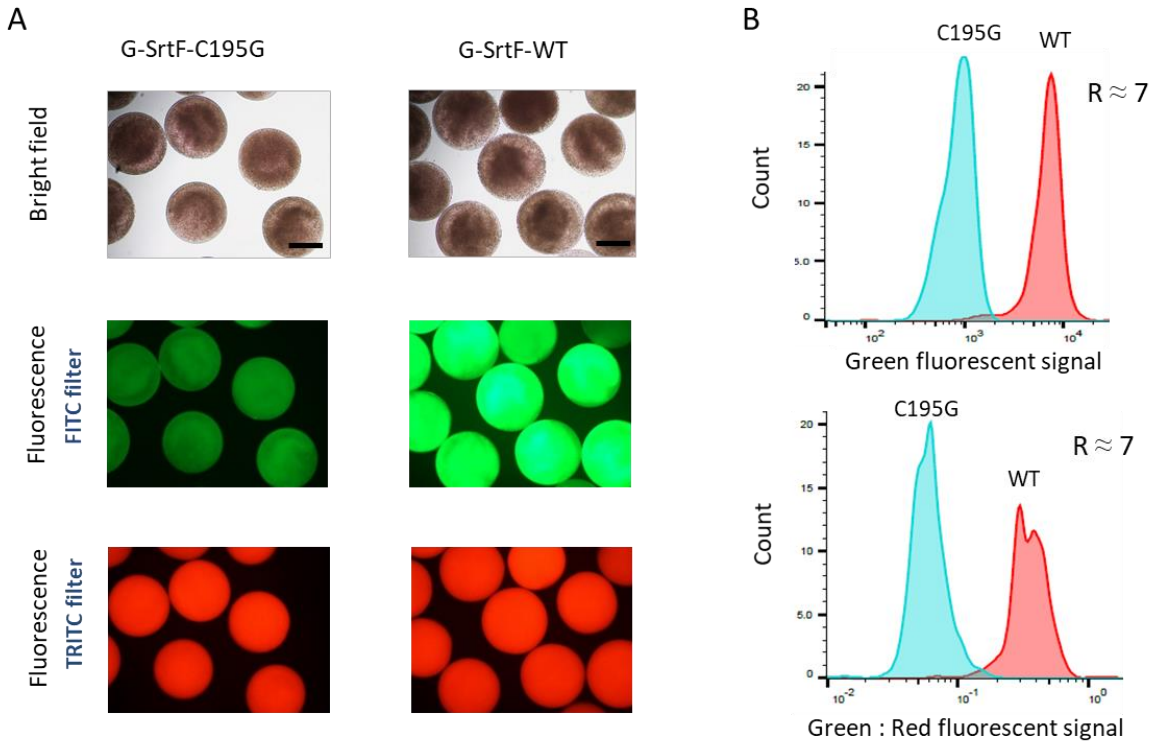


**Figure 3.60.** Microscope and COPAS analysis showing successful conjugation and capture of the fluorescent peptide FITC-LPETGE within microreactors expressing G-SrtF wild type. Microreactors expressing G-SrtF-C195G were used as negative control. After encapsulation within hollow-core microcapsules, cells were grown in TB medium for 20 hours at 28 °C then induced for protein expression with 0.2 mM IPTG for 20 hours at 16 °C. Following PSS-PAH coating, microreactors were lysed and incubated with 50 µM FITC-LPETGE in 50 mM Tris-HCl pH 7.65, 500 mM NaCl, 10 mM $CaCl_2$ for 21 hours at 25 °C. (**A**) Bright field (upper panel) and fluorescence pictures of reacted microreactors using FITC and TRITC filters (middle and lower panel respectively). Fluorescence exposure time was 1/25s and 1/2000s for FITC and TRITC filter respectively; the size bar corresponds to 200 µm. (**B**) Histogram overlays showing fluorescence distribution of G1-SrtF wild type (red) and G1-SrtF-195G (blue)-expressing microreactors populations before (upper panel) and after (lower panel) green signal normalization for the red fluorescent signal obtained by using propidium iodide. The ratio (R) between the median value of the green fluorescent signal of microreactors expressing the wild type and the inactive PaSrtF is given.

## 3.3 Directed evolution of PaSrtF

### 3.3.1 Library construction and analysis

In the absence of a reliable structure-function relationship, diversification of the SrtF-Pa gene was achieved by error prone PCR (ep-PCR). First described by Goeddel and co-workers (Goeddel D, 1989), epPCR became the most used and convenient random mutagenesis technique for the diversification of a defined segment of DNA and has been successfully applied to evolve a large number of enzymes including SaSrtA.

By taking advantage of the low fidelity of some DNA polymerases under certain conditions, random point mutations can be introduced into the gene of interest through a simple PCR amplification reaction and the average number of mutations can be controlled by the number of PCR cycle performed.

Random mutagenesis of the SrtF-Pa gene by ep-PCR was achieved by following the protocol described by Wilson and Keefe (Wilson and Keefe, 2000) which is based on the method of Cadwell and Joyce (Cadwell and Joyce, 1992). The method relies on increasing magnesium concentrations, increasing and unbalancing the concentration of the four nucleotides and on the addition of manganese in the PCR reaction buffer to reduce base-pairing fidelity to increase the polymerase mutation rate while maintaining low the mutational bias.

For this random mutagenesis protocol, Wilson and Keefe calculated the average of amino acid mutations per open reading frame as a function of ORF length and number of ep-PCR doublings (**Figure 3.61)**.

| EP-PCR doublings | Mutations per codon | ORF length | | | | |
|---|---|---|---|---|---|---|
| | | 100 bp | 200 bp | 400 bp | 800 bp | 1600 bp |
| 5 | 0.0076 | 0.25 | 0.50 | 1.0 | 2.0 | 4.0 |
| 10 | 0.015 | 0.50 | 1.0 | 2.0 | 4.0 | 8.0 |
| 20 | 0.030 | 1.0 | 2.0 | 4.0 | 8.1 | 16 |
| 30 | 0.045 | 1.5 | 3.0 | 6.0 | 12 | 24 |
| 50 | 0.076 | 2.5 | 5.0 | 10 | 20 | 40 |

**Figure 3.61.** Average number of amino acid mutations per open reading frame (ORF) as a function of ORF length and number of ep-PCR doublings (Wilson and Keefe, 2000).

Taking this calculation as a guide, the number of doublings required to introduce the desired average of 1.5 amino acid in PaSrtF ORF of 522 base pairs was determined to be 5.4.

Prior to performing the actual ep-PCR reaction, known amounts of the template (2.5, 5 and 10 ng) were amplified under mutagenic conditions for 10 cycles. The total yield of epPCR product after 10 cycles, estimated by comparing the intensity of the epPCR samples with the intensity of the gel standard loaded alongside on an ethidium bromide-stained agarose allowed to calculate an amplification efficiency of 1.6. The number of cycles required to duplicate the template DNA 5.4 times with an amplification efficiency of 1.6.was therefore determined to be 8.

After the reaction, successful amplification was confirmed by DNA gel electrophoresis and the resulting ep-PCR products were cloned into the recipient digested expression vector to yield a full size library of ligation product that encode for N-terminal single glycine-modified PaSrtF mutants. By electroporating an aliquot of the purified ligation into electrocompetent BL21 (DE3) cells, a total library size of $10^7$ transformants was estimated.

In order to verify the success of the epPCR and analyze the library composition, plasmid DNA was isolated and sequenced from 14 clones. Alignment of each PCR product with the unmutated parental gene revealed the presence of point mutations randomly distributed throughout the target sequence demonstrating the positive outcome of the mutagenesis method (**Table 3.3**).

**Table 3.3**. Summary of mutational events of 14 sequenced clones after ep-PCR

| Clone | Codon | Nucleotide change | Amino acid change |
|---|---|---|---|
| 1 | 101 | AAT ---> GAT | Asn ---> Asp |
| 2 | 55<br>126<br>183 | GGT ---> GGC<br>GCC ---> ACC<br>ATT ---> TTT | ---<br>Ala ---> Thr<br>Ile ---> Phe |
| 3 | 129<br>179 | TAT ---> AAT<br>CCG ---> TCG | Tyr ---> Asn<br>Pro ---> Ser |
| 4 | 74 | TCC ---> TCT | --- |
| 5 | 105<br>124<br>160 | TCT ---> CCT<br>GTG ---> GTA<br>CAG ---> CTG | Ser ---> Pro<br>---<br>Gln ---> Leu |
| 6 | 181 | AGC ---> TGC | Ser ---> Cys |
| 7 | 53<br>188 | AAA ---> AGA<br>AAT ---> TAT | ---<br>Asn ---> Tyr |
| 8 | --- | --- | --- |
| 9 | 160 | CAG ---> CGG | Gln ---> Arg |
| 10 | 74<br>79<br>92<br>160 | TCC ---> ACC<br>AAA ---> TAA<br>ACC---> -CC<br>CAG ---> TAG | Ser ---> Thr<br>Lys ---> STOP<br>Frameshift<br>Gln ---> STOP |
| 11 | 54<br>175 | AAA---> GAA<br>AAA ---> TAA | Lys ---> Glu<br>Lys --->STOP |

| | | | |
|---|---|---|---|
| 12 | --- | --- | --- |
| 13 | 151 | ATT ---> ACT | Ile --->Thr |
| 14 | --- | --- | --- |

Although the total number of these mutations was low for a significant statistical analysis, the average number of mutations introduced in the SrtF gene was in agreement with the expected value of 1.5. However, the calculated ratio of transitions (purine-to-purine and pyrimidine-to-pyrimidine mutations) to transversions (purine-to-pyrimidine and pyrimidine-to-purine mutations) of 1.6, revealed a notable bias towards transitions over transvertions.

Moreover, the analysis of the library compositions with the web program *PEDEL-AA* (Firth and Patrick, 2008) allowed to estimate that the library will contain about 94% of variants without additional stop codons or insertion and deletions and that about the 66% of the library will contain at least one mutation.

### 3.3.2 Library encapsulation

For library encapsulation, an aliquot of the purified library ligation was electroporated into an aliquot of electrocompetent BL21 and the total number of viable clones was estimated by counting the number of transformants achieved after plating on a LB agar plate an aliquot of the recovery.

As the encapsulation of randomly dispersed cells follows the Poisson distribution, the average number of cells per bead was controlled by adjusting the number of cells added to the alginate solution prior to microbeads formation. To reduce the probability that multiple cells are encapsulated and avoid ambiguous results during analysis, the number of viable transformants was therefore used to calculate the volume of the recovery culture to disperse in the alginate solution to achieve a satisfactory degree of monoclonality. For instance, when a dilution of one cell per five beads was made (0.2 cells/bead), 16% of the alginate beads were expected to harbor a single cell while only 1% of them were expected to harbor more than one cell. On the other hand, 82% of beads do not contain cells and are expected to generate empty microcapsules. Analysis of microreactor after cell proliferation showed that about 20% of the total were colonized demonstrating the reliability of the method used for the encapsulation of the library and confirming that the procedure to prepare microreactors have a minimal effect on cell viability.

Although the low degree of cell occupancy allows to increase the fraction of monoclonal microreactors, the higher the degree of dilution the higher will be the number of empty microcapsules meaning larger production volumes and longer sorting and analysis times. To overcome this problem, in a previous study (Walser et al., 2008), a COPAS-based technology was developed to enrich microcompartments colonized

by green fluorescent *E. coli* from empty ones. However, in this work, the use of hollow-core microcapsules for library encapsulation offers the great advantage to provide a fast and efficient gravity-driven separation of colonized microcapsules from empty microcapsules. In fact, due the high specific weight, colonized microreactors sediment faster than the not-colonized ones and can be easily separated from the latter (**see section 3.2.2, figure 3.25**).

### 3.3.3 Preliminary library screening

To validate the assay workflow a preliminary library screening was performed.
Starting from 25 ml alginate that generate about $10^6$ compartments, 2 x $10^5$ transformants were encapsulated to achieve a cell/droplet ratio of 1:5. As expected, after cell proliferation about 20% of total microcapsules were colonized by cells. Following separation from empty microcapsules through gravity separation, microreactors were coated with a layer of PSS and a layer of PAH and after cell lysis incubated with the 50 µM FITC-LPETGE for 20 hours at 25 °C. After unreacted peptide removal, the brightest 3% of the microreactors were separated on the basis of the green fluorescent signal and following the addition of propidium iodide microreactor were re-sorted on the basis of the green: red fluorescence ratio. Best hits were subsequently dispensed into a microtiter plate. Two of the selected microreactors were dissolved and plasmid recovered by electroporation. Sequencing analysis performed in triplicate confirmed the presence of one or three point mutations. Interestingly, both isolated clones contained a point mutation at the same position that resulted in the conversion of the threonine residue 213 (T213) into either a serine or an alanine residue. (**figure 6.3 A**).
To assess whether the two isolated G1-SrtF mutants showed improved catalytic properties, their ability to conjugate the fluorescent recognition peptide FITC-LPETGE to Gly6-AlgQ2 in comparison to the wild type G1-SrtF was investigated in whole cell extracts through a gel-based conjugation assay.
As can be seen in **figure 6.3 B** the assay did not reveal any significant catalytic improvement for the two SrtF mutants as compared to the wild type variant. Although the library screening efforts described are only preliminary, the successful execution of the whole assay workflow proof the validity of the directed evolution strategy developed.

A

| | |
|---|---|
| **G-SrtF-Mut 1:** | N98D/K139E/T213S |
| **G-SrtF-Mut 2:** | T213A |

B

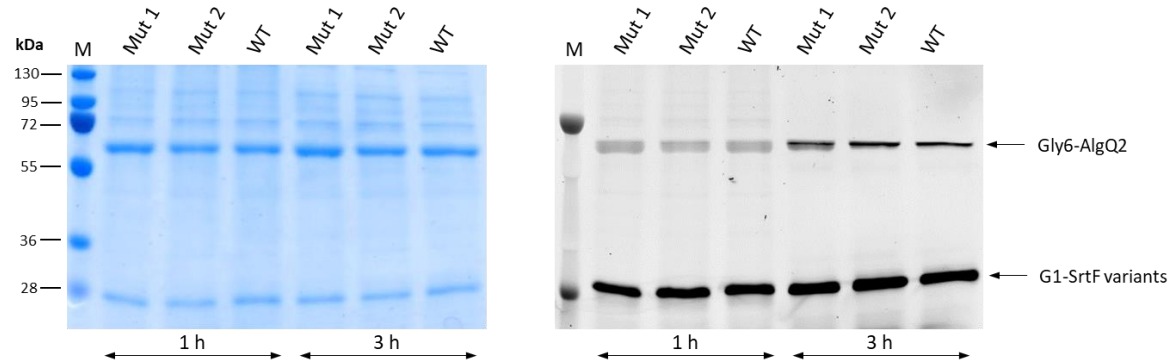


**Figure 6.3.** (**A**) Amino acid mutations found in the two isolated SrtF clones. (**B**) Analysis of the conjugation efficiency of G1-SrtF mutants and G1-SrtF wild type. Whole cell extracts of *E. coli* cultures expressing SrtF wild type or SrtF mutants were mixed with 10 µM Gly6-AlgQ2 and 50 µM of fluorescent peptide FITC-LPQTGE in 50 mM sodium phosphate pH 8.5, 500 mM NaCl and incubated for 1 or 3 three hours at 25 °C. The extent of the transpeptidation reaction was analyzed by SDS-PAGE gel fluorescence scanning (right panel) and quantified with *imageJ*. Equal protein loading was assessed by staining the gel with Coomassie (left panel). Lane M designates the protein ladder; Mut1 and Mut2 indicate the G1-SrtF mutants (as in A) while WT the wild type variant.

# 4 Conclusions and outlook

In recent years, sortase enzymes have emerged as powerful tools for protein engineering applications. Sortase-mediated ligation methods have proven effective for building a diverse range of peptide and protein conjugates in a site-specific fashion and can now be considered a valuable alternative to chemical ligation methods. Sortase-mediated ligations proceed under physiological conditions and require only two short motifs, the C-terminal sortase recognition sequence (i.e. LPXTG) and an N-terminal glycine tag, which can easily be introduced into proteins or other molecular probes, either by genetic engineering or by chemical synthesis. A major shortcoming of sortase enzymes concerns their general poor reaction rates. The most active naturally occurring sortase enzyme identified so far, as well as the best characterized, is the class A member from the Gram-positive *Staphylococcus aureus* (SaSrtA). An evolved pentamutant variant of SaSrtA (eSaSrtA) exhibiting more than 2 orders of magnitude increase in activity was identified in a yeast-display-based directed evolution screen (I. Chen et al., 2011). At present, the majority of the sortase-mediated ligation protocols rely on the use of the wild type SaSrtA and its evolved variant eSaSrtA. The industrial partner of this work, *NBE therapeutics AG*, designed and developed a new platform known as SMAC-technology (sortase-mediated antibody conjugation technology) for the site-specific conjugation of drugs to antibodies using sortase enzymes (Beerli et al., 2015). Antibody-drug conjugates (ADCs) generated using eSaSrtA were found to display *in vitro* and *in vivo* potencies similar to ADCs prepared by conventional chemical conjugation methods. One promising feature of the SMAC-technology concerns the possibility to conjugate different drugs onto one single antibody using sortases with different specificities (biorthogonal conjugation) thereby increasing the cancer killing effectiveness of ADCs. In order to identify novel sortase enzymes that can be used, for instance, in combination with eSaSrtA for biorthogonal conjugation, seven naturally occurring sortases were selected as targets for activity and specificity characterization. Focus was laid on sortases from classes with a predicted specificity orthogonal to the LPXTG-specificity of SaSrtA.

Among sortases investigated in this work, sortase B from *B. anthracis* (BaSrtB) yielded sufficient transpeptidation products that enabled for the first time the detailed sequence specificity analysis of a non-class A sortase (Puorger et al., 2017). By recognizing the consensus sequence NPNTG, BaSrtB exhibits sequence specificity orthogonal to SaSrtA and could be used for dual sortagging applications. However, the disappointingly catalytic activity of BaSrtB (estimated $10^4$-fold lower than eSaSrtA) precludes its use for biorthogonal sortagging but makes this sortase an ideal target for directed evolution.

Unlike BaSrtB, the member of the not-yet-characterized class F from *Propionibacterium acnes* (PaSrtF) exhibits excellent catalytic features and set itself to become a valid alternative to the most thoroughly employed SaSrtA. With an activity comparable to SaSrtA, PaSrtF proved to tolerate high salt concentrations which would enable broader applicability for sortagging approaches. Determination of the substrate specificity showed that, similar to eSaSrtA, PaSrtF prefers substrates carrying the consensus recognition sequence LPXTG. Although the overlap of the substrate spectrum prevents the use of PaSrtF in combination with eSaSrtA for biorthogonal sortagging, PaSrtF was successfully used for generation of highly

homogeneous ADCs displaying target-specific cell killing activity and potency similar to eSaSrtA-conjugated ADCs (Di Girolamo et al., 2019). The use of SrtF for sortagging was patent protected by *NBE Therapeutics AG*.

Apart from the use of PaSrtF for protein engineering, the characterization of PaSrtF paves the way for the discovery of drugs targeting *Propionibacterium acnes*. This organism, which is an oportunistic pathogen of the skin, is, among other factors, responsible for the occurrence of *acne vulgaris*. As PaSrtF is the sole sortase expressed in *P. acnes*, it is most likely the housekeeping sortase that attachs proteins bearing the LPXTG motif to the cell wall such as CAMP factor, DsA1 and other proteins known to be important virulence factors. Consequently, the identification of molecules inhibiting PaSrtF represents a promising route for the prevention and the treatment of *P. acnes*-related diseases. In this context, the structure determination of PaSrtF, in combination with *in silico* modeling and docking approaches, would allow to identify structures which are most likely to bind PaSrtF, threby facilitating the selection of the most promising candidates for PaSrtF inhibition.

Other sortase enzymes investigated in this work either showed very low solubility and could not be purified or displayed only marginal activities and could not be further characterized. Besides sampling natural diversity of sortases, a chimeric enzyme that ideally displayed an altered sequence specificity was also constructed and investigated but without success.

In the second part of the work, a novel assay that allows for the directed evolution of sortases with increased activity and/or altered specificity was developed. The assay, conceived to provide enough sensitivity for the detection of low active sortases, relies on the use of alginate bead-based microreactors as individual evolutionary units that are suitable for high-throughput screening using the large particle flow cytometer COPAS (*Complex Object Parametric Analyzer and Sorter*).

The assay consists of different steps individually optimized to achieve the best outcome. First, three types of alginate-beads based microcapsules were investigated as miniature size culture and reaction vessels. Among them, hollow-core chitosan-coated alginate microcapsule (HC-CAM) were recognized as the best choice as they enable *E. coli* colonies to grow and occupy the whole capsule core without affecting capsule stability. Colonies as big as the capsules allow to maximize the amount of enzyme that can be assayed in a single microreactor thereby increasing the chance to detect the activity of poorly active enzymes. Due to their high specific weight, HC-CAM-based microreactors can be easily separated from empty microcapsules allowing a considerable reduction of working volumes and sorting analysis times. In addition, the homogeneity in colony size and shape enables an accurate optical readout during sorting increasing the chance to isolate sortase variants with the improved properties.

Using the highly active SaSrtA, two different strategies were investigated for the optimal sortase-mediated conjugation reaction and for the efficient retention of the fluorescent transpeptidation products within microreactors. The first strategy relied on the use of an N-terminally oligo-glycine-modified alginate binding protein (Gly6-AlgQ2) as the nucleophilic component of the sortase-mediated conjugation reaction that, by interacting with alginate, would enable the fluorescent transpeptidation product FITC-

LPETG6-AlgQ2 to be specifically retained within alginate bead-based microreactors. In this context, the sortase moiety in the fusion protein Gly6-AlgQ2-SrtA was found to attach the fluorescent-labeled substrate peptide to the glycine stretch at its N-terminus in an intramolecular fashion that results in improved reaction rate as compared to the reaction performed with separate SaSrtA and AlgQ2. Although significant fluorescence change was observed with microreactors expressing Gly6-AlgQ2-SrtA wild type in comparison to those expressing the fusion construct with the inactive sortase A (Gly6-AlgQ2-SrtA-C184G), protein release analysis from microreactors have shown that the fusion protein and the relative fluorescent transpeptidation products are not specifically retained within microreactors thereby compromising the faithful measurement of the sortase activity. To overcome this limitation and ensure a direct correlation between the sortase activity and the fluorescent output signal, a second strategy was therefore investigated. The second strategy also relied on an intramolecular transpeptidation reaction catalyzed by a sortase A modified at the N-terminus by the addition of a single glycine residue (G-SrtA). In comparison to the fusion protein Gly6-AlgQ2-SrtA, G-SrtA showed higher expression yields that resulted in higher levels of fluorescence and therefore higher sensitivity. In this case, experiments with mixtures of microreactors expressing G-SrtA wild type and the relative inactive version G-SrtA-C184G and protein release analysis from microreactors have shown that coating microreactors with a size selective shell made of the polyelectrolyte pair PSS and PAH ensure an efficient retention of the enzyme and of the relative transpeptidation products. Following the development of the strategy with SaSrtA, the functionality of the microreactor-based assay in this format was optimized and validated with the newly characterized PaSrtF. The results demonstrated the suitability of the assay for its directed evolution. A preliminary screening of a random mutagenized library of PaSrtF was performed.

Although the validity of the microreactor-based assay could not be demonstrated with the very low active sortase B from *B. anthracis* (BaSrtB), the results have shown that the assay has the potential to be sensitive enough to enable BaSrtB and other sortases with very low catalytic efficiency to become accessible for directed evolution.

The microreactor-based assay developed in this work enables the completion of a whole screening cycle in 4-5 days with an effective hands-on time of about 20 hours and can easily be scaled up without any substantial change in the procedure. Compared to microtiter plate screening approaches, the microreactor-based assay, in combination with the large particle flow cytometer COPAS, enables a considerable reduction of reaction volume and allows the screening of clones about one order of magnitude faster than the maximum screening capacity achievable using advanced robotic systems ($10^5$ clones per day). However, compared to single cell and microfluidics-based screening systems which make use of FACS (up to $10^4$ clones per second), our system has significantly lower throughput. Producing hydrogel-based microreactors with a diameter size compatible with FACS, for instance through microfluidics techniques, would allow to increase the throughput and therefore reduce the time required to identify sortase variants with desired properties.

# 5 Experimental procedures

## 5.1 General information

Unless otherwise specified in the following experimental procedures, all commercial products used in this work were of analytical grade and purchased from Applichem, Fluka, Invitrogen, Merck, Promega, Roth Sigma-Aldrich, ThermoFisher. All the cloning procedures reported in this work were performed by using the FX cloning strategy (Geertsma, 2013). Primer design, PCRs and DNA ligations methods followed the FX cloning manual's instructions. After cloning sequences of interest were analyzed by restriction analysis and verified by DNA sequencing with universal primers T7 promoter or T7 terminal. Unless otherwise specified, competent cells preparation, bacterial transformations, DNA restriction reactions and DNA gel electrophoresis were performed following standard protocols as described in the laboratory methods collection of Prof. Georg Lipps. Small scale plasmid preparation and DNA gel purification were performed using commercial kits according to the manufacturer's instructions. Unless otherwise specified, all the *E. coli* cultures were performed in growth media containing 50 µg/ml kanamycin. FITC-labeled peptides and peptide mixtures were purchased from Genscript and dissolved in DMF or DMSO to a final concentration of about 20 mM. Dilutions were performed in the buffer used for the sortase-mediated reaction. FITC-labeled peptides and protein concentration was calculated from the measured absorbance at 495 nm and 280 nm respectively using the relative extinction coefficients. All the SDS-PAGE and western blot analysis reported in this work were performed using the standard Laemmli SDS-PAGE method as described in the laboratory methods collection of Prof. Georg Lipps. After gel electrophoresis, proteins bands were stained with a colloidal Coomassie staining solution and destained with water. Alternatively, following electroblotting of proteins onto a nitrocellulose membrane, proteins were detected by using a primary antibody against the histidine tag (1:1000 dilutions of anti-His mouse antibody; ThermoFisher, MA1-21315) and a secondary antibody linked to alkaline phosphatase for colorimetric detection (1:8000 dilutions of anti-mouse antibody-AP; Roth, 4760.1).

## 5.2 PCR oligonucleotide primers, vectors and strains

### List of oligo deoxyribonucleotides used in this work

| Name | Sequence (5'→ 3') |
|---|---|
| F1 | ATATATGCTCTTCTAGTGGGACTATTGGTATCCTGAAAATTCCG |
| R2 | GGCTCGTATGTTGTGTGGAA |
| F2 | ATATATGCTCTTCTAGTGGACAAGGGTTTGCCCTCTTGC |
| R2 | GGCTCGTATGTTGTGTGGAA |
| F3 | ATATATGCTCTTCTAGTGCGGCGAAAAAAGGTCCG |
| R3 | TATATAGCTCTTCATGCGGCAACCGGATAGGTATAGAAGATG |
| F4 | ATATATGCTCTTCTAGTACCCCGAAACCGATTGTGC |
| R4 | TATATAGCTCTTCATGCGGCAACCGGATAGGTATAGAAGATG |
| F5 | ATATATGCTCTTCTAGTCAGGCCAAACCGCAAATTCC |
| R5 | TATATAGCTCTTCATGCCTTGACTTCCGTTGCAACAAAGATC |
| F6 | ATATATGCTCTTCTAGTCAAGCTAAACCTCAAATTCCG |
| R6 | TATATAGCTCTTCATGCTTCCAGTTTGACTTCTGTAGC |
| F7 | GGAGATATACATATGGGTGGTGGTGGCGGTGG |
| R7 | CCACCGCCACCACCACCCATATGTATATCTCC |
| F8 | ATATATGCTCTTCTGCACACCATCATCATCACCATCATCATC |
| R8 | TATATAGCTCTTCAACTTGAGCCTGAGCCGTTCTTGTATTGTCTGTCATAAGCCTGC |
| F9 | TATATAAGTTGAAGAGCGACCTGCAGACTGGCTGTGTATAA |
| R9 | ATATATTGCAGAAGAGCTGAACTAGTGGATCCCCAAAAAAG |
| F10 | ATATATGCTCTTCTGCACACCATCATCATCACCATCATCATC |
| R10 | TATATAGCTCTTCAACTTGAGCCTGAGCCATAAGCCTGCTGCATCATTTGTAAAACC |
| F11 | ATATATGCTCTTCTGCACACCATCATCATCACCATCATCATC |
| R11 | TATATAGCTCTTCAACTTGAGCCTGAGCCTTGTAAAACCTGGTATAAGCCTCTCAG |
| F12 | ATATATGCTCTTCTGCACACCATCATCATCACCATCATCATC |
| R12 | TATATAGCTCTTCAACTTGAGCCTGAGCCGCCTCTCAGTTTCAACTGACGTTG |
| F13 | ATATATGCTCTTCTGCATTAGAAGTTTTGTTTCAAGGTCC |
| R13 | TATATAGCTCTTCAACTACCACCGCCGCCACCCATATGTATATCTCCTTCTTAAAGTTAAAC |
| F14 | ATATATGCTCTTCTGCAGGTAGTTGGTCCCACCCG |
| R14 | TATATAGCTCTTCAACTACCACCGCCGCCACCCATATGTATATCTCCTTCTTAAAGTTAAAC |

| | |
|---|---|
| F15 | ATATATGCTCTTCTGCATTAGAAGTTTTGTTTCAAGGTCC |
| R15 | TATATAGCTCTTCAACTACCCATATGTATATCTCCTTCTTAAAGTTAAAC |
| F16 | ATATATGCTCTTCTGCATTAGAAGTTTTGTTTCAAGGTCC |
| R16 | TATATAGCTCTTCAACTGCCACCCATATGTATATCTCCTTCTTAAAGTTAAAC |
| F17 | ATATATGCTCTTCTGCATTAGAAGTTTTGTTTCAAGGTCC |
| R17 | TATATAGCTCTTCAACTGCCGCCACCCATATGTATATCTCCTTCTTAAAGTTAAAC |
| F18 | GGAGATATACATATGGGCAGTACCACCACGTCAAGCACG |
| R18 | CGTGCTTGACGTGGTGGTACTGCCCATATGTATATCTCC |
| F19 | GGAGATATACATATGGGCGGCAGTACCACCACGTCAAGCACG |
| R19 | CGTGCTTGACGTGGTGGTACTGCCGCCCATATGTATATCTCC |
| F20 | GGAGATATACATATGGGCGGCGGCAGTACCACCACGTCAAGCACG |
| R20 | CGTGCTTGACGTGGTGGTACTGCCGCCGCCCATATGTATATCTCC |
| F21 | CTGACCCTGATTACGGGCGATGACTATAACG |
| R21 | CGTTATAGTCATCGCCCGTAATCAGGGTCAG |
| F22 | GTAACCCTGTCTACTGGTGATTACGCATTG |
| R22 | CAATGCGTAATCACCAGTAGACAGGGTTAC |
| F23 | AGCTATTGTGATTGCCTGGGATTACGTG |
| R23 | CACGTAATCCCAGGCAATCACAATAGCT |
| F24 | ATATATGCTCTTCTAGTCAATTCAGCAAAGGAGAAGAACTTTTCACTGG |
| R24 | TATATAGCTCTTCATGCACTAGTTTTGTAGAGCTCATCCGTGCC |
| F25 | ATATATGCTCTTCTAGTCATATGACTACCACCGCCAG |
| R25 | TATATAGCTCTTCATGCCTTATTGGTGTCCAAAGGTAGCTTAG |
| F26 | GAGAGGCTTATACCAAGTCTTACAAATGATGC |
| R26 | GCATCATTTGTAAGACTTGGTATAAGCCTCTC |
| F27 | ATATATGCTCTTCTAGTACCACCACGTCAAGCACGAG |
| R27 | TATATAGCTCTTCATGCTTATTATTTTTCAAACTGCGGATGGG |
| F28 | CATCTGTTGTCAAAGACAGCATCC |
| R28 | GCCTTCTGCTTAATTTGATGCCTG |
| T7 promoter | TAATACGACTCACTATAGGG |
| T7 terminator | GCTAGTTATTGCTCAGCGG |

## List of vectors used in this work

| Vector name | Source | Application |
|---|---|---|
| pUC57-BaSrtBΔ34 | Genscript | Subcloning |
| pUC57-BaSrtDΔ24 | Genscript | Subcloning |
| pUC57-MkSrtEΔ24 | Genscript | Subcloning |
| pEX-A2-CaSrtDΔ23 | Eurofins | Subcloning |
| pEX-A2-CpSrtDΔ22 | Eurofins | Subcloning |
| pEX-A2-ScSrtEΔ157 | Eurofins | Subcloning |
| pEX-A2-PaSrtFΔ34 | Eurofins | Subcloning |
| pEX-A2-Chimeric eSaSrtA/D | Eurofins | Subcloning |
| pUC57-Gly5-AlgQ2 | Genscript | Subcloning |
| pEX-A2-AlgX-C | Eurofins | Subcloning |
| pEX-A2-CBM | Eurofins | Subcloning |
| pUC57-eSaSrtA | Kindly provided by NBE therapeutics | Subcloning |
| p7XC3H | Geertsma 2013 | FX recipient expression vector |
| p7XC3GH | Geertsma 2013 | FX recipient expression vector |
| pINITIAL | Geertsma 2013 | FX recipient cloning vector |
| p7X-Ccdb-Cat-Streptag | Constructed in this work | FX recipient expression vector |
| p7X-Gly6-AlgQ2-GSGS-CcdB-Cat-His10 | Constructed in this work | FX recipient expression vector |
| p7X-Gly6-AlgQ2ΔC6-GSGS-CcdB-Cat-His10 | Constructed in this work | FX recipient expression vector |
| p7X-Gly6-AlgQ2ΔC12-GSGS-CcdB-Cat-His10 | Constructed in this work | FX recipient expression vector |
| p7X-Gly6-AlgQ2ΔC18-GSGS-CcdB-Cat-His10 | Constructed in this work | FX recipient expression vector |
| p7X-G1-CcdB-Cat-His10 | Constructed in this work | FX recipient expression vector |
| p7X-G2-CcdB-Cat-His10 | Constructed in this work | FX recipient expression vector |
| p7X-G3-CcdB-Cat-His10 | Constructed in this work | FX recipient expression vector |
| p7X-G5-CcdB-Cat-His10 | Constructed in this work | FX recipient expression vector |
| p7X-G1-CcdB-Cat-Streptag | Constructed in this work | FX recipient expression vector |
| p7X-G5-CcdB-Cat-Streptag | Constructed in this work | FX recipient expression vector |
| p7X-BaSrtBΔ34-His10 | Constructed in this work | Expression of BaSrtBΔ34-His10 |
| p7X-BaSrtDΔ24-His10 | Constructed in this work | Expression of BaSrtDΔ24-His10 |
| p7X-CpSrtDΔ22-His10 | Constructed in this work | Expression of CpSrtDΔ22-His10 |
| p7X-CaSrtDΔ23-His10 | Constructed in this work | Expression of CaSrtDΔ23-His10 |
| p7X-CaSrtDΔ66-His10 | Constructed in this work | Expression of CaSrtDΔ66-His10 |
| p7X-ScSrtEΔ157-His10 | Constructed in this work | Expression of ScSrtEΔ157-His10 |

| | | |
|---|---|---|
| p7X-ScSrtEΔ193-His10 | Constructed in this work | Expression of ScSrtEΔ193-His10 |
| p7X-MkSrtEΔ24-His10 | Constructed in this work | Expression of MkSrtEΔ24-His10 |
| p7X-PaSrtFΔ34-His10 | Constructed in this work | Expression of PaSrtFΔ34-His10 |
| p7X-PaSrtFΔ34-Streptag | Constructed in this work | Expression of PaSrtFΔ34-Streptag |
| p7X-PaSrtFΔ47-Streptag | Constructed in this work | Expression of PaSrtFΔ47-Streptag |
| p7X-PaSrtFΔ60-Streptag | Constructed in this work | Expression of PaSrtFΔ60-Streptag |
| p7X-Chimeric eSrtA/D-His10 | Constructed in this work | Expression of Chimeric eSrtA/D-His10 |
| p7X-Ser-Gly5-AlgQ2-His10 | Constructed in this work | Expression of Ser-Gly5-AlgQ2-His10 |
| p7X-Gly6-AlgQ2-His10 | Constructed in this work | Expression of Gly6-AlgQ2-His10 |
| p7X-Gly6-AlgQ2-GFP-His10 | Constructed in this work | Expression of Gly6-AlgQ2-GFP-His10 |
| p7X-AlgX-C-GFP-His10 | Constructed in this work | Expression of AlgX-C-GFP-His10 |
| p7X-CBM-GFP-His10 | Constructed in this work | Expression of CBM-GFP-His10 |
| p7X-GFP-His10 | Constructed in this work | Expression of GFP-His10 |
| p7X-VvGT5-GFP-His10 | Constructed in this work | Expression of VvGT5-GFP-His10 |
| p7X-Gly6-AlgQ2-wtSaSrtA-His10 | Constructed in this work | Expression of Gly6AlgQ2-SaSrtA-His10 |
| p7X-Gly6-AlgQ2-eSaSrtA-His10 | Constructed in this work | Expression of Gly6-AlgQ2-eSaSrtA-His10 |
| p7X-Gly6-AlgQ2-BaSrtB-His10 | Constructed in this work | Expression of Gly6-AlgQ2-BaSrtB-His10 |
| p7X-Gly6-AlgQ2ΔC6-eSrtA-His10 | Constructed in this work | Expression of Gly6-AlgQ2ΔC6-eSrtA-His10 |
| p7X-Gly6-AlgQ2ΔC12-eSrtA-His10 | Constructed in this work | Expression of Gly6-AlgQ2ΔC12-eSrtA-His10 |
| p7X-Gly6-AlgQ2ΔC18-eSrtA-His10 | Constructed in this work | Expression of Gly6-AlgQ2ΔC18-eSrtA-His10 |
| p7X-G1-wtSaSrtA-His10 | Constructed in this work | Expression of G1-SaSrtA-His10 |
| p7X-G2-wtSaSrtA-His10 | Constructed in this work | Expression of G2-wtSaSrtA-His10 |
| p7X-G3-wtSaSrtA-His10 | Constructed in this work | Expression of G3-wtSaSrtA-His10 |
| p7X-G5-wtSaSrtA-His10 | Constructed in this work | Expression of G5-wtSaSrtA-His10 |
| p7X-G1-BaSrtB-His10 | Constructed in this work | Expression of G1-BaSrtB-His10 |
| p7X-G2-BaSrtB-His10 | Constructed in this work | Expression of G2-BaSrtB-His10 |
| p7X-G3-BaSrtB-His10 | Constructed in this work | Expression of G3-BaSrtB-His10 |
| p7X-G1-PaSrtFΔ34-Streptag | Constructed in this work | Expression of G1-PaSrtFΔ34-Streptag |
| p7X-G2-PaSrtFΔ34-Streptag | Constructed in this work | Expression of G2-PaSrtFΔ34-Streptag |
| p7X-G3-PaSrtFΔ34-Streptag | Constructed in this work | Expression of G3-PaSrtFΔ34-Streptag |
| p7X-Gly6-AlgQ2-SaSrtAC184G-His10 | Constructed in this work | Expression of Gly6-AlgQ2-SaSrtAC184G-His10 |
| p7X -G1-SaSrtAC184G-His10 | Constructed in this work | Expression of G1-SaSrtAC184G-His10 |
| p7X-Gly6-AlgQ2-BaSrtBC233G-His10 | Constructed in this work | Expression of Gly6-AlgQ2-BaSrtBC233G-His10 |
| p7X-G1-BaSrtBC233G-His10 | Constructed in this work | Expression of G1-BaSrtBC233G-His10 |
| p7X-G1-PaSrtFC195G-Streptag | Constructed in this work | Expression of G1-PaSrtFC195G-Streptag |
| p7X-GFP-His10 | Constructed in this work | Expression of GFP-His10 |
| p7X-VvGT5-GFP-His10 | Constructed in this work | Expression of VvGT5-GFP-His10 |
| p7X-Gly6-AlgQ2-eSaSrtA(RBS) | Constructed in this work | Expression of Gly6-AlgQ2-eSaSrtA(RBS) |

**List of bacterial strains used in this work**

| Strain | Genotype | Application |
|---|---|---|
| *Escherichia coli* BL21 (DE3) | *F-, ompT, gal, dcm, lon, hsdSB (rB⁻mB⁺), λ(DE3 [lacI lacUV5-T7 gene 1 ind1 sam7 nin5]).* | Protein expression |
| *XJb autolysis* (DE3) (Zymo research) | *F- ompT hsdSB(rB- mB-) gal dcm ΔaraB::λR, cat (CmR), λ(DE3)* | Protein expression |
| *Escherichia coli* DB3.1 | *F-, gyrA462, endA1, glnV44, Δ(sr1-recA), mcrB, mrr, hsdS20(rB-, mB-), ara14, galK2, lacY1, proA2, rpsL20(Smr), xyl5, Δleu mtl1.* | FX cloning |
| *Escherichia coli* Top10 | *F-, mcrA, Δ(mrr-hsdRMS-mcrBC), φ80lacZΔM15, ΔlacX74, nupG, recA1, araD139, Δ(ara-leu)7697, galE15, galK16, rpsL(StrR), endA1, λ-.* | FX Cloning |
| *Escherichia coli* XL1-Blue | *endA1, gyrA96(nal$^R$), thi-1, recA1, relA1, lac, glnV44, F'[Tn10 pro AB$^+$ lacIq Δ(lacZ)M15], hsdR17(rK⁻mK$^+$).* | Cloning |

## 5.3 Molecular biology

### 5.3.1 Gene synthesis and cloning

**Cloning of selected sortases**

Sequences of selected sortases were subjected to an *in silico* analysis using the bioinformatics tools TMpred, PredictProtein, SignalP and Phobius to delineate signal peptides and identify transmembrane regions. Sequences encoding for the putative soluble domains were codon optimized for *E. coli* expression and custom-synthesized by GenScript or Eurofins with FX cloning-compatible SapI sites at each end. Synthetic genes from GenScript or Eurofins were delivered in pUC57 or in pEX-A2 vectors respectively. For protein expression, sortases sequences were transferred in the FX expression vector p7XC3H to produce sortases with a 3C cleavage site and a histidine tag (10xHis) at the C-terminus under control of T7 RNA polymerase promoter. To produce variants of $CaSrtD_{\Delta 23}$ and $ScSrtE_{\Delta 157}$ with a shorter N-terminal region ($CaSrtD_{\Delta 66}$ and $ScSrtE_{\Delta 193}$ respectively) sequences were amplified from the relative pEX-A2 vectors with primer pairs F1/R1 and F2/R2 respectively and subsequently cloned in the expression vector p7XC3H. Sequence encoding for $PaSrtF_{\Delta 34}$ was also transferred from the vector pEX-A2 in the FX expression vector p7X-CcdB-Cat-Streptag to produce the C-terminal twin-strep-tagged PaSrtF. Sequences encoding for the $PaSrtF_{\Delta 34}$ length variants $PaSrtF_{\Delta 47}$ and $PaSrtF_{\Delta 60}$ flanked by SapI restriction sites were amplified from p7X-PaSrtFΔ34-Streptag with primer pairs F3/R3 and F4/R4 respectively. The resulting

PCR products were cloned in the expression vector p7X-CcdB-Cat-Streptag yielding p7X-PaSrtFΔ47-Streptag and p7X-PaSrtFΔ60-Streptag.

**Cloning of SaSrtA variants**

Sequences encoding for the wild type SaSrtA (wtSaSrtA) or for the enhanced SaSrtA (eSaSrtA) flanked by SapI restriction sites were amplified from the vector pBX-SaSrtA-EstA (vector number 1013 from Prof. Georg Lipps plasmid collection) or pUC57-eSaSrtA (kindly provided by NBE Therapeutics) using primer pairs F5/R5 or F6/R6 for the wild type and the enhanced SaSrtA respectively. Resulting PCR products were cloned in the intermediate FX vector pINITIAL to obtain pINITIAL-wtSaSrtA and pINITIAL-eSaSrtA which were used for subsequent subcloning.

**Gene synthesis and cloning of the chimeric sortase eSrtA/D**

Following the identification of putative recombination sites through the SCHEMA algorithm, the sequence of the chimeric sortase that consists of the N-terminal region of eSaSrtA (residues Gln59-Arg151) fused to the C-terminal region of BaSrtD (Thr 143-Lys 198) was codon optimized for expression in *E. coli* and custom-synthesized by Eurofins. Sequence encoding for the chimeric enzyme, delivered in the cloning vector pEX-A2, was transferred into the expression vector p7XC3H to obtain p7X-Chimeric eSaSrtA/BaSrtD-His10 for the production of a C-terminal His-tagged protein.

**Gene synthesis and cloning of the putative alginate binding proteins**

The amino acid sequence of the periplasmic protein AlgQ2 from Sphingomonas species (GI: 9501762) was analysed with Signal P. In agreement with a previous study (Momma et al., 2002) the *in silico* analysis of the protein sequence allowed to delineate a 24 amino acids long signal. Sequences encoding for $AlgQ2_{\Delta 24,}$ for the conserved C-terminal carbohydrate-binding domain of AlgX (AlgX-C) from *Pseudomonas aeruginosa* (GI: 15598742; residue 337-461), and for the carbohydrate-binding motif (CBM) of the sugar binding protein from Bacteroides thetaiotamicron (WP_032841246.1; residues 505-635) were codon optimized for *E. coli* expression and custom-synthesized by Genscript or Eurofins with 5 glycine codifying codons at the 5'end. Synthetic genes were flanked by FX cloning-compatible SapI sites. To investigate the alginate binding ability of the selected putative alginate binding proteins, synthetic genes from delivered in pUC57 or in pEX-A2 vectors (from Genscript and Eurofins respectively) were transferred in the FX expression vector p7XC3GH to yield p7X-Gly6-AlgQ2-GFP-His10, p7X-AlgX-C-GFP-His10 and p7X-CBM-GFP-His10 for the production of proteins fused at their C-terminus with the green fluorescent protein (GFP). To investigate whether AlgQ2 works as nucleophile in a sortase-mediated conjugation reaction, sequence encoding for Gly5-AlgQ2 was first transferred in the expression vector p7XC3H to obtain the vector p7X-Ser-Gly5-AlgQ2 that encodes for AlgQ2 with the N-terminus

SGGGGG (Ser-Gly5-AlgQ2). For the expression of AlgQ2 with 6 glycines at the N-terminus (Gly6-AlgQ2), the "cloning scar" serine codon in p7X-Ser-Gly5-AlgQ2 was changed by site-directed mutagenesis PCR (described below) into another glycine residue by using primer pair F7/R7 yielding p7X- Gly6-AlgQ2.

**Construction of Gly6-AlgQ2-sortases fusion proteins**

For the production of the fusion proteins Gly6-AlgQ2-sortases, SapI restriction sites were introduced into the expression vector p7X-Gly6-AlgQ2 by PCR with primer pair F8/R8. R8 was designed so that a GSGS linker is introduced between the two components of the fusion. The resulting PCR product was ligated with the *Ccdb-Cat* cassette previously amplified from the FX cloning vector pINITIAL with primer pair F9/R9 yielding the FX vector p7X-Gly6-AlgQ2-GSGS-CcdB-Cat. Sequences encoding for wtSaSrtA, eSaSrtA and BaSrtB were then transferred from pINITIAL or pUC57 in the vector p7X-Gly6-AlgQ2-GSGS-CcdB-Cat obtaining the expression vectors p7X-Gly6-AlgQ2-wtSaSrtA-His10, p7X-Gly6-AlgQ2-eSaSrtA-His10 and p7X-Gly6-AlgQ2-BaSrtB-His10 respectively.

**Shortening of the C-terminal region of AlgQ2**

For the production of the fusions Gly6-AlgQ2-eSrtA in which the C-terminal region of AlgQ2 was shortened by 6, 12 and 18 amino acids, SapI restriction sites were first introduced into the vector p7X-Gly6-AlgQ2-GSGS-CcdB-Cat by PCR with primer pairs F10/R10, F11/R11 and F12/R12 respectively. Reverse primers were designed so that a GSGS linker is introduced between the AlgQ2 variants and eSaSrtA. The resulting PCR products were ligated with the *Ccdb-Cat* cassette (obtained as described above) yielding the FX expression vectors p7X-Gly6-AlgQ2ΔC6-GSGS-CcdB-Cat, p7X-Gly6-AlgQ2ΔC12-GSGS-CcdB-Cat and p7X-Gly6-AlgQ2ΔC18-GSGS-CcdB-Cat. Sequence encoding for eSaSrtA was transferred from pUC57 in these vectors to obtain the expression vectors p7X-Gly6-AlgQ2ΔC6-eSrtA-His10, p7X-Gly6-AlgQ2ΔC12-eSaSrtA-His10 and p7X-Gly6-AlgQ2ΔC18-eSrtA-His10.

**Construction of N-terminal glycine-modified sortases**

For the construction of sortases with 5 glycine residues at the N-terminus, SapI restriction sites were introduced in the vector p7XC3H with primer pair F13/R13 or in the vector p7X-CcdB-Cat-Streptag with primer pair F14/R14. The resulting PCR products were ligated with the *Ccdb-Cat* cassette (obtained as described above) yielding the FX expression vectors p7X-G5-CcdB-Cat-His10 and p7X-G5-CcdB-Cat-Streptag respectively. Sequence encoding for the wild type SaSrtA was then transferred from pINITIAL in the expression vector p7X-G5-CcdB-Cat-His10 to yield p7X-G5-wtSaSrtA-His10. Sequence encoding

for PaSrtF was transferred from the cloning vector pEX-A2-PaSrtFΔ34 in the expression vector p7X-G5-CcdB-Cat-Streptag yielding p7X-G5-PaSrtF-Streptag.

For the construction of the wild type SaSrtA and BaSrtB with either 1, 2 or 3 glycine residues at the N-terminus, SapI restriction sites and glycine codifying codons were introduced in the expression vector p7XC3H with primer pairs F15/R15, F16/R16 and F17/R17 respectively. The resulting PCR products were ligated with the *Ccdb-Cat* cassette (obtained as described above) yielding the expression vectors p7X-G1-CcdB-Cat-His10, p7X-G2-CcdB-Cat-His10 and p7X-G3-CcdB-Cat-His10. Sequences encoding for the wild type SaSrtA and BaSrtB were therefore transferred in the latter vectors to produce p7X-G1-wtSaSrtA-His10, p7X-G2-wtSaSrtA-His10, p7X-G3-wtSaSrtA-His10, p7X-G1-BaSrtB-His10, p7X-G2-BaSrtB-His10 and p7X-G3-BaSrtB-His10. For the construction of PaSrtF with either 1, 2 or 3 glycine residues at the N-terminus, site-directed mutagenesis PCR (described below) of the vector p7X-PaSrtFΔ34-Streptag was performed with primer pairs F18/R18, F19/R19 and F20/R20 respectively yielding p7X-G1-PaSrtFΔ34-Streptag, p7X-G2-PaSrtFΔ34-Streptag and p7X-G3-PaSrtFΔ34-Streptag.

**Inactivation of sortases**

Inactive sortases were obtained by replacing the cysteine in the active site with glycine by site-directed mutagenesis PCR. Expression vectors encoding for Gly6-AlgQ2-SaSrtAC184G (p7X-Gly6-AlgQ2-SaSrtAC184G-His10) and G1-SaSrtAC184G (p7X -G1-SaSrtAC184G-His10) were obtained by mutating the vector p7X-Gly6-AlgQ2-wtSaSrtA-His10 and p7X-G1-wtSaSrtA-His10 with the primer pair F21/R21 respectively. Similarly, expression vectors encoding for Gly6-AlgQ2-BaSrtBC233G (p7X-Gly6-AlgQ2-BaSrtBC233G-His10) and G1-BaSrtBC233G (p7X-G1-BaSrtBC233G-His10) were obtained by mutating the vector p7X-Gly6-AlgQ2-BaSrtB and p7X-G1-BaSrtB respectively with the primer pair F22/R22. The expression vector encoding for G1-PaSrtFC195G (p7X-G1-PaSrtFC195G-Streptag) was obtained by mutating the vector p7X-G1-PaSrtF-Streptag using the primer pair F23/R23.

**Construction of the expression vectors encoding for GFP and VvGT5-GFP**

For the expression of the green fluorescence protein (GFP), sequence encoding for GFP flanked by SapI restriction sites was amplified from the FX vector p7XC3GH with the primer pair F24/R24.The resulting PCR product was cloned in the expression vector p7XC3H yielding p7X-GFP-His10.

For the production of the fusion protein VvGT5-GFP, sequence encoding VvGT5 flanked by SapI restriction sites was amplified from the vector pET-VvGT5 (vector number 571 from Prof. Georg Lipps plasmid collection) with the primer pair F25/R25 and the resulting PCR product cloned in the expression vector p7XC3GH yielding p7X-VvGT5-GFP-His10.

**Modification of Gly6-AlgQ2-eSrtA upon RBS translation rate analysis**

For the production of the fusion protein Gly6-AlgQ2-eSrtA in which codons encoding for AlgQ2 residues Gln501 and Val502 were changed from CAG and GTT to CAA and GTC respectively, site-directed mutagenesis PCR (described below) of the vector p7X-Gly6-AlgQ2-eSaSrtA was performed with primer pair F26/R26 yielding p7X-Gly6-AlgQ2-eSaSrtA(RBS).

### 5.3.2 Site-directed mutagenesis

Site-directed mutagenesis PCR reactions were carried out with 0.5 μM of each primer, 3 units Phusion HF DNA Polymerase (NEB), 1 X Phusion HF Buffer (NEB), 200 μM of each dNTP and 15 ng of template in a total volume of 30 μl. The PCR program employed consisted of 95 °C for 5 minutes as initial step, followed by 16 cycles of denaturation at 95 °C for 30 seconds, annealing at 55 °C for 30 seconds, elongation at 72 °C for 1 minute/kilobase. A final elongation step of 5 minutes at 72 °C was performed. Following digestion of parental template with 3 units of DpnI for 1 hour at 37 °C, an aliquot of XL1blue chemical competent cells was transformed with 5 μl of the PCR reaction mix. Cells were plated on LB agar plates supplemented with 50 μg/ml kanamycin for selection of positive clones. The resulting mutagenized vectors were purified from a 10 ml overnight culture in LB medium by using a plasmid extraction kit (Peqlab) according to manufacturer's instructions. Vectors concentration was measured with the NanoDrop 2000c spectrophotometer (ThermoFisher) and sequences verified by DNA sequencing

## 5.4 Biochemistry

### 5.4.1 Protein expression and purification

**Expression and purification of BaSrtB, BaSrtD and CpSrtD**

With the exception of PaSrtF, selected sortases were expressed and purified using the same following procedure. *E. coli* BL21 (DE3) cells carrying the relative expression vector were inoculated in 20 ml LB medium and incubated for about 16 hours at 37 °C. The overnight culture was inoculated in 4 liters LB medium within a 4 liters' flask. Proper shaking was ensured by blowing air at 0.6 Bar. The culture was grown until an $OD_{600}$ of 0.6 was reached. Protein expression was induced by adding 1 mM IPTG followed by 3 additional hours of growth. Cells were harvested by centrifugation (4,500*g* for 15 minutes at 4 °C) and resuspended in 20 ml of 300 mM KCl, 100 mM $KH_2PO_4$, pH 8.0. Cells suspensions were incubated

on ice with 1 mg/ml lysozyme, 20 mM $MgCl_2$ and 50 units Super Nuclease (Sino Biological) for 30 minutes and then sonicated 6-8 cycles for 60 seconds (followed by intervals of 30 seconds for cooling) with 80% amplitude and 70% cycle duty. Cell lysates were centrifuged at 12,000*g* for 20 minutes at 4 °C and the cleared lysates were applied to a column filled with 5 ml TALON Superflow (GE Healthcare) metal affinity resin connected to the protein purification system Profinia (Biorad). Column was pre-equilibrated in 300 mM KCl, 100 mM $KH_2PO_4$, 10 mM imidazole pH 8.0 and after lysate loading washed twice with the same buffer containing 10 and 20 mM imidazole respectively. Bound proteins were eluted with 300 mM KCl, 100 mM $KH_2PO_4$, 250 mM imidazole pH 8.0. The purification progress was analyzed with SDS-PAGE and elution fractions dialyzed against 50 mM Tris/HCl, 200 mM NaCl pH 8.0, 60 % glycerol and stored at -20 °C.

**Expression and purification of PaSrtF variants**

*E. coli* BL21 (DE3) cells transformed with the specific expression vector were inoculated in 5 ml of LB medium and allowed to grow overnight at 37 °C. The overnight cultures were inoculated in 1 liter of LB medium (250 ml LB medium in 4 flasks of 1 liter) and allowed to grow at 37 °C until the optical density at 600 nm was 0.6. The cultures were cooled down and protein expression induced by the addition of 0.5 mM IPTG for 24 hours at 16 °C. Cells were harvested by centrifugation (16.800 *g* for 15 minutes at 4 °C), washed once in 100 mM Tris/HCl pH 8.0, 300 mM NaCl, 1 mM EDTA and pelleted again for 15 minutes at 4,500*g* and resuspended in 5 ml of the same buffer. Following 30 minutes' incubation on ice with 1 mg/ ml lysozyme and 0.1 % Triton X-100, cells were sonicated and the lysates clarified by centrifugation at 31,000*g* for 15 minutes at 4 °C. The cleared lysates were adjusted to a final concentration of 5 mM DTT and slowly applied onto a gravity flow column containing 1 ml Strep-Tactin® Superflow sepharose (IBA Lifesciences), pre-equilibrated with 2 column bed volume (CV) of wash buffer (100 mM Tris/HCl pH 8.0, 500 mM NaCl, 1mM EDTA, 5mM DTT). Following 6 column wash steps with 3 CV of wash buffer, proteins were eluted in 5 fractions: 1 CV elution buffer (100 mM Tris/HCl pH 8.0, 500 mM NaCl, 1mM EDTA, 5mM DTT, 2.5 mM desthiobiotin (IBA Lifesciences)) for the first fraction, 2 CV for the second and third fraction and again 1 CV for the remaining 2 fractions. After SDS-PAGE analysis, fractions containing PaSrtF were pooled together and diluted 10 fold with 10 mM sodium phosphate, pH 7.0 for further purification by ion exchange chromatography. The dilution was loaded onto a 1 ml HiTrap SP XL column (GE Healthcare) connected to the chromatography system Äkta Explorer (GE Healthcare) and eluted with a linear gradient from 0 to 1 M NaCl, in 10 mM sodium phosphate pH 7.0. Fractions corresponding to the main peak of the chromatogram were analyzed by SDS-PAGE and fractions containing PaSrtF were pooled and dialyzed against 50 mM sodium phosphate, pH 8.5, 500 mM NaCl, 1 mM EDTA, 10% glycerol before concentrating with an Amicon Ultra-4 (10 kDa) centrifuge filter (Millipore). Proteins were frozen in liquid nitrogen and stored at -20 °C.

**Solubility studies and purification of the chimeric SaSrtA**

*E. coli* BL21 (DE3) cells transformed with the expression vector p7X-ChimericSaSrtA/BaSrtD-His10 were inoculated in 5 ml of LB medium and grown overnight at 37 °C. The overnight culture was inoculated into 25 ml LB ($OD_{600}$= 0.05) and grown at 37 °C until optical density nm was about 0.6. Following protein expression with 1 mM IPTG for 3 hours at 37 °C, optical density at 600 nm was measured. Cells from 2 ml of culture were harvested by centrifugation at 5,000 rpm for 5 minutes and resuspended in one of the selected extraction buffer so that optical density at 600 nm was 10. Cell suspensions were sonicated on ice three times for 20 seconds (80% amplitude and 70% cycle duty) and then centrifuged 10 minutes at 16,000*g*. Supernatants (here referred to as soluble fractions) were taken and cell pellets resuspended in the same volume of 100 mM Tris/HCl pH 8, 8M Urea, 0.2 % β-mercaptoethanol. Following vortexing, for 1 minute samples were centrifuged 10 minutes at 16,000*g* and supernatants (here referred to as insoluble fractions) were taken. 5 µl of soluble and insoluble fractions from each sample were analyzed by SDS-PAGE.

Large scale expression and purification of the chimeric SaSrtA was performed following the procedure described above for BaSrtB, BaSrtD and CpSrtD. In this case, cells were lysed in 50 mM Tris/HCl pH 7.5, 150 mM NaCl, 0.5 M Urea, and cell lysate clarified by centrifugation at 50,000*g* for 15 minutes at 4 °C. The same buffer supplemented with 10 mM imidazole was used for column equilibration and for the first column wash. Second column wash and protein elution were performed using the same buffer supplemented with 20 mM and 250 mM imidazole respectively. Following SDS-PAGE analysis, the eluate was dialyzed against 50 mM Tris/HCl pH 7.5, 150 mM NaCl, 0.5 M Urea, 50% glycerol, concentrated with an Amicon Ultra-4 (10 kDa) centrifuge filter (Millipore) and stored at -20 °C.

**Expression and purification of G1-SaSrtA**

*E. coli* BL21 (DE3) cells carrying the expression vector p7X-G1-SaSrtA-His10 were inoculated in 20 ml TB medium and incubated for about 16 hours at 37 °C. The overnight culture was diluted in 1.2 liters of TB medium (600 ml LB medium in 2 conical flasks of 2 liter) and cell grown until an optical density at 600 nm was 0.6. The culture was cooled down and protein expression induced with 0.5 mM IPTG for 22 hours at 16 °C. Cells were harvested by centrifugation (4,500*g* for 15 minutes at 4 °C) and resuspended in 50 mM Tris/HCl, 150 mM NaCl, 5 mM imidazole, pH 8.5. Cells suspensions were incubated on ice with 1 mg/ml lysozyme, 20 mM $MgCl_2$ and 50 units Super Nuclease (Sino Biological) for 30 minutes and sonicated 6-8 cycles for 60 seconds (followed by intervals of 30 seconds for cooling) with 80% amplitude and 70% cycle duty. The cell lysate was centrifuged at 20,000*g* for 20 minutes at 4 °C and the cleared supernatant applied to a column filled with 5 ml TALON Superflow (GE Healthcare) metal affinity resin connected to the protein purification system Profinia (Biorad) pre-equilibrated in the buffer used for cell

lysis. Following the loading of the lysate, the column was washed twice with the same buffer supplemented with 10 and 20 mM imidazole and protein eluted from the column with 250 mM imidazole. The eluate was dialyzed against 25 mM Tris/HCl pH 8.2, 150 mM NaCl and concentrated with an Amicon Ultra-4 (10 kDa) centrifuge filter (Millipore). The protein was frozen in liquid nitrogen and stored at -20 °C.

**Expression and purification of Gly6-AlgQ2 and Ser-Gly5-AlgQ2**

Gly6-AlgQ2 and Ser-Gly5-AlgQ2 were expressed and purified following the procedure described above for BaSrtB, BaSrtD and CpSrtD. In this case, before induction with IPTG, the culture was cooled down to room temperature and protein expression induced for 16 hours at 25 °C.

**Expression and purification of fusion proteins with AlgQ2**

Gly6-AlgQ2-eSrtA and variants thereof, Gly6-AlgQ2-BaSrtB and Ser-Gly6-AlgQ2-GFP were expressed and purified following the procedure described above for BaSrtB, BaSrtD and CpSrtD. As for Gly6-AlgQ2 and Ser-Gly5-AlgQ2 protein expression was induced for 16 hours at 25 °C. During cell lysis a tablet of cOmplete EDTA-free Protease Inhibitor (Roche) was added to prevent protein degradation. For further purification through size exclusion chromatography, proteins were loaded onto a HiLoad 16/60 Superdex 200 prepacked column (GE Healthcare) connected to the chromatography system Äkta Explorer (GE Healthcare) and eluted with 50 mM Tris/HCl, 200 mM NaCl pH 7.8. Following SDS-PAGE analysis, fractions containing proteins were pooled together and concentrated with an Amicon Ultra-4 (10 kDa) centrifuge filter (Millipore). Proteins were frozen in liquid nitrogen and stored at -20 °C.

**Expression and purification of GFP and VvGT5-GFP**

The GFP and the fusion protein VvGT5-GFP were expressed and purified following the same procedure described for G1-SaSrtA. In this case, the pH of the buffers used was 7.8. The eluate was dialyzed against 25 mM Tris/HCl pH 7.8, 150 mM NaCl, 50 % glycerol and stored at -20 °C.

**Thioacyl intermediate formation and purification**

Gly6-AlgQ2-eSrtA (10 µM) were incubated with 20 µM of donor peptide FITC-LPXTGE in 25 mM Tris/HCl pH 8.3, 150 mM NaCl, 10 mM $CaCl_2$ in a final volume of 1.5 ml for 90 minutes at 30 °C. The reaction was centrifuged at 16,000*g* for 5 minutes at 4 °C then applied onto a 5 ml Bio-Scale™ Mini Bio-Gel® P-6 desalting cartridge (Biorad) using a peristaltic pump at a flow rate of 0.5 ml/minute. Fractions of 1 ml were collected and analyzed by SDS-PAGE. Fractions containing FITC-labeled Gly6-AlgQ2-

eSrtA were concentrated with an Amicon Ultra-4 (10 kDa) centrifuge filter (Millipore), frozen in liquid nitrogen and stored at -20 °C.

## 5.4.2 Sortase activity assays

**Gel-based conjugation assays**

To monitor the activity of sortases through the gel-based conjugation assay, purified sortases or whole cell extracts of sortases were mixed with the FITC-labeled substrate peptides in presence or in absence of the nucleophile Gly6-AlgQ2 in the specific reaction buffer. Following incubation, reactions were quenched by the addition of the SDS-PAGE loading buffer and separated on a 12% SDS–PAGE gel. Transpeptidation products were visualized by scanning the gel for FITC emission (Excitation wavelength: 473 nm; Filter LPB ≥ 510 nm) using the FLA-9000 imager (Fujifilm) and quantified by densitometry using the image analysis software *ImageJ*. To assess equal protein loading gels were stained with Coomassie after the fluorescence scan.

**FRET-based cleavage assays**

To monitor the transpeptidation activity of PaSrtF in presence of different metal bivalent cations or at different temperatures, 5 µM of purified PaSrtF was incubated with 2 mM tryglycine and 20 µM of bacterial sortase substrate II Dabcyl-QALPETGEE-Edans (Anaspec). Dabcyl (4-{[4-(dimethylamino) phenyl]azo}benzoic acid) is the quencher and Edans (5-[(2-aminoethyl)amino] naphthalene-1-sulfonic acid) the fluorophore. Fluorophore release was monitored as an increase in fluorescence for 1 hour (excitation: 350 nm, emission 495 nm) with a plate reader (Infinite M200, TECAN) or a fluorescence spectrophotometer (Clary eclipse, Agilent). Initial rates of fluorescence change were transformed to rates of concentration change by using the specific fluorescence of the product in the different buffers used.

**HPLC-based assays**

For the analysis of the activity of length variants of PaSrtF by RP-HPLC, 5 µM of each variant was incubated with 250 µM FITC-LPQTGE and 1 mM GGGK-biotin in 50 mM sodium phosphate, pH 8.5, 5 mM DTT at 25 °C. For the analysis of the activity of the chimeric sortase, 20 µM of enzyme were incubated with 250 µM FITC-LPQTGE and 250 µM GGGK-biotin in 25 mM Tris/HCl pH 8.2, 150 mM NaCl, 10 mM $CaCl_2$ at 30 °C. After different time points, 5 µl samples were taken and the reaction was stopped by the addition of 95 µl of 50 mM HCl. Samples were analyzed with an XBridge C18 column (Waters) equilibrated in 0.1% NH4OH in 5% MeOH at 30 °C. Elution was performed with a linear gradient from 0 to 100% of 0.1% NH4OH in 95% MeOH over 10 ml at a flow rate of 0.5 ml/min. Eluted peptides were detected by absorbance at 497 nm and fluorescence at 522 nm (excitation at 497 nm) and peak areas were analyzed for quantification employing the software *Unicorn*.

**Sortase-mediated conjugation within alginate beads**

To analyze the activity of eSaSrtA and derivatives within alginate beads, 50 µl (about 1000) of homogenous alginate beads (prepared as described in **section 5.5**) were transferred into a 2 ml centrifuge tubes. For protein loading, beads were washed once with 25 mM Tris/HCl pH 8, 10 mM $CaCl_2$ and incubated with specific proteins in 500 µl final volume of the same buffer for 30 minutes at 25 °C and 850 rpm shaking. To remove unbound proteins, beads were washed three times with 2 ml of the same buffer for 2 minutes. The sortase-mediated reaction was initiated by incubating the beads with the specific fluorescent labeled peptide in a final volume of 500 µl for 1 hour at 30 °C. Beads were washed three times with 2 ml of the same buffer for 2 minutes for unreacted peptide removal and subsequently analyzed by fluorescence microscopy. For the SDS-PAGE analysis, 10 µl of beads were taken and dissolved with 5 µl of 200 mM EDTA.

### 5.4.3 Structure determination of sortase D from *C. perfringens*

Protein crystallization, data collection and structure determination were performed by the research group of Professor Tim Mayer (Biozentrum, Universiy of Basel).

Plate-like crystals of sortase D2 form Clostridium perfringens (CpSrtD) were grown at room temperature in a sitting drop experiment in 25 % PEG3350, 0.1 M Bis-Tris pH 5.5, 0.2 M NaCl within one week. Crystals were cryo-preserved by a quick soak in a reservoir solution containing of 25 % ethylene glycol and flash-cooled in liquid nitrogen. Diffraction data were collected at Swiss Light source X06DA beamline and processed using XDS software (Kabsch, 2010a, 2010b). The crystals belong to space group $P2_1$ with cell dimensions $a$ = 38.8 Å, $b$ = 67.4 Å, and $c$ = 68.0 Å, β= 91.5° and contain two protein molecules per asymmetric unit. The structure of CpSrtD was determined by molecular replacement using the crystals structure of sortase C from *Streptococcus pneumoniae* (3G66.pdb) (Neiers et al., 2009) with the program Phaser (McCoy et al., 2007). Model building was carried out with Buccaneer (Cowtan, 2006) and Coot (Emsley and Cowtan, 2004). The structure was refined using PHENIX (Adams et al., 2002) and Refmac5 (Murshudov et al., 2011) and validated with MolProbity (Chen et al., 2010).

## 5.5 Microreactors preparation, processing and analysis

### Alginate and chitosan solution preparation

Alginate solutions (3% w/v) were prepared by dissolving low viscosity sodium alginate (no. A112, Sigma-Aldrich) in 25 mM Tris/HCl pH 7.8. Solutions were clarified by centrifugation for 10 minutes at 5,000*g* then filtered-sterilized by using a vacuum filtration system equipped with a 0.22 µm membrane filter (steriflip, Millipore). For the preparation of chitosan solutions (0.3% w/v) low molecular weight chitosan (no. 448869, Sigma-Aldrich) was added to 25 mM sodium acetate pH 5, 200 mM $CaCl_2$ and stirred for 30 minutes. The pH was adjusted to 5 with glacial acetic acid. Following centrifugation at 15,000*g* for 20 minutes the supernatant was poured in a glass bottle and autoclaved at 121 °C for 20 minutes.

### Alginate bead-based microcompartments production

*Gel-core alginate microbeads* (GCABs) were prepared using the semi-automated encapsulator B-395 Pro (Encapsulator Biotech/Buchi). The syringe pump of the encapsulator was used to extrude 5 ml of freshly prepared alginate solution through a 150-µm diameter nozzle into a gently stirred beaker filled with 100 ml hardening solution. For *inhomogeneous* or *homogeneous* beads preparation the hardening solution consisted of 25 mM Tris/HCl pH 7.8, 100 mM $CaCl_2$, 0.1% Tween 20 or 25 mM Tris/HCl pH 7.8, 50 mM $CaCl_2$, 200 mM NaCl, 0.1% Tween 20 respectively. Typically, uniform and monodispersed beads were produced at a rate of 2480 Hz (Amplitude =5) with a flow rate of 3.12 ml/ minute and an electrode tension of 1080 V. The resulting alginate beads were allowed to harden for 10-15 minutes and then collected at the bottom of a 50 ml tube by sedimentation. The hardening solution was discarded and beads washed twice with 40 ml of a washing solution consisting of 20 mM Tris/HCl pH 7.8, 100 mM NaCl, 10 mM $CaCl_2$ and 0.05% Tween 20. To obtain *gel-core chitosan-coated alginate microcapsules* (GC-CAMs), alginate beads were transferred into a gently stirred beaker filled with 15 ml of chitosan solution for 3 minutes. To stop the coating reaction and remove excess of chitosan, GC-CAMs were first collected by sedimentation into a 50 ml tube filled with 30 ml of 150 mM NaCl, 10 mM $CaCl_2$, 0.05% Tween 20 and after sedimentation washed twice with the same solution. To obtain *hollow-core chitosan-alginate micro-capsules* (HC-CAMs) GC-CAMs were suspended in 25 ml of 150 mM NaCl, 10 mM $CaCl_2$, 0.05% Tween 20 supplemented with 20 mM sodium citrate for 1 minute with gentle agitation for alginate core liquefaction. Following sedimentation at the bottom of the tube, HC-CAMs were washed twice with 20 mM Tris/HCl pH 7.8, 100 mM NaCl, 10 mM $CaCl_2$ and 0.05% Tween 20. After preparation, alginate bead-based microcompartments were immediately used or stored in their washing buffers at 4 °C up to 1 month.

**Cell encapsulation and growth in alginate bead-based microcompartments**

Cultures of *E. coli* BL21 (DE3) harboring the plasmid of interest were grown in LB or TB medium until exponential phase (OD600 = 0.4-0.8), then diluted to an $OD_{600}$ of 0.1 with 50 mM Tris/HCl pH 7.6, 100 mM NaCl. Typically, an aliquot of this diluted cell suspension was added to 5 ml alginate solution to obtain an average of 2 encapsulated cells per microcompartment. After mixing by gentle inversion for 1 minute, the resulting cell suspension was transferred into a 20 ml syringe and immediately used to prepare alginate bead-based microcompartments as described above. Following preparation *gel-core alginate microbeads* (GCABs) or *gel-core chitosan-coated alginate microcapsules* (GC-CAMs) entrapping cells were transferred into a 100 ml conical flask filled with 25 ml LB medium supplemented with 10 mM $CaCl_2$ and incubated at 28 °C for 16-18 hours, 160 rpm shaking. To grow cells in *hollow-core chitosan-alginate microcapsules* (HC-CAMs) *gel-core chitosan-coated alginate microcapsules* (GC-CAMs) encapsulating cells were treated with sodium citrate (as described above) before incubation in LB or TB medium for 16-20 hours at 28-30 °C, 160 rpm shaking. Alternatively, dissolution of the alginate gel core was achieved by the addition of 20 mM sodium citrate into the growth medium. Expression of recombinant proteins in the cytoplasm of encapsulated BL21 (DE3) cells was induced by the addition of 0.2-1 mM IPTG to overnight cultures of microreactors followed by 3 hours of growth at 37 °C for GFP, AlgQ2-fusions, G-SrtA and G-SrtB or 20 hours at 16 °C for G-SrtF. Alternatively, protein expression was induced by growing encapsulated cells overnight in an auto-induction medium (TB auto). Following cell growth and protein expression, colonized microreactors were collected at the bottom of a 50 ml tube by sedimentation and washed three times with 40 ml of 20 mM Tris/HCl pH 7.8, 100 mM NaCl, 10 mM $CaCl_2$ and 0.05% Tween 20. Microreactors were immediately used or stored in this buffer at 4 °C up to one week.

**Survival rates and encapsulated cell number determination**

Cell survival rates upon encapsulation in gel-core alginate microcompartments were determined by plating an aliquot of the alginate-cell suspension used for cell encapsulation on LB agar plates. Upon overnight incubation at 37 °C the number of colonies on the plate was compared with the number of *E. coli* colonies detected in the microcompartments by microscopy after 18 hours of growth at 28 °C. Cell survival rates upon encapsulation in hollow-core alginate microcapsules was estimated by comparing the total number of colonized gel-core and hollow-core microcompartments.

The total number of BL21 cells grown in a single gel-core or hollow-core-based microreactor was estimated by using a modified MTT reduction assay as described by Wang and colleagues (Wang et al., 2010). About 150 microreactors (10 µl) were transferred in 1.5-ml centrifuge tubes and residual buffer was pipetted off. Following the addition of 200 µl of LB medium pre-warmed to 37 °C the reduction reaction was initiated by the addition of 20 µl of 5.0 mg/ml of MTT in water pre-warmed to 37 °C. Tubes were incubated at 37 °C for 15 minutes and 1000 rpm shaking with the tube cap open. The medium was

pipetted off from microreactors and the purple formazan crystals produced by the reaction were dissolved with 1 ml of DMSO by vortexing for 1 minute. Samples were transferred into clean tubes and diluted four fold with DMSO. Absorbance values, recorded after 10 minutes at 550 nm in a spectrophotometer using DMSO as the blank, were used to estimate the number of cells in a single microreactor from a standard curve constructed as follows. 200 µl cell suspensions at $OD_{600}$ values between 0.05 and 0.6 (in triplicate) were prepared in 1.5-ml tubes from an exponentially growing culture of BL21 in LB medium using pre-warmed LB medium. Cell suspensions were incubated with 20 µl of 5.0 mg/ml of MTT at 37 °C for 15 minutes. Formazan crystals were collected at the bottom of the tubes by centrifugation at 10,000*g* for 1 minute and following the removal of the supernatant dissolved with 1 ml of DMSO by vortexing for 1 minute. Suspensions were diluted four fold with DMSO and absorbance values recorded after 10 minutes at 550 nm in a spectrophotometer using DMSO as the blank. The standard curve was obtained by plotting averaged values of absorbance at 550 nm against relative cell densities.

**Encapsulated cell lysis optimization**

Lysis of *E. coli* cells within microreactors was performed with detergent mixture BugBuster (10 X, no. 70921, Merck Millipore). The concentration of BugBuster necessary to obtain efficient cell lysis was determined using two different assays. The first assay consisted of determining the cell viability of encapsulated cells after treatment of microreactors with increasing BugBuster concentration by using the MTT assay described above. Samples of 100 µl of microreactors (about 2000) were transferred into 2 ml centrifuge tubes and incubated in 500 µl final volume of 25 mM Tris/HCl pH 8.2, 150 mM NaCl, 10 mM $CaCl_2$ in presence of BugBuster (between 0.1 and 1 X) for 30 minutes at 25 °C and 850 rpm shaking. Following two washing steps with 2 ml of the same buffer to remove the detergent, about 150 microreactors (10 µl) were transferred in 1.5 ml centrifuge tubes and the MTT assay performed. In the second assay efficient cell lysis was evaluated by analyzing the relative amount of GFP released from GFP-expressing microreactors treated with increasing BugBuster concentrations for different time points. 100 µl of GFP-expressing microreactors were incubated in 500 µl final volume of 25 mM Tris/HCl pH 8.2, 150 mM NaCl, 10 mM $CaCl_2$ in presence of 0.1-0.5 X BugBuster for 5, 15 and 30 minutes at 25 °C and 850 rpm shaking for cell lysis. The GFP released in solution from uncoated and coated microreactors was measured by using a fluorescence microplate reader (Infinite M200, TECAN) at 490 nm for excitation and 520 nm for emission. Relative percentage of GFP diffusion for each sample was then calculated using as reference the amount of GFP diffused from microreactors treated with the highest BugBuster concentration and the longest incubation time. The same assay was employed to analyze the lysis efficiency of the commercial autolytic strain XJb (DE3) in comparison to the standard expression strain BL21 (DE3).

**Layer-by layer coating analysis**

Layer-by layer coating of microreactors was performed using the polyelectrolyte coating pair PSS (poly-styrene sulfonate, no. 243051, Sigma) and PAH (poly-allylamine hydrochloride, no. 283223 Sigma). To find out coating conditions that enable microreactors to retain the GFP inside after cell lysis, the permeability of differently coated microreactors to GFP was analyzed. To this end, samples of 100 µl of GFP-expressing microreactors (about 2000) were transferred into 2 ml centrifuge tubes and incubated with 900 µl of PSS (2 mg/ml, 0.5 M NaCl, 0.1 M $CaCl_2$) or PAH solution (2 mg/ml, 0.5 M NaCl) for 5 minutes at 25 °C and 850 rpm shaking. Before proceeding with the deposition of the next layer of the opposite charged polyelectrolyte samples were washed three times with 2 ml of 150 mM NaCl, 10 mM $CaCl_2$ and 0.05% Tween 20 for 1 minute and 850 rpm shaking. Three washing steps were also performed at the end of the coating procedure. Layer-by-layer-coated microreactors were incubated in 500 µl final volume of 25 mM Tris/HCl pH 8.2, 150 mM NaCl, 10 mM $CaCl_2$ in presence of 0.5 X BugBuster for 15 minutes at 25 °C and 850 rpm shaking for cell lysis. The GFP released in solution from uncoated and coated microreactors was measured by using a fluorescence microplate reader (Infinite M200, TECAN) at 490 nm for excitation and 520 nm for emission. Relative percentage of GFP diffusion for each sample was then calculated using as reference the amount of GFP diffused from uncoated microreactors.

**Unreacted peptide washing optimization**

To determine best washing conditions for the removal of unreacted fluorescent peptide, microreactors expressing either Gly6-AlgQ2-SrtA or the inactive Gly6-AlgQ2-SrtA-C184G were prepared and treated in the same manner in parallel. Samples of 100 µl of microreactors (about 2000) were transferred into 2 ml centrifuge tubes and incubated in 500 µl final volume of 25 mM Tris/HCl pH 8.2, 150 mM NaCl, 10 mM $CaCl_2$ in presence of 0.5 X BugBuster for 30 minutes at 25 °C and 850 rpm shaking. Following cell lysis, microreactors were incubated in 500 µl of the same buffer in presence of 50 µl of FITC-LPETGE for 18 hours at 30 °C. After the reaction, microreactors were washed three times with 2 ml of the selected washing buffer for 5 minutes at 25 °C and 850 rpm shaking. Microreactors were rinsed twice with 2 ml of 10 mM Tris/HCl pH 8.5, 10 mM $CaCl_2$ for 1 minute and 850 rpm shaking and subsequently analysed by fluorescence microscopy and or COPAS.

**Recovery of the plasmid**

For plasmid recovery, a single microreactor was taken along with 1µl of buffer and transferred in 1.5 ml centrifuge tube. Uncoated microreactors were dissolved by the addition of 10 µl of 10 mM Tris HCl pH 8, 20 mM $NaHCO_3$ followed by vortexing for 1 minute. Differently, PSS-PAH-coated microreactors were

mixed with 5 µl of 50 mM NaOH for disassembly of the polyelectrolyte shell. Following 1 minute vortexing and 5 minutes at 1000 rpm, 5 µl of 50 mM Acetic acid were added and the sample vortexed again. For plasmid recovery by electroporation, 4 µl of sample were added to 40 µl of electrocompetent BL21 (DE3) cells (Sigma) diluted 1 to 4 with sterile 10 % glycerol and incubated for 1 minute on ice. Cells were electroporated at 2.5 kV, 200 Ω, and 25 µF using a 2 mm electroporation cuvette in a Gene Pulser Xcell unit (Biorad). After the pulse, 960 µl of recovery medium (No. CMR0001, Sigma) were added to the cuvette and cell suspension transferred into a 15 ml tube which was incubated for 1 hour at 37 °C and 200 rpm for cell recovery. The culture was centrifuged for 3 minutes at 3000*g* and the supernatant discarded. Cells were spread on LB agar plate and incubated overnight at 37 °C.

For genotype recovery by PCR, 1 µl of sample was mixed with 0.5 µM of each primers (F27 and R27), 3 units Phusion HF DNA Polymerase, 1 X Phusion HF Buffer, 200 µM of each dNTP in a total volume of 30 µl. The PCR program employed consisted of 95 °C for 5 minutes as initial step, 14 cycles of denaturation at 95 °C for 30 seconds and annealing at 61 °C for 30 seconds (decrease 0.5 °C per cycle) and elongation at 72 °C for 1 minute followed by 14 cycles at 95 °C for 30 seconds and annealing at 53 °C for 30 seconds and elongation at 72 °C for 1 minute. A final elongation step of 5 minutes at 72 °C was performed.

**Validation of the microreactor-based assay**

For the validation of the microreactor-based assay, microreactors expressing wild type sortases or derivatives and the respective inactive versions were prepared and treated in the same manner in parallel. Details for each experiments are reported in the captions of the figures in the "results and discussion" section. Following encapsulation and cell growth within hollow-core chitosan-coated alginate microcapsules (HC-CAMs), microreactors were incubated in presence of IPTG for protein expression. Typically, samples of 100 µl of microreactors (about 2000) were used for the assay. For cell lysis, uncoated or PSS-PAH-coated microreactor were transferred into 2 ml centrifuge tubes and incubated in 500 µl final volume of the specific buffer in presence of 0.5 X BugBuster for 30 minutes at 25 °C and 850 rpm shaking. Buffers used for cell lysis were always employed for the reaction. Following the removal of the detergent by washing, microreactors were incubated in the specific reaction buffer in presence of the specific FITC-labeled peptide substrate. Fluorescent labeled peptide removal was achieved by washing microreactors three times with about 2 ml of 50 mM Glycine pH 9.5, 500 mM NaCl, 10 mM $CaCl_2$, 0.1% Zwittergent 3:14 for 5 minutes and 850 rpm shaking. For fluorescence microscopy and COPAS analysis, microreactors were rinsed twice with 2 ml of 10 mM Tris/HCl pH 8.5, 10 mM $CaCl_2$ for 1 minute and 850 rpm shaking. For the analysis with propidium iodide, 100 µl of 1 mg/ml propidium iodide solution were added to microreactors samples in a final volume of 1 ml of 10 mM Tris/HCl pH 8.5, 10 mM $CaCl_2$ in for 5 minutes and 850 rpm shaking. Excess of Propidium iodide was removed by rinsing microreactors twice with 2 ml of the same buffer.

For the SDS-PAGE analysis, 10 µl of uncoated microreactors were transferred in a 1.5 ml tube and the residual buffer was removed. Microreactors were dissolved with 10 µl 1M $NaHCO_3$ and 10 µl 0.5 M EDTA. Similarly, 10 µl of PSS-PAH-coated microreactors were transferred in a 1.5 ml tube and after removal of the residual buffer were mixed with 5 µl of 1 M NaOH and 0 µl 0.5 M EDTA. Proper dissolution was achieved by pipetting up and down.

**Fluorescence microscopy and COPAS analysis**

Microcompartments and microreactors were typically analyzed by fluorescence microscopy and by complex object parametric analyzer and sorter (COPAS). Fluorescence microscopy was performed with an Olympus BX41 microscope. Nonfiltered white light (bright field) was used for the illumination of the microreactors structure. Two filter set that allows for blue excitation and green emission (excitation filter at 480/20; longpass emission filter at 510 nm) or green excitation and red emission (excitation filter at 535/30; longpass emission filter at 580 nm) were used to analyze FITC and propidium iodide-based fluorescence respectively. Picture were taken using 10 X and 20 X magnification lens. Exposure times ranged from 1/25 seconds to 1/1000 seconds for FITC-based fluorescence and from 1/1000 seconds to 1/8000 seconds for propidium iodide-based fluorescence.
Microreactors were spectrophotometrically imaged with a COPAS Plus particle analyzer and sorter (1000 µm flow-cell) equipped with the Flow pilot software (Union Biometrica). Fluorescence signals were recorded at 510 nm, appropriate for the emission maximum of FITC and at 615 nm appropriate for PI [ex: 488 nm, photon multiplier settings (PMT green): 450-650 V, (PMT red): 450 V; gain factor: 1.0. The COPAS-device was operated at frequencies between 10 and 20 Hz; At least 600 microbeads were collected any time to perform statistical analysis. Data analysis was done using the FlowJo software.

## 5.6 PaSrtF library preparation and screening

**Random mutagenesis of PaSrtF by error prone-PCR**

Diversification of the PaSrtF gene was performed by error prone-PCR (ep-PCR) based on the protocol described by Wilson and Keefe (Wilson and Keefe, 2000). The protocol was adapted in order to obtain the best experimental outcome. The 1.7 kb fragment obtained upon digestion of the vector carrying the sequence encoding for $PaSrtF_{\Delta N34}$ (pINITIAL- $PaSrtF_{\Delta N34}$) with *KpnI* and *PvuI* (NEB) was used as template. The ep-PCR reaction mixture consisted of 10 mM Tris/HCl pH 8.7, 50 mM KCl, 7 mM $MgCl_2$, 1 mM of dCTP and dTTP, 0.2 mM dATP and dGTP, 450 ng of template, 0.5 µM of each primer (F28/R28), 0.4 mM $MnCl_2$ and 50 U Firepol DNA polymerase (Solis BioDyne) in a final volume of

500 µl. The reaction mixture was set up on ice and subsequently spilt in 50 µl aliquots in PCR tubes. Cycling conditions consisted of 95° C for 5 minutes as initial step, followed by 8 cycles of denaturation at 94 °C for 1 minute, annealing at 56 °C for 1 minute, elongation at 72 °C for 2 minutes. A final elongation step of 5 minutes at 72 °C was performed. Reactions were pooled together and ep-PCR product was cleaned up using the NucleoSpin® Gel and PCR Clean-up kit (Macherey-Nagel). Purified ep-PCR product concentration was measured with the NanoDrop 2000c (ThermoFisher).

**Preparation of ep-PCR product and recipient expression vector for cloning**

For the construction of the library both the ep-PCR product and the recipient FX expression vector p7X-G1-CcdB-Cat-Streptag were prepared as described below. 5 µg of the vector were digested with 15 U SapI (NEB), 10 U *NcoI* (NEB) in 1 X Cutsmart buffer (NEB) in a total volume of 200 µl for 5 hours at 37 °C. Following heat inactivation of the restriction enzymes at 80 °C for 20 minutes, the digestion mixture was run on a 0.8% (w/v) agarose gel stained with Redsafe (iNtRON). The DNA band corresponding to the SapI-digested vector (5.4 kb) was excised from the gel and purified by using the NucleoSpin® Gel and PCR Clean-up kit. DNA elution was made in 30 µl of sterile water pre-warmed to 50 °C. 6 µg of epPCR product were digested with 15 U SapI and 10 U DpnI (NEB) in 1 X Cutsmart Buffer in a total volume of 200 µl for 16 hours at 30 °C. Following heat inactivation of the restriction enzymes at 80 °C for 20 minutes the digestion, the mixture was run on a 2% (w/v) agarose gel stained with Redsafe (iNtRON). The DNA band corresponding to the SapI-digested epPCR product (552 bp) was excised from the gel and purified by using the NucleoSpin Gel and PCR Clean-up kit (Macherey-Nagel). DNA elution was made in 30 µl of sterile water pre-warmed to 50 °C.

**Test library preparation and analysis of library composition**

Before proceeding with the full-sized library construction, a series of test libraries were performed using different ligation and electroporation conditions in order to maximize the final size of the ep-PCR library. Best experimental conditions found for the test library were subsequently used for the construction of the full-sized library. For the preparation of test library 50 ng of the digested vector were mixed with a three-fold molar excess of the digested ep-PCR product, 20 U of T4 DNA ligase (NEB) and 1 X T4 DNA ligase buffer (NEB) in a final volume of 10 µl. A control reaction containing only the digested vector but not the epPCR product was used to calculate the fraction of ligation products made of recircularized vector. Following incubation for 16 hours at 16 °C, the ligase was heat inactivated at 65 °C for 20 minutes and either 1 µl of the test ligation reaction or of the control reaction was added to 40 µl of electrocompetent BL21(DE3) cells (Sigma) diluted 1 to 1 with sterile 10 % glycerol. Electroporation was performed following the electrocompetent cells manufacturer's instructions and advices. Best electroporation conditions were obtained at 2.5 kV, 200 Ω, and 25 µF using a 2 mm electroporation cuvette in a Gene Pulser

Xcell unit (Biorad). After the pulse, 960 µl of recovery medium (No. CMR0001, Sigma) were added to the cuvette and cell suspension transferred into a 15 ml tube which was incubated for 1 hour at 37 °C and 200 rpm for cell recovery. 100 µl of cell suspensions were spread on LB agar plates and incubated overnight at 37 °C. For the analysis of library composition, small-scale plasmid preparation was performed from 14 clones and the mutagenized gene insert sequenced using the universal T7 promoter primer. To identify mutations, sequenced samples were aligned with the sequence of the unmutated PaSrtF gene by using the software Vector NTI. Identified mutations were used to calculate the overall mutation rate and to assess bias in the mutation spectrum of the library. Library analysis was also performed using the online program PEDEL-AA (Firth and Patrick, 2008).

**Full-sized library construction**

For the construction of the full-sized ep-PCR library 500 ng of digested vector was mixed with a threefold molar excess of digested ep-PCR product, 200 U of T4 DNA ligase (NEB) and 1 X T4 DNA ligase buffer (NEB) in a final volume of 100 µl. Following incubation for 16 hours at 16 °C, the ligase was heat inactivated at 65 °C for 20 minutes and the ligation product was cleaned up using the NucleoSpin Gel and PCR Clean-up kit (Macheray-Nagel). Ligation products were eluted in 75 µl of sterile water pre-warmed to 50 °C. After elution, the library ligation product was split into 10 µl aliquots and stored at -20 °C. The size of final epPCR library was estimated by counting the number of transformants obtained after electroporation of 1 µl of the full-sized library ligation into electrocompetent BL21 (DE3) using the procedure described above for the test library.

**Library encapsulation and preliminary library screening**

For the encapsulation and preliminary screening of the PaSrtF library, one aliquot of the full-sized library ligation was thawed on ice. 1 µl was added to 40 µl of electrocompetent BL21 (DE3) cells (Sigma) diluted 1 to 4 with sterile 10 % glycerol. After 1-minute incubation on ice, the mix was transferred into a 2 mm electroporation cuvette and immediately electroporated at 2.5 kV, 200 Ω, and 25 µF in a Gene Pulser Xcell unit (Biorad). After the pulse, 960 µl of recovery medium (No. CMR0001, Sigma) were added to the cuvette and cell suspension transferred into a 15 ml tube which was incubated for 1 hour at 37 °C and 200 rpm for cell recovery. At this point, 50 µg/ml kanamycin were added to the culture which was grown for two additional hours to allow only transformants to replicate. Following 2 hours of growth the culture was chilled on ice for 15 minutes and subsequently stored overnight at 4 °C. By plating on LB agar plates an aliquot of cells after 1-hour recovery and after 2 additional hours of growth, a 7-fold cell number replication was determined. The number of transformants on the plate after 2 hour of growth was then used to calculate the volume of the culture to mix with the alginate solution prior to encapsulation to have an average number of cells per bead of 0.25. Two batches of 25 ml of alginate solution were used for encapsulation. Alginate beads encapsulating cells from each batch were prepared and collected into a

gently stirred beaker filled with 250 ml of 25 mM Tris/HCl pH 7.8, 50 mM $CaCl_2$, 200 mM NaCl, 0.1% Tween 20 and allowed to harder for about 15 minutes. Beads were collected at the bottom of four 50 ml tube by sedimentation and subsequently washed twice with 40 ml of 20 mM Tris/HCl pH 7.8, 100 mM NaCl, 10 mM $CaCl_2$ and 0.05% Tween 20. Alginate beads were transferred into a gently stirred beaker filled with 75 ml of chitosan solution for 2 minutes then recovered again by sedimentation into four 50 ml tube. The chitosan solution was discarded and beads washed twice with 40 ml of 150 mM NaCl, 10 mM $CaCl_2$, 0.05% Tween 20. Chitosan-coated alginate beads were transferred into 200 ml of TB medium supplemented with kanamycin and 20 mM sodium citrate for 1 hour at 37 °C then for 20 hours at 28 °C and 160 rpm shaking. According to Poisson distribution, about 20 % of microcompartments were colonized. Empty and colonized microcompartments were collected into 50 ml tubes. By exploiting the different specific weight, microreactors (5 ml) were gradually separated from empty microcompartments and incubated into 40 ml TB medium supplemented with 0.5 mM IPTG at 16 °C and 160 rpm shaking for protein expression. The day after, microreactors were properly washed with 150 mM NaCl, 10 mM $CaCl_2$, 0.05% Tween 20 to remove traces of medium and subsequently coated with PSS and PAH. For the deposition of PSS, microreactors were incubated with 40 ml of 2 mg/ml PSS in 0.5 M NaCl, 100 mM $CaCl_2$ for 5 minutes in a rotating mixer then washed three times with 40 ml of 150 mM NaCl, 10 mM $CaCl_2$, 0.05% Tween 20. For the deposition of PAH, microreactors were incubated with 40 ml of 2 mg/ml PAH in 0.5 M NaCl for 5 minutes in a rotating mixer then washed three times with 40 ml of the same washing solution. After coating, microreactors were washed once with 25 mM Tris/HCl pH 7.65, 500 mM NaCl, 10 mM $CaCl_2$ and incubated in 25 ml of the same buffer supplemented with 0.5 X BugBuster for 30 minutes in a rotating mixer at room temperature for cell lysis. Microreactors were washed three times with the same buffer without the detergent and subsequently transferred into a 100 ml conical flask containing 25 ml of the same buffer supplemented with 25 µM FITC-LPQTGE and incubated at 25 °C for 20 hours. After the reaction, microreactors were collected into a 50 ml tube and washed three times with 40 ml of 50 mM Glycine pH 9.5, 500 mM NaCl, 10 mM $CaCl_2$, 0.1% Zwittergent 3:14 for unreacted fluorescent labeled peptide removal. After washing microreactors three times with 40 ml of 10 mM Tris/HCl pH 8.5, 10 mM $CaCl_2$ to remove the detergent, microreactors were analysed using the large particle flow cytometer COPAS (BioSorter, Union Biometrica). The device was operated with 10 mM Tris/HCl pH 8.5, 10 mM $CaCl_2$ as sheath fluid. For library screening, microreactors displaying the highest green fluorescence intensity levels (about 3%of the total) were sorted into a 50 ml centrifugation tube prefilled with 10 ml of 10 mM Tris/HCl pH 8.5, 10 mM $CaCl_2$ ('enrichment mode', max. 100 Hz sorting rate). Isolated microreactors were incubated for 5 minutes with propidium iodide (≈ 100 µl of 1 mg/ml for 100 µl microreactors) and two washing steps with 10 mM Tris/HCl pH 8.5, 10 mM $CaCl_2$ subjected to another sorting ('pure mode', maximum 1 Hz sorting rate) on the basis of the green to red fluorescence ratio. Single microreactors were dispensed into Nunc MicroWell 96-well plates filled with 100 µl of 10 mM Tris/HCl pH 8.5, 10 mM $CaCl_2$. The two clones displaying the highest green to red fluorescence ratio were dissolved and plasmid recovered by electroporation as described above.

# 6 Bibliography

Adams, P.D., Grosse-Kunstleve, R.W., Hung, L.-W., Ioerger, T.R., McCoy, A.J., Moriarty, N.W., Read, R.J., Sacchettini, J.C., Sauter, N.K., Terwilliger, T.C., 2002. PHENIX: building new software for automated crystallographic structure determination. Acta Crystallogr. D Biol. Crystallogr. 58, 1948–1954. https://doi.org/10.1107/S0907444902016657

Agresti, J.J., Antipov, E., Abate, A.R., Ahn, K., Rowat, A.C., Baret, J.-C., Marquez, M., Klibanov, A.M., Griffiths, A.D., Weitz, D.A., 2010. Ultrahigh-throughput screening in drop-based microfluidics for directed evolution. Proc. Natl. Acad. Sci. U. S. A. 107, 4004–4009. https://doi.org/10.1073/pnas.0910781107

Aharoni, A., Amitai, G., Bernath, K., Magdassi, S., Tawfik, D.S., 2005. High-Throughput Screening of Enzyme Libraries: Thiolactonases Evolved by Fluorescence-Activated Sorting of Single Cells in Emulsion Compartments. Chem. Biol. 12, 1281–1289. https://doi.org/10.1016/j.chembiol.2005.09.012

Ahmed, E.M., 2015. Hydrogel: Preparation, characterization, and applications: A review. J. Adv. Res. 6, 105–121. https://doi.org/10.1016/j.jare.2013.07.006

Amer, B.R., Macdonald, R., Jacobitz, A.W., Liauw, B., Clubb, R.T., 2016. Rapid Addition of Unlabeled Silent Solubility Tags to Proteins Using a New Substrate-Fused Sortase Reagent. J. Biomol. NMR 64, 197–205. https://doi.org/10.1007/s10858-016-0019-z

Antipov, A.A., Sukhorukov, G.B., 2004. Polyelectrolyte multilayer capsules as vehicles with tunable permeability. Adv. Colloid Interface Sci., Plenary and Invited Lectures From the XVIth European Chemistry at Interfaces Conference, Vladimir, Russia, May 2003 111, 49–61. https://doi.org/10.1016/j.cis.2004.07.006

Antos, J.M., Chew, G.-L., Guimaraes, C.P., Yoder, N.C., Grotenbreg, G.M., Popp, M.W.-L., Ploegh, H.L., 2009a. Site-Specific N- and C-Terminal Labeling of a Single Polypeptide Using Sortases of Different Specificity. J. Am. Chem. Soc. 131, 10800–10801. https://doi.org/10.1021/ja902681k

Antos, J.M., Ingram, J., Fang, T., Pishesha, N., Truttmann, M.C., Ploegh, H.L., 2017. Site-Specific Protein Labeling via Sortase-Mediated Transpeptidation. Curr. Protoc. Protein Sci. 89, 15.3.1-15.3.19. https://doi.org/10.1002/cpps.38

Antos, J.M., Popp, M.W.-L., Ernst, R., Chew, G.-L., Spooner, E., Ploegh, H.L., 2009b. A Straight Path to Circular Proteins. J. Biol. Chem. 284, 16028–16036. https://doi.org/10.1074/jbc.M901752200

Antos, J.M., Truttmann, M.C., Ploegh, H.L., 2016. Recent advances in sortase-catalyzed ligation methodology. Curr. Opin. Struct. Biol. 38, 111–118. https://doi.org/10.1016/j.sbi.2016.05.021

Beerli, R.R., Hell, T., Merkel, A.S., Grawunder, U., 2015. Sortase enzyme-mediated generation of site-specifically conjugated antibody drug conjugates with high in vitro and in vivo potency. PloS One 10, e0131177.

Bellucci, J.J., Bhattacharyya, J., Chilkoti, A., 2015. A non-canonical function of sortase enables site-specific conjugation of small molecules to lysine residues in proteins. Angew. Chem. Int. Ed Engl. 54, 441–445. https://doi.org/10.1002/anie.201408126

Beneyton, T., Coldren, F., Baret, J.-C., Griffiths, A.D., Taly, V., 2014. CotA laccase: high-throughput manipulation and analysis of recombinant enzyme libraries expressed in *E. coli* using droplet-based microfluidics. The Analyst 139, 3314–3323. https://doi.org/10.1039/C4AN00228H

Beneyton, T., Thomas, S., Griffiths, A.D., Nicaud, J.-M., Drevelle, A., Rossignol, T., 2017. Droplet-based microfluidic high-throughput screening of heterologous enzymes secreted by the yeast Yarrowia lipolytica. Microb. Cell Factories 16. https://doi.org/10.1186/s12934-017-0629-5

Bentley, M.L., Gaweska, H., Kielec, J.M., McCafferty, D.G., 2007. Engineering the Substrate Specificity of Staphylococcus aureus Sortase A: THE β6/β7 LOOP FROM SrtB CONFERS NPQTN RECOGNITION TO SrtA. J. Biol. Chem. 282, 6571–6581. https://doi.org/10.1074/jbc.M610519200

Bierne, H., Mazmanian, S.K., Trost, M., Pucciarelli, M.G., Liu, G., Dehoux, P., Jänsch, L., Portillo, F.G., Schneewind, O., Cossart, P., 2002. Inactivation of the srtA gene in Listeria monocytogenes inhibits anchoring of surface proteins and affects virulence. Mol. Microbiol. 43, 869–881. https://doi.org/10.1046/j.1365-2958.2002.02798.x

Boekhorst, J., de Been, M.W.H.J., Kleerebezem, M., Siezen, R.J., 2005. Genome-Wide Detection and Analysis of Cell Wall-Bound Proteins with LPxTG-Like Sorting Motifs. J. Bacteriol. 187, 4928–4934. https://doi.org/10.1128/JB.187.14.4928-4934.2005

Brüggemann, H., Henne, A., Hoster, F., Liesegang, H., Wiezer, A., Strittmatter, A., Hujer, S., Dürre, P., Gottschalk, G., 2004. The Complete Genome Sequence of Propionibacterium Acnes, a Commensal of Human Skin. Science 305, 671–673. https://doi.org/10.1126/science.1100330

Cadwell, R.C., Joyce, G.F., 1992. Randomization of genes by PCR mutagenesis. Genome Res. 2, 28–33. https://doi.org/10.1101/gr.2.1.28

Carmody, W.R., 1961. Easily prepared wide range buffer series. J. Chem. Educ. 38, 559–560. https://doi.org/10.1021/ed038p559

Cascioferro, S., Raffa, D., Maggio, B., Raimondi, M.V., Schillaci, D., Daidone, G., 2015. Sortase A Inhibitors: Recent Advances and Future Perspectives. J. Med. Chem. 58, 9108–9123. https://doi.org/10.1021/acs.jmedchem.5b00779

Chan, A.H., Yi, S.W., Terwilliger, A.L., Maresso, A.W., Jung, M.E., Clubb, R.T., 2015. Structure of the Bacillus anthracis Sortase A Enzyme Bound to Its Sorting Signal. J. Biol. Chem. 290, 25461–25474. https://doi.org/10.1074/jbc.M115.670984

Chan, L., Cross, H.F., She, J.K., Cavalli, G., Martins, H.F.P., Neylon, C., 2007. Covalent Attachment of Proteins to Solid Supports and Surfaces via Sortase-Mediated Ligation. PLOS ONE 2, e1164. https://doi.org/10.1371/journal.pone.0001164

Chávarri, M., Marañón, I., Ares, R., Ibáñez, F.C., Marzo, F., Villarán, M. del C., 2010. Microencapsulation of a probiotic and prebiotic in alginate-chitosan capsules improves survival in simulated gastro-intestinal conditions. Int. J. Food Microbiol. 142, 185–189. https://doi.org/10.1016/j.ijfoodmicro.2010.06.022

Chen, Irwin, Dorr, B.M., Liu, D.R., 2011. A general strategy for the evolution of bond-forming enzymes using yeast display. Proc. Natl. Acad. Sci. 108, 11399–11404.

Chen, I., Dorr, B.M., Liu, D.R., 2011. A general strategy for the evolution of bond-forming enzymes using yeast display. Proc. Natl. Acad. Sci. U. S. A. 108, 11399–11404. https://doi.org/10.1073/pnas.1101046108

Chen, L., Cohen, J., Song, X., Zhao, A., Ye, Z., Feulner, C.J., Doonan, P., Somers, W., Lin, L., Chen, P.R., 2016. Improved variants of SrtA for site-specific conjugation on antibodies and proteins with high efficiency. Sci. Rep. 6. https://doi.org/10.1038/srep31899

Chen, V.B., Arendall, W.B., Headd, J.J., Keedy, D.A., Immormino, R.M., Kapral, G.J., Murray, L.W., Richardson, J.S., Richardson, D.C., 2010. MolProbity: all-atom structure validation for macromolecular crystallography. Acta Crystallogr. D Biol. Crystallogr. 66, 12–21. https://doi.org/10.1107/S0907444909042073

Comfort, D., Clubb, R.T., 2004. A Comparative Genome Analysis Identifies Distinct Sorting Pathways in Gram-Positive Bacteria. Infect. Immun. 72, 2710–2722. https://doi.org/10.1128/IAI.72.5.2710-2722.2004

Cowtan, K., 2006. The Buccaneer software for automated model building. 1. Tracing protein chains. Acta Crystallogr. D Biol. Crystallogr. 62, 1002–1011. https://doi.org/10.1107/S0907444906022116

Das, S., Pawale, V.S., Dadireddy, V., Singh, A.K., Ramakumar, S., Roy, R.P., 2017. Structure and specificity of a new class of Ca2+-independent housekeeping sortase from Streptomyces avermitilis provide insights into its non-canonical substrate preference. J. Biol. Chem. 292, 7244–7257. https://doi.org/10.1074/jbc.M117.782037

Dasgupta, S., Samantaray, S., Sahal, D., Roy, R.P., 2011. Isopeptide Ligation Catalyzed by Quintessential Sortase A: MECHANISTIC CUES FROM CYCLIC AND BRANCHED OLIGOMERS OF INDOLICIDIN. J. Biol. Chem. 286, 23996–24006. https://doi.org/10.1074/jbc.M111.247650

Déjugnat, C., Sukhorukov, G.B., 2004. pH-responsive properties of hollow polyelectrolyte microcapsules templated on various cores. Langmuir ACS J. Surf. Colloids 20, 7265–7269. https://doi.org/10.1021/la049706n

Di Girolamo, S., Puorger, C., Castiglione, M., Vogel, M.S., Gebleux, R., Briendl, M., Hell, T., Beerli, R.R., Grawunder, U., Lipps, G., 2019. Characterization of the housekeeping sortase from the human pathogen Propionibacterium acnes - first investigation of a class F sortase. Biochem. J. BCJ20180885. https://doi.org/10.1042/BCJ20180885

Dorr, B.M., Ham, H.O., An, C., Chaikof, E.L., Liu, D.R., 2014. Reprogramming the specificity of sortase enzymes. Proc. Natl. Acad. Sci. 111, 13343–13348. https://doi.org/10.1073/pnas.1411179111

Dramsi, S., Trieu-Cuot, P., Bierne, H., 2005. Sorting sortases: a nomenclature proposal for the various sortases of Gram-positive bacteria. Res. Microbiol. 156, 289–297. https://doi.org/10.1016/j.resmic.2004.10.011

Duong, A., Capstick, D.S., Di, B.C., Findlay, K.C., Hesketh, A., Hong, H.J., Elliot, M.A., 2012. Aerial development in Streptomyces coelicolor requires sortase activity. Mol.Microbiol. 83, 992–1005.

Duong, Andrew, Capstick, D.S., Di Berardo, C., Findlay, K.C., Hesketh, A., Hong, H.-J., Elliot, M.A., 2012. Aerial development in Streptomyces coelicolor requires sortase activity: Sortase activity in S. coelicolor. Mol. Microbiol. 83, 992–1005. https://doi.org/10.1111/j.1365-2958.2012.07983.x

Emsley, P., Cowtan, K., 2004. Coot: model-building tools for molecular graphics. Acta Crystallogr. D Biol. Crystallogr. 60, 2126–2132. https://doi.org/10.1107/S0907444904019158

Erickson, H.P., 2009. Size and Shape of Protein Molecules at the Nanometer Level Determined by Sedimentation, Gel Filtration, and Electron Microscopy. Biol. Proced. Online 11, 32–51. https://doi.org/10.1007/s12575-009-9008-x

Espah Borujeni, A., Channarasappa, A.S., Salis, H.M., 2014. Translation rate is controlled by coupled trade-offs between site accessibility, selective RNA unfolding and sliding at upstream standby sites. Nucleic Acids Res. 42, 2646–2659. https://doi.org/10.1093/nar/gkt1139

Fallah-Araghi, A., Baret, J.-C., Ryckelynck, M., Griffiths, A.D., 2012. A completely in vitro ultrahigh-throughput droplet-based microfluidic screening system for protein engineering and directed evolution. Lab. Chip 12, 882–891. https://doi.org/10.1039/C2LC21035E

Finn, R.D., Coggill, P., Eberhardt, R.Y., Eddy, S.R., Mistry, J., Mitchell, A.L., Potter, S.C., Punta, M., Qureshi, M., Sangrador-Vegas, A., Salazar, G.A., Tate, J., Bateman, A., 2016. The Pfam protein families database: towards a more sustainable future. Nucleic Acids Res. 44, D279–D285. https://doi.org/10.1093/nar/gkv1344

Firth, A.E., Patrick, W.M., 2008. GLUE-IT and PEDEL-AA: new programmes for analyzing protein diversity in randomized libraries. Nucleic Acids Res. 36, W281–W285. https://doi.org/10.1093/nar/gkn226

Fischlechner, M., Schaerli, Y., Mohamed, M.F., Patil, S., Abell, C., Hollfelder, F., 2014. Evolution of enzyme catalysts caged in biomimetic gel-shell beads. Nat. Chem. 6, 791–796. https://doi.org/10.1038/nchem.1996

Foster, T.J., Geoghegan, J.A., Ganesh, V.K., Höök, M., 2014. Adhesion, invasion and evasion: the many functions of the surface proteins of Staphylococcus aureus. Nat. Rev. Microbiol. 12, 49–62. https://doi.org/10.1038/nrmicro3161

Frankel, B.A., Kruger, R.G., Robinson, D.E., Kelleher, N.L., McCafferty, D.G., 2005. Staphylococcus aureus Sortase Transpeptidase SrtA: Insight into the Kinetic Mechanism and Evidence for a Reverse Protonation Catalytic Mechanism. Biochemistry 44, 11188–11200. https://doi.org/10.1021/bi050141j

Frottin, F., Martinez, A., Peynot, P., Mitra, S., Holz, R.C., Giglione, C., Meinnel, T., 2006. The proteomics of N-terminal methionine cleavage. Mol. Cell. Proteomics 5, 2336–2349.

Gåserød, O., Gudmund Skjask-Brñk, Andrea Sannes, 1999. Microcapsules of alginate–chitosan. II. A study of capsule stability and permeability. Biomaterials 20, 773–783.

Gåserød, O., Smidsrød, O., Skj\a ak-Br\a ek, G., 1998. Microcapsules of alginate-chitosan–I: a quantitative study of the interaction between alginate and chitosan. Biomaterials 19, 1815–1825.

Geertsma, E.R., 2013. FX Cloning: A Versatile High-Throughput Cloning System for Characterization of Enzyme Variants, in: Enzyme Engineering, Methods in Molecular Biology. Humana Press, Totowa, NJ, pp. 133–148. https://doi.org/10.1007/978-1-62703-293-3_10

Ghadessy, F.J., Ong, J.L., Holliger, P., 2001. Directed evolution of polymerase function by compartmentalized self-replication. Proc. Natl. Acad. Sci. U. S. A. 98, 4552–4557. https://doi.org/10.1073/pnas.071052198

Gianella, P., Snapp, E., Levy, M., 2016. An in vitro compartmentalization based method for the selection of bond-forming enzymes from large libraries. Biotechnol. Bioeng. 113, 1647–1657. https://doi.org/10.1002/bit.25939

Glasgow, J.E., Salit, M.L., Cochran, J.R., 2016. In Vivo Site-Specific Protein Tagging with Diverse Amines Using an Engineered Sortase Variant. J. Am. Chem. Soc. 138, 7496–7499. https://doi.org/10.1021/jacs.6b03836

Goeddel D, L.D., 1989. A method for random mutagenesis of a defined DNA segment using a modified polymerase chain reaction. Technique 1, 11–15.

Goh, C.H., Heng, P.W.S., Chan, L.W., 2012. Alginates as a useful natural polymer for microencapsulation and therapeutic applications. Carbohydr. Polym. 88, 1–12. https://doi.org/10.1016/j.carbpol.2011.11.012

Heck, T., Pham, P.-H., Hammes, F., Thöny-Meyer, L., Richter, M., 2014a. Continuous Monitoring of Enzymatic Reactions on Surfaces by Real-Time Flow Cytometry: Sortase A Catalyzed Protein Immobilization as a Case Study. Bioconjug. Chem. 25, 1492–1500. https://doi.org/10.1021/bc500230r

Heck, T., Pham, P.-H., Yerlikaya, A., Thöny-Meyer, L., Richter, M., 2014b. Sortase A catalyzed reaction pathways: a comparative study with six SrtA variants. Catal. Sci. Technol. 4, 2946–2956. https://doi.org/10.1039/C4CY00347K

Hendrickx, A.P.A., Budzik, J.M., Oh, S.-Y., Schneewind, O., 2011. Architects at the bacterial surface - sortases and the assembly of pili with isopeptide bonds. Nat. Rev. Microbiol. 9, 166–176. https://doi.org/10.1038/nrmicro2520

Hirakawa, H., Ishikawa, S., Nagamune, T., 2015. Ca2+ -independent sortase-A exhibits high selective protein ligation activity in the cytoplasm of *Escherichia coli*. Biotechnol. J. 10, 1487–1492. https://doi.org/10.1002/biot.201500012

Hirakawa, H., Ishikawa, S., Nagamune, T., 2012. Design of Ca2+-independent Staphylococcus aureus sortase A mutants. Biotechnol. Bioeng. 109, 2955–2961.

Ilangovan, U., Ton-That, H., Iwahara, J., Schneewind, O., Clubb, R.T., 2001. Structure of sortase, the transpeptidase that anchors proteins to the cell wall of Staphylococcus aureus. Proc. Natl. Acad. Sci. U. S. A. 98, 6056–6061. https://doi.org/10.1073/pnas.101064198

Jacobitz, A.W., Kattke, M.D., Wereszczynski, J., Clubb, R.T., 2017. Sortase Transpeptidases: Structural Biology and Catalytic Mechanism. Adv. Protein Chem. Struct. Biol. 109, 223–264. https://doi.org/10.1016/bs.apcsb.2017.04.008

Jacobitz, A.W., Wereszczynski, J., Yi, S.W., Amer, B.R., Huang, G.L., Nguyen, A.V., Sawaya, M.R., Jung, M.E., McCammon, J.A., Clubb, R.T., 2014. Structural and Computational Studies of the Staphylococcus aureus Sortase B-Substrate Complex Reveal a Substrate-stabilized Oxyanion Hole. J. Biol. Chem. 289, 8891–8902. https://doi.org/10.1074/jbc.M113.509273

Jeong, H.-J., Abhiraman, G.C., Story, C.M., Ingram, J.R., Dougan, S.K., 2017. Generation of Ca2+-independent sortase A mutants with enhanced activity for protein and cell surface labeling. PLOS ONE 12, e0189068. https://doi.org/10.1371/journal.pone.0189068

Kabsch, W., 2010a. XDS. Acta Crystallogr. D Biol. Crystallogr. 66, 125–132. https://doi.org/10.1107/S0907444909047337

Kabsch, W., 2010b. Integration, scaling, space-group assignment and post-refinement. Acta Crystallogr. D Biol. Crystallogr. 66, 133–144. https://doi.org/10.1107/S0907444909047374

Kang, H.J., Coulibaly, F., Proft, T., Baker, E.N., 2011. Crystal Structure of Spy0129, a Streptococcus pyogenes Class B Sortase Involved in Pilus Assembly. PLoS ONE 6. https://doi.org/10.1371/journal.pone.0015969

Kattke, M. D., Chan, A.H., Duong, A., Sexton, D.L., Sawaya, M.R., Cascio, D., Elliot, M.A., Clubb, R.T., 2016. Crystal Structure of the Streptomyces coelicolor Sortase E1 Transpeptidase Provides Insight into the Binding Mode of the Novel Class E Sorting Signal. PLoS ONE 11, e0167763-. https://doi.org/10.1371/journal.pone.0167763

Kattke, Michele D., Chan, A.H., Duong, A., Sexton, D.L., Sawaya, M.R., Cascio, D., Elliot, M.A., Clubb, R.T., 2016. Crystal structure of the Streptomyces coelicolor sortase E1 transpeptidase provides insight into the binding mode of the novel class E sorting signal. PloS One 11, e0167763.

Kemp, K.D., Singh, K.V., Nallapareddy, S.R., Murray, B.E., 2007. Relative Contributions of Enterococcus faecalis OG1RF Sortase-Encoding Genes, srtA and bps (srtC), to Biofilm Formation and a Murine Model of Urinary Tract Infection. Infect. Immun. 75, 5399–5404. https://doi.org/10.1128/IAI.00663-07

Kharat, A.S., Tomasz, A., 2003. Inactivation of the srtA Gene Affects Localization of Surface Proteins and Decreases Adhesion of Streptococcus pneumoniae to Human Pharyngeal Cells In Vitro. Infect. Immun. 71, 2758–2765. https://doi.org/10.1128/IAI.71.5.2758-2765.2003

Kintses, B., Hein, C., Mohamed, M.F., Fischlechner, M., Courtois, F., Lainé, C., Hollfelder, F., 2012. Picoliter Cell Lysate Assays in Microfluidic Droplet Compartments for Directed Enzyme Evolution. Chem. Biol. 19, 1001–1009. https://doi.org/10.1016/j.chembiol.2012.06.009

Krasaekoopt, W., Bhandari, B., Deeth, H., 2004. The influence of coating materials on some properties of alginate beads and survivability of microencapsulated probiotic bacteria. Int. Dairy J. 14, 737–743. https://doi.org/10.1016/j.idairyj.2004.01.004

Kruger, Ryan G, Dostal, P., McCafferty, D.G., 2004. Development of a high-performance liquid chromatography assay and revision of kinetic parameters for the Staphylococcus aureus sortase transpeptidase SrtA. Anal. Biochem. 326, 42–48. https://doi.org/10.1016/j.ab.2003.10.023

Kruger, Ryan G., Otvos, B., Frankel, B.A., Bentley, M., Dostal, P., McCafferty, D.G., 2004. Analysis of the substrate specificity of the Staphylococcus aureus sortase transpeptidase SrtA. Biochemistry 43, 1541–1551. https://doi.org/10.1021/bi035920j

Kubica, M., Guzik, K., Koziel, J., Zarebski, M., Richter, W., Gajkowska, B., Golda, A., Maciag-Gudowska, A., Brix, K., Shaw, L., Foster, T., Potempa, J., 2008. A Potential New Pathway for Staphylococcus aureus Dissemination: The Silent Survival of S. aureus Phagocytosed by Human Monocyte-Derived Macrophages. PLOS ONE 3, e1409. https://doi.org/10.1371/journal.pone.0001409

Leeuwen, H.C. van, Klychnikov, O.I., Menks, M.A.C., Kuijper, E.J., Drijfhout, J.W., Hensbergen, P.J., 2014. Clostridium difficile sortase recognizes a (S/P)PXTG sequence motif and can accommodate diaminopimelic acid as a substrate for transpeptidation. FEBS Lett. 588, 4325–4333. https://doi.org/10.1016/j.febslet.2014.09.041

Leong, J.-Y., Lam, W.-H., Ho, K.-W., Voo, W.-P., Lee, M.F.-X., Lim, H.-P., Lim, S.-L., Tey, B.-T., Poncelet, D., Chan, E.-S., 2016. Advances in fabricating spherical alginate hydrogels with controlled particle designs by ionotropic gelation as encapsulation systems. Particuology 24, 44–60. https://doi.org/10.1016/j.partic.2015.09.004

Levary, D.A., Parthasarathy, R., Boder, E.T., Ackerman, M.E., 2011. Protein-Protein Fusion Catalyzed by Sortase A. PLOS ONE 6, e18342. https://doi.org/10.1371/journal.pone.0018342

Li, R.H., Altreuter, D.H., Gentile, F.T., 1996. Transport characterization of hydrogel matrices for cell encapsulation. Biotechnol. Bioeng. 50, 365–373. https://doi.org/10.1002/(SICI)1097-0290(19960520)50:4<365::AID-BIT3>3.0.CO;2-J

Lim, F., Sun, A.M., 1980. Microencapsulated islets as bioartificial endocrine pancreas. Science 210, 908–910. https://doi.org/10.1126/science.6776628

Lodes, M.J., Secrist, H., Benson, D.R., Jen, S., Shanebeck, K.D., Guderian, J., Maisonneuve, J.-F., Bhatia, A., Persing, D., Patrick, S., Skeiky, Y.A.W., 2006. Variable expression of immunoreactive surface proteins of Propionibacterium acnes. Microbiology 152, 3667–3681. https://doi.org/10.1099/mic.0.29219-0

MA Xiao-Jun, X.W.-M., 2004. Chemical Method of Breaking the Cell-loaded Sodium Alginate/Chitosan Microcapsules. Chem. J. Chin. Univ. 25, 1342–1346.

Mak, W.C., Cheung, K.Y., Trau, D., 2008. Diffusion Controlled and Temperature Stable Microcapsule Reaction Compartments for High-Throughput Microcapsule-PCR. Adv. Funct. Mater. 18, 2930–2937. https://doi.org/10.1002/adfm.200800388

Mandlik, A., Swierczynski, A., Das, A., Ton-That, H., 2008. Pili in Gram-positive bacteria: assembly, involvement in colonization and biofilm development. Trends Microbiol. 16, 33–40. https://doi.org/10.1016/j.tim.2007.10.010

Manzano, C., Contreras-Martel, C., El Mortaji, L., Izoré, T., Fenel, D., Vernet, T., Schoehn, G., Di Guilmi, A.M., Dessen, A., 2008. Sortase-Mediated Pilus Fiber Biogenesis in Streptococcus pneumoniae. Structure 16, 1838–1848. https://doi.org/10.1016/j.str.2008.10.007

Manzano, C., Izoré, T., Job, V., Di Guilmi, A.M., Dessen, A., 2009. Sortase activity is controlled by a flexible lid in the pilus biogenesis mechanism of gram-positive pathogens. Biochemistry 48, 10549–10557. https://doi.org/10.1021/bi901261y

Maresso, A.W., Chapa, T.J., Schneewind, O., 2006. Surface Protein IsdC and Sortase B Are Required for Heme-Iron Scavenging of Bacillus anthracis. J. Bacteriol. 188, 8145–8152. https://doi.org/10.1128/JB.01011-06

Marraffini, L.A., DeDent, A.C., Schneewind, O., 2006. Sortases and the Art of Anchoring Proteins to the Envelopes of Gram-Positive Bacteria. Microbiol. Mol. Biol. Rev. 70, 192–221. https://doi.org/10.1128/MMBR.70.1.192-221.2006

Marraffini, L.A., Schneewind, O., 2007. Sortase C-Mediated Anchoring of BasI to the Cell Wall Envelope of Bacillus anthracis. J. Bacteriol. 189, 6425–6436. https://doi.org/10.1128/JB.00702-07

Marraffini, L.A., Schneewind, O., 2006. Targeting proteins to the cell wall of sporulating Bacillus anthracis. Mol. Microbiol. 62, 1402–1417. https://doi.org/10.1111/j.1365-2958.2006.05469.x

Marraffini, L.A., Schneewind, O., 2005. Anchor Structure of Staphylococcal Surface Proteins V. ANCHOR STRUCTURE OF THE SORTASE B SUBSTRATE IsdC. J. Biol. Chem. 280, 16263–16271. https://doi.org/10.1074/jbc.M500071200

Marraffini, L.A., Ton-That, H., Zong, Y., Narayana, S.V.L., Schneewind, O., 2004. Anchoring of Surface Proteins to the Cell Wall of Staphylococcus aureus A CONSERVED ARGININE RESIDUE IS REQUIRED FOR EFFICIENT CATALYSIS OF SORTASE A. J. Biol. Chem. 279, 37763–37770. https://doi.org/10.1074/jbc.M405282200

Mastrobattista, E., Taly, V., Chanudet, E., Treacy, P., Kelly, B.T., Griffiths, A.D., 2005. High-Throughput Screening of Enzyme Libraries: In Vitro Evolution of a β-Galactosidase by Fluorescence-

Activated Sorting of Double Emulsions. Chem. Biol. 12, 1291–1300. https://doi.org/10.1016/j.chembiol.2005.09.016

Matsumoto, T., Takase, R., Tanaka, T., Fukuda, H., Kondo, A., 2012. Site-specific protein labeling with amine-containing molecules using Lactobacillus plantarum sortase. Biotechnol. J. 7, 642–648. https://doi.org/10.1002/biot.201100213

Mazmanian, S.K., Liu, G., Jensen, E.R., Lenoy, E., Schneewind, O., 2000. Staphylococcus aureus sortase mutants defective in the display of surface proteins and in the pathogenesis of animal infections. Proc. Natl. Acad. Sci. U. S. A. 97, 5510–5515.

Mazmanian, S.K., Liu, G., Ton-That, H., Schneewind, O., 1999. Staphylococcus aureus Sortase, an Enzyme that Anchors Surface Proteins to the Cell Wall. Science 285, 760–763. https://doi.org/10.1126/science.285.5428.760

Mazmanian, S.K., Skaar, E.P., Gaspar, A.H., Humayun, M., Gornicki, P., Jelenska, J., Joachmiak, A., Missiakas, D.M., Schneewind, O., 2003. Passage of Heme-Iron Across the Envelope of Staphylococcus aureus. Science 299, 906–909. https://doi.org/10.1126/science.1081147

McConnell, S.A., Amer, B.R., Muroski, J., Fu, J., Chang, C., Ogorzalek Loo, R.R., Loo, J.A., Osipiuk, J., Ton-That, H., Clubb, R.T., 2018. Protein Labeling via a Specific Lysine-Isopeptide Bond using the Pilin Polymerizing Sortase from Corynebacterium diphtheriae. J. Am. Chem. Soc. 140, 8420–8423. https://doi.org/10.1021/jacs.8b05200

McCoy, A.J., Grosse-Kunstleve, R.W., Adams, P.D., Winn, M.D., Storoni, L.C., Read, R.J., 2007. Phaser crystallographic software. J. Appl. Crystallogr. 40, 658–674. https://doi.org/10.1107/S0021889807021206

Momma, K., Mikami, B., Mishima, Y., Hashimoto, W., Murata, K., 2002. Crystal structure of AlgQ2, a macromolecule (alginate)-binding protein of Sphingomonas sp. A1 at 2.0 Å resolution. J. Mol. Biol. 316, 1051–1059. https://doi.org/10.1006/jmbi.2001.5393

Momma, K., Mishima, Y., Hashimoto, W., Mikami, B., Murata, K., 2005. Direct Evidence for Sphingomonas sp. A1 Periplasmic Proteins as Macromolecule-Binding Proteins Associated with the ABC Transporter: Molecular Insights into Alginate Transport in the Periplasm. Biochemistry 44, 5053–5064. https://doi.org/10.1021/bi047781r

Murshudov, G.N., Skubák, P., Lebedev, A.A., Pannu, N.S., Steiner, R.A., Nicholls, R.A., Winn, M.D., Long, F., Vagin, A.A., 2011. REFMAC5 for the refinement of macromolecular crystal structures. Acta Crystallogr. D Biol. Crystallogr. 67, 355–367. https://doi.org/10.1107/S0907444911001314

Naik, M.T., Suree, N., Ilangovan, U., Liew, C.K., Thieu, W., Campbell, D.O., Clemens, J.J., Jung, M.E., Clubb, R.T., 2006. Staphylococcus aureus Sortase A Transpeptidase CALCIUM PROMOTES SORTING SIGNAL BINDING BY ALTERING THE MOBILITY AND STRUCTURE OF AN ACTIVE SITE LOOP. J. Biol. Chem. 281, 1817–1826. https://doi.org/10.1074/jbc.M506123200

Navarre, W.W., Schneewind, O., 1999. Surface Proteins of Gram-Positive Bacteria and Mechanisms of Their Targeting to the Cell Wall Envelope. Microbiol. Mol. Biol. Rev. MMBR 63, 174–229.

Navarre, W.W., Schneewind, O., 1994. Proteolytic cleavage and cell wall anchoring at the LPXTG motif of surface proteins in gram-positive bacteria. Mol. Microbiol. 14, 115–121.

Neiers, F., Madhurantakam, C., Fälker, S., Manzano, C., Dessen, A., Normark, S., Henriques-Normark, B., Achour, A., 2009. Two Crystal Structures of Pneumococcal Pilus Sortase C Provide Novel

Insights into Catalysis and Substrate Specificity. J. Mol. Biol. 393, 704–716. https://doi.org/10.1016/j.jmb.2009.08.058

Nikghalb, K.D., Horvath, N.M., Prelesnik, J.L., Banks, O.G.B., Filipov, P.A., Row, R.D., Roark, T.J., Antos, J.M., 2018. Expanding the Scope of Sortase-Mediated Ligations by Using Sortase Homologues. ChemBioChem 19, 185–195. https://doi.org/10.1002/cbic.201700517

O'Neill, E., Pozzi, C., Houston, P., Humphreys, H., Robinson, D.A., Loughman, A., Foster, T.J., O'Gara, J.P., 2008. A Novel Staphylococcus aureus Biofilm Phenotype Mediated by the Fibronectin-Binding Proteins, FnBPA and FnBPB. J. Bacteriol. 190, 3835–3850. https://doi.org/10.1128/JB.00167-08

Ostafe, R., Prodanovic, R., Lloyd Ung, W., Weitz, D.A., Fischer, R., 2014. A high-throughput cellulase screening system based on droplet microfluidics. Biomicrofluidics 8, 041102. https://doi.org/10.1063/1.4886771

Pallen, M.J., Lam, A.C., Antonio, M., Dunbar, K., 2001. An embarrassment of sortases–a richness of substrates? Trends Microbiol. 9, 97–101.

Peppas, N.A., Hilt, J.Z., Khademhosseini, A., Langer, R., 2006. Hydrogels in Biology and Medicine: From Molecular Principles to Bionanotechnology. Adv. Mater. 18, 1345–1360. https://doi.org/10.1002/adma.200501612

Petersen, T.N., Brunak, S., Heijne, G. von, Nielsen, H., 2011. SignalP 4.0: discriminating signal peptides from transmembrane regions. Nat. Methods 8, 785–786. https://doi.org/10.1038/nmeth.1701

Pettersen, E.F., Goddard, T.D., Huang, C.C., Couch, G.S., Greenblatt, D.M., Meng, E.C., Ferrin, T.E., 2004. UCSF Chimera--a visualization system for exploratory research and analysis. J. Comput. Chem. 25, 1605–1612. https://doi.org/10.1002/jcc.20084

Piotukh, K., Geltinger, B., Heinrich, N., Gerth, F., Beyermann, M., Freund, C., Schwarzer, D., 2011a. Directed Evolution of Sortase A Mutants with Altered Substrate Selectivity Profiles. J. Am. Chem. Soc. 133, 17536–17539. https://doi.org/10.1021/ja205630g

Piotukh, K., Geltinger, B., Heinrich, N., Gerth, F., Beyermann, M., Freund, C., Schwarzer, D., 2011b. Directed Evolution of Sortase A Mutants with Altered Substrate Selectivity Profiles. J. Am. Chem. Soc. 133, 17536–17539. https://doi.org/10.1021/ja205630g

Popp, M.W., Antos, J.M., Grotenbreg, G.M., Spooner, E., Ploegh, H.L., 2007. Sortagging: a versatile method for protein labeling. Nat. Chem. Biol. 3, 707–708. https://doi.org/10.1038/nchembio.2007.31

Price, A.D., Zelikin, A.N., Wark, K.L., Caruso, F., 2010. A Biomolecular "Ship-in-a-Bottle": Continuous RNA Synthesis Within Hollow Polymer Hydrogel Assemblies. Adv. Mater. 22, 720–723. https://doi.org/10.1002/adma.200903411

Puorger, C., Di Girolamo, S., Lipps, G., 2017. Elucidation of the Recognition Sequence of Sortase B from Bacillus anthracis by Using a Newly Developed Liquid Chromatography–Mass Spectrometry-Based Method. Biochemistry 56, 2641–2650. https://doi.org/10.1021/acs.biochem.7b00108

Rabuka, D., 2010. Chemoenzymatic Methods for Site-Specific Protein Modification. Curr. Opin. Chem. Biol. 14, 790–796. https://doi.org/10.1016/j.cbpa.2010.09.020

Raeeszadeh-Sarmazdeh, M., Parthasarathy, R., Boder, E.T., 2015. Site-specific immobilization of protein layers on gold surfaces via orthogonal sortases. Colloids Surf. B Biointerfaces 128, 457–463. https://doi.org/10.1016/j.colsurfb.2015.02.044

Rashidian, M., Dozier, J.K., Distefano, M.D., 2013. Chemoenzymatic Labeling of Proteins: Techniques and Approaches. Bioconjug. Chem. 24, 1277–1294. https://doi.org/10.1021/bc400102w

Rathore, S., Desai, P.M., Liew, C.V., Chan, L.W., Heng, P.W.S., 2013. Microencapsulation of microbial cells. J. Food Eng. 116, 369–381. https://doi.org/10.1016/j.jfoodeng.2012.12.022

Riley, L.M., Weadge, J.T., Baker, P., Robinson, H., Codée, J.D.C., Tipton, P.A., Ohman, D.E., Howell, P.L., 2013. Structural and Functional Characterization of *Pseudomonas aeruginosa* AlgX: ROLE OF AlgX IN ALGINATE ACETYLATION. J. Biol. Chem. 288, 22299–22314. https://doi.org/10.1074/jbc.M113.484931

Robson, Scott A., Jacobitz, A.W., Phillips, M.L., Clubb, R.T., 2012. Solution Structure of the Sortase Required for Efficient Production of Infectious Bacillus anthracis Spores. Biochemistry 51, 7953–7963. https://doi.org/10.1021/bi300867t

Robson, S. A., Jacobitz, A.W., Phillips, M.L., Clubb, R.T., 2012. Solution structure of the sortase required for efficient production of infectious Bacillus anthracis spores. Biochemistry 51, 7953–7963.

Salis, H.M., Mirsky, E.A., Voigt, C.A., 2009. Automated design of synthetic ribosome binding sites to control protein expression. Nat. Biotechnol. 27, 946. https://doi.org/10.1038/nbt.1568

Schmohl, L., Bierlmeier, J., Gerth, F., Freund, C., Schwarzer, D., 2017. Engineering sortase A by screening a second-generation library using phage display. J. Pept. Sci. Off. Publ. Eur. Pept. Soc. 23, 631–635. https://doi.org/10.1002/psc.2980

Schneewind, O., Model, P., Fischetti, V.A., 1992. Sorting of protein A to the staphylococcal cell wall. Cell 70, 267–281.

Serp, D., Cantana, E., Heinzen, C., Stockar, U.V., Marison, I.W., 2000. Characterization of an encapsulation device for the production of monodisperse alginate beads for cell immobilization. Biotechnol. Bioeng. 70, 41–53. https://doi.org/10.1002/1097-0290(20001005)70:1<41::AID-BIT6>3.0.CO;2-U

Shaik, M.M., Lombardi, C., Trindade, D.M., Fenel, D., Schoehn, G., Guilmi, A.M.D., Dessen, A., 2015. A Structural Snapshot of Type II Pilus Formation in Streptococcus pneumoniae. J. Biol. Chem. 290, 22581–22592. https://doi.org/10.1074/jbc.M115.647834

Skjåk-Bræk, G., Grasdalen, H., Smidsrød, O., 1989. Inhomogeneous polysaccharide ionic gels. Carbohydr. Polym. 10, 31–54. https://doi.org/10.1016/0144-8617(89)90030-1

Spirig, T., Weiner, E.M., Clubb, R.T., 2011. Sortase enzymes in Gram-positive bacteria. Mol. Microbiol. 82, 1044–1059. https://doi.org/10.1111/j.1365-2958.2011.07887.x

Stefan, N., Gébleux, R., Waldmeier, L., Hell, T., Escher, M., Wolter, F.I., Grawunder, U., Beerli, R.R., 2017. Highly Potent, Anthracycline-based Antibody–Drug Conjugates Generated by Enzymatic, Site-specific Conjugation. Mol. Cancer Ther. 16, 879–892. https://doi.org/10.1158/1535-7163.MCT-16-0688

Suliman, M., Santosh, V., Seegar, T.C.M., Dalton, A.C., Schultz, K.M., Klug, C.S., Barton, W.A., 2017. Directed evolution provides insight into conformational substrate sampling by SrtA. PLOS ONE 12, e0184271. https://doi.org/10.1371/journal.pone.0184271

Suree, N., Liew, C.K., Villareal, V.A., Thieu, W., Fadeev, E.A., Clemens, J.J., Jung, M.E., Clubb, R.T., 2009. The Structure of the Staphylococcus aureus Sortase-Substrate Complex Reveals How the Universally Conserved LPXTG Sorting Signal Is Recognized. J. Biol. Chem. 284, 24465–24477. https://doi.org/10.1074/jbc.M109.022624

Suryadinata, R., Seabrook, S.A., Adams, T.E., Nuttall, S.D., Peat, T.S., 2015. Structural and biochemical analyses of a Clostridium perfringens sortase D transpeptidase. Acta Crystallogr. D Biol. Crystallogr. 71, 1505–1513. https://doi.org/10.1107/S1399004715009219

Tawfik, D.S., Griffiths, A.D., 1998. Man-made cell-like compartments for molecular evolution. Nat. Biotechnol. 16, 652–656. https://doi.org/10.1038/nbt0798-652

Ton-That, H., Liu, G., Mazmanian, S.K., Faull, K.F., Schneewind, O., 1999. Purification and characterization of sortase, the transpeptidase that cleaves surface proteins of Staphylococcus aureus at the LPXTG motif. Proc. Natl. Acad. Sci. U. S. A. 96, 12424–12429.

Ton-That, H., Mazmanian, S.K., Alksne, L., Schneewind, O., 2002. Anchoring of Surface Proteins to the Cell Wall of Staphylococcus aureus CYSTEINE 184 AND HISTIDINE 120 OF SORTASE FORM A THIOLATE-IMIDAZOLIUM ION PAIR FOR CATALYSIS. J. Biol. Chem. 277, 7447–7452. https://doi.org/10.1074/jbc.M109945200

Ton-That, H., Mazmanian, S.K., Faull, K.F., Schneewind, O., 2000. Anchoring of Surface Proteins to the Cell Wall of Staphylococcus aureus SORTASE CATALYZED IN VITRO TRANSPEPTIDATION REACTION USING LPXTG PEPTIDE AND NH2-GLY3SUBSTRATES. J. Biol. Chem. 275, 9876–9881.

Ton-That, H., Schneewind, O., 2003. Assembly of pili on the surface of Corynebacterium diphtheriae. Mol. Microbiol. 50, 1429–1438. https://doi.org/10.1046/j.1365-2958.2003.03782.x

Vanier, G., Sekizaki, T., Domínguez-Punaro, M.C., Esgleas, M., Osaki, M., Takamatsu, D., Segura, M., Gottschalk, M., 2008. Disruption of srtA gene in Streptococcus suis results in decreased interactions with endothelial cells and extracellular matrix proteins. Vet. Microbiol. 127, 417–424. https://doi.org/10.1016/j.vetmic.2007.08.032

Voigt, C.A., Martinez, C., Wang, Z.-G., Mayo, S.L., Arnold, F.H., 2002. Protein building blocks preserved by recombination. Nat. Struct. Mol. Biol. 9, 553–558. https://doi.org/10.1038/nsb805

Walser, M., Leibundgut, R.M., Pellaux, R., Panke, S., Held, M., 2008. Isolation of monoclonal microcarriers colonized by fluorescent E. coli. Cytometry A 73A, 788–798. https://doi.org/10.1002/cyto.a.20597

Wang, B.L., Ghaderi, A., Zhou, H., Agresti, J., Weitz, D.A., Fink, G.R., Stephanopoulos, G., 2014. Microfluidic high-throughput culturing of single cells for selection based on extracellular metabolite production or consumption. Nat. Biotechnol. 32, 473–478. https://doi.org/10.1038/nbt.2857

Wang, H., Cheng, H., Wang, F., Wei, D., Wang, X., 2010. An improved 3-(4,5-dimethylthiazol-2-yl)-2,5-diphenyl tetrazolium bromide (MTT) reduction assay for evaluating the viability of Escherichia coli cells. J. Microbiol. Methods 82, 330–333. https://doi.org/10.1016/j.mimet.2010.06.014

Weiss, W.J., Lenoy, E., Murphy, T., Tardio, L., Burgio, P., Projan, S.J., Schneewind, O., Alksne, L., 2004. Effect of srtA and srtB gene expression on the virulence of Staphylococcus aureus in animal models of infection. J. Antimicrob. Chemother. 53, 480–486. https://doi.org/10.1093/jac/dkh078

Wilson, D.S., Keefe, A.D., 2000. Random Mutagenesis by PCR. Curr. Protoc. Mol. Biol. 51, 8.3.1-8.3.9. https://doi.org/10.1002/0471142727.mb0803s51

Witte, M.D., Wu, T., Guimaraes, C.P., Theile, C.S., Blom, A.E.M., Ingram, J.R., Li, Z., Kundrat, L., Goldberg, S.D., Ploegh, H.L., 2015. Site-specific protein modification using immobilized sortase in batch and continuous-flow systems. Nat. Protoc. 10, 508–516. https://doi.org/10.1038/nprot.2015.026

Wuethrich, I., Peeters, J.G.C., Blom, A.E.M., Theile, C.S., Li, Z., Spooner, E., Ploegh, H.L., Guimaraes, C.P., 2014. Site-Specific Chemoenzymatic Labeling of Aerolysin Enables the Identification of New Aerolysin Receptors. PLOS ONE 9, e109883. https://doi.org/10.1371/journal.pone.0109883

Zhang, J., Yamaguchi, S., Nagamune, T., 2015. Sortase A-mediated synthesis of ligand-grafted cyclized peptides for modulating a model protein-protein interaction. Biotechnol. J. 10, 1499–1505. https://doi.org/10.1002/biot.201500013

Zong, Y., Bice, T.W., Ton-That, H., Schneewind, O., Narayana, S.V.L., 2004. Crystal Structures of Staphylococcus aureus Sortase A and Its Substrate Complex. J. Biol. Chem. 279, 31383–31389. https://doi.org/10.1074/jbc.M401374200

Zou, Z., Alibiglou, H., Mate, D.M., Davari, M.D., Jakob, F., Schwaneberg, U., 2018. Directed sortase A evolution for efficient site-specific bioconjugations in organic co-solvents. Chem. Commun. 54, 11467–11470. https://doi.org/10.1039/C8CC06017G

# Acknowledgments

I would like to thank all the people I have met during the past 6 years at the FHNW. They made great this life experience and deeply contributed to my scientific and personal development.

I would like to express my deepest gratitude to Prof. Dr. Georg Lipps. Besides giving me this huge opportunity, he gave the freedom and independence to work on this project from which I learnt so much. I am thankful to him for the trust in me, for his support and for his time and dedication. I really wish him and his family all the best.

A special thank goes to my lab and project mate Dr. Chasper Puorger for the great right-hand he was, for all the fruitful scientific discussions we had and for the precious advices and help he gave me since I started the PhD.

Special thanks also to my lab mates Maren, Valeria, Sabrina, Jan, Jean-Christophe and Raphael for the support and for all the nice moments we spent together inside and outside the lab.

Many thanks to my colleague and friend Rosario for the help he gave me since I arrived in Basel and for the company and nice conversations we had during our coffee breaks. Many thanks also to Anna Weston, Salvo Mannino, all the professors, post Docs, PhD students, practical students and all the people and friends I have met during this period.

I am thankful to all the students from the University of Palermo who have followed over the years and who made me feel like home. In particular, I am grateful to Elisabetta Calà and Mara Castiglione who worked on this project and contributed to clarify important issues of the research. I wish them all a beautiful career.

Thanks to Dr. Roger Beerli and Dr. Ulf Grawunder from *NBE therapeutics* for the scientific collaboration and for the interesting and fruitful discussion we had during our meetings.

Thanks to Prof. Dr. Timm Maier and Dr. Roman Jacob (Biozentrum, Unibas) for accepting the collaboration on protein structure determination. Many thanks also go to the research group of Prof. Dr. Svan Panke (D-BSSE, ETH) for letting me use the COPAS and in particular to Dr. Steven Schmitt for his support with the instrument and Philip Koch for his friendliness.

I would like to thank Prof. Dr. Florian Seebeck for overseeing me during these years, Prof. Dr. Michael Nash for accepting to co-examine my PhD thesis and Prof. Dr. Dennis Gillingham to chair my PhD defense.

I would like to thank the Swiss Commission for Technology (CTI) for funding the project of this thesis, the entire FHNW as well as the University of Basel.

Finally, I would like to address my gratitude to my family and to my girlfriend Carla for their constant support and encouragement on my way. Without them, this would not have happened. I love you!